Landau States and Astrophysical Jets

By

Hervé Guy

A thesis submitted to the Faculty of Graduate Studies and Research
in partial fulfillment of the requirements for the degree of

Master of Science

In

Physics

Carleton University
Ottawa, Ontario

Your file Votre référence
ISBN: 978-0-494-68620-1
Our file Notre référence
ISBN: 978-0-494-68620-1

Abstract

Since the beginning of the twentieth century, astrophysical jets have been observed at all scales and with a wide range of parameters, in terms of jet sources, sizes, speeds and emitted wavelengths. Several models that explained the origin of astrophysical jets have been created over time with varying degrees of success! Surprisingly, none of them have used Landau states to explain the origin of the astrophysical jets, which are always formed in the vicinity of a bizarre object, such as a black hole or a neutron star. Among the exotic properties shared by these, one in particular is that they often have an extremely strong magnetic field, which is precisely the environment where the Landau states are present.

The purpose of this work is then to examine the role that Landau States could play in explaining the origin of astrophysical jets.

After having determined how Landau states behave in uniform varying magnetic fields, two models will be proposed: 1) a Quasi-Realistic Astrophysical Jet Model that will try to explain how an astrophysical jet could be formed in the atmosphere of a neutron star, and 2) a Quasi-Realistic Jet Propulsion Mechanism that will try to explain how photons could be emitted when the density in the Landau states changes in the vicinity of a neutron stars surface and propelled via the astrophysical jets formed in the atmosphere of the neutron star.

Please note:

The original title page for this thesis has been removed due to formatting problems.

All information has been transferred to the Carleton University standard title page template for theses.

Acknowledgements

I would like to thank all the people who have helped and inspired me during my master's study.

I especially want to thank my advisor, Prof. Peter J. Watson, for his guidance during my research and study at Carleton University. He taught me my first course when I initiated this crazy adventure. Once successfully completed, he was so generous in sharing me his thoughts about the potential role that Landau States could play in explaining the origin of astrophysical jets. In this regard, he showed me all roads that allowed me to complete this project. His perpetual energy and enthusiasm in research had always motivated me. In addition, he was always accessible and willing to help his students with their research.

The generous support from my employer CANARIE Inc. is greatly appreciated. In retrospect, I am amazed by the confidence of managers and colleagues. Without their great patience and support, my ambition to study at part-time would hardly be realized.

My deepest gratitude goes to my wonderful spouse, my two adorable sons, as well as my family, for their unflagging love and support throughout my life; this dissertation would have been simply impossible without them.

Contents

List of Tables

List of Figures

Chapter 1

Introduction

1.1 Jet phenomena

We have gradually become aware that jets are ubiquitous phenomena in astrophysics. They have been observed since the beginning of the twentieth century on all scales and with a wide range of parameters, in terms of jet sources, sizes, speeds and emitted wavelengths.

The first evidence of jet-like features emanating from the nuclei of galaxies goes back to the discovery by Curtis in 1918 [11] of the optical jet from the elliptical galaxy M87 in the Virgo cluster. The figure 1.1 shows some evidence that relativistic jets in some of these compact sources are found by means of multiwavelength observations with ground-based or satellite-based telescopes. The jet of M87 extends at least 5000 light-years from the nucleus and is made up of matter ejected from the galaxy. It is showing apparent relativistic motion close to the speed of light.

The finding that jets can also be produced in larger scale by distant quasars (con-

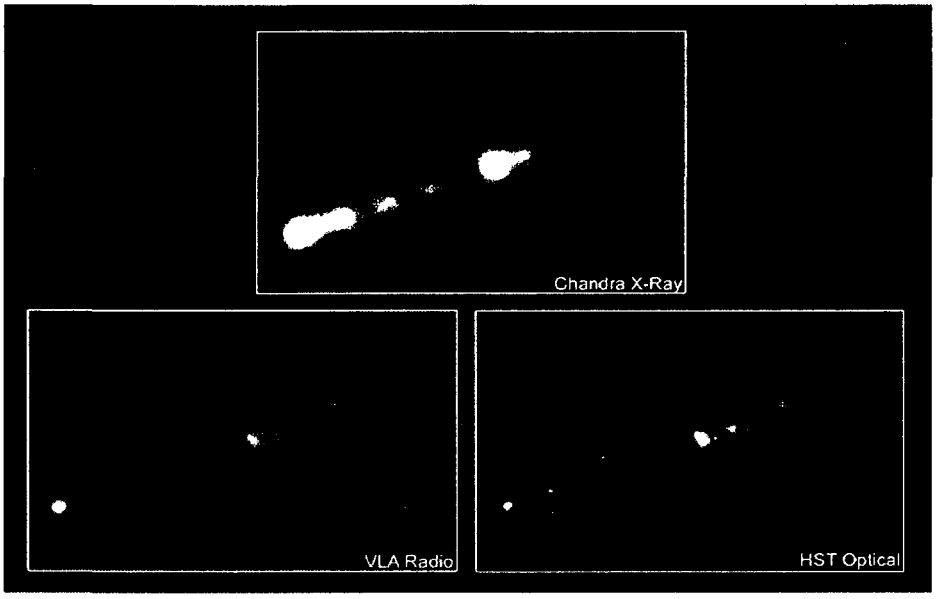

Figure 1.1: Multifrequency images of M87 jet structure with arcsecond resolution instruments. [4].

traction of *QUASi*-stell*AR* radio source) systems is more recent. The first quasars were discovered with radio telescopes in the late 1950s. Shortly after, scientists began to observe the quasars and they discovered something very unusual. After careful observations, Maarten Schmidt concluded in 1962 [34] that light from quasars was red-shifted by large amounts, in some cases as large as z = 5[1]. As a result, quasars must be traveling at a sizeable fraction of the speed of light. The first evidence of jet-like features emanating from quasars has been recorded in the 1960s as well. Figure 1.2 shows two observations of the Quasar 3C 273 with a jet in different wavelengths.

[1]Redshift (and blue shift) may be characterized by the relative difference between the observed and emitted wavelengths (or frequency) of an object. It is customary to refer to this change using a dimensionless quantity called z. If λ represents wavelength, then z is defined by the equations: $1 + z = \frac{\lambda_{obsv}}{\lambda_{emit}}$

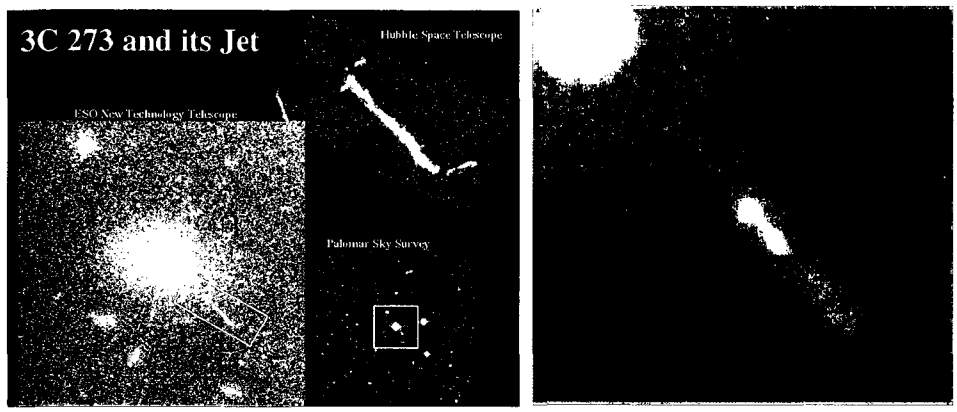

Figure 1.2: (left) Visible [22] and (right) X-ray observation [1] of the Quasar 3C 273 with a jet.

It became clear during the 1960s that the above-mentioned quasars and the elliptical galaxy "M87" fall within a class including other, related kinds of objects. These are now all collectively known as "active galactic nuclei" or *AGN*. They share the common feature of powerful energy release from a small volume at their centre, assumed to be a super-massive black hole many times the mass of the sun.

But that was not the end of the story. More recently, it has been found that jets can also be produced in smaller scale by binary stellar systems. The detection by Margon *and al.* in 1979 [29] of large, periodic doppler drifts in the optical lines of SS 433 resulted in the proposition of a kinematic model [13] [30].

At first glance, it may seem paradoxical that relativistic jets were first discovered in the nuclei of galaxies and distant quasars, and that for more than a decade SS 433, which is located in our galaxy, was the only known object of its class [28]. This can be explained by the fact that a black hole is accreting at the Eddington limit, which has the consequence

that the resulting black body temperature at the last stable orbit in the surrounding accretion disk is approximately inversely proportional to the one-fourth power of the mass of the black hole [32]. Consequently, the more massive the black hole, the cooler the surrounding accretion disk is. Thus, the disks around supermassive black holes emit then strongly at optical and UV wavelengths. If we apply the same principle for some much lighter systems, such as the ones formed by a black hole or neutron star binaries in our galaxy, it is not a surprise that they have been identified for the first time by their X-ray emission. Therefore, it is understandable that there was an impasse in the discovery of new stellar sources of relativistic jets until the recent developments in X-ray astronomy.

Figure 1.3: Artist's rendition of SS 433 and its Relativistic Jet [42]

However, SS 433, here represented in figure 1.3, is a quite unusual object. Because of its

proximity, its study opens the way for a better understanding of the relativistic jets seen elsewhere in the universe. Many observations have then been made since its discovery. It has been found over time that this visible "*intragalactic-object*" mimics, on a much smaller scale, many of the above-mentioned phenomena seen in quasars. For instance, it emits some strong emission across a broad range of wavelengths from radio wave to X-ray. It also combines two relevant aspects of relativistic astrophysics: 1) accreting black hole or neutron stars (of stellar origin) that produces hard X-rays from the surrounding accretion disk and 2) relativistic jets of particles. This was why these kinds of unusual objects are often referred to in the literature as *microquasars*. Figure 1.4 shows two spectra of SS 433 observed in different visible and X-ray wavelengths.

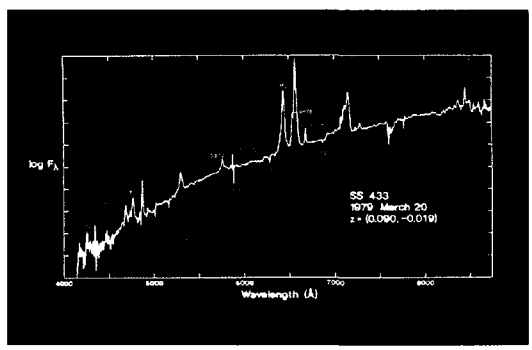

Figure 1.4: SS 433: Optical and X-ray spectrums [23]

1.2 Purpose of this thesis

Unfortunately, the mechanism responsible for the formation, acceleration and collimation of relativistic jets is poorly understood at present. Several models have been created over

time, such as [6], [28], [32], etc., with varying degrees of success! It might seem hardly necessary to add another one here.

It is surprising that there are no relativistic jet models that have tried to explain the origin of astrophysical jets using Landau states [24]. The relativistic jet is always formed in the vicinity of a bizarre object, such as a black hole or a neutron star. Among the exotic properties shared by these, one in particular is that they often have an extremely strong magnetic field [35], which is precisely the environment where the Landau states are present. [25]

The purpose of this work is then to examine the role that Landau States could play in explaining the origin of astrophysical jets, in particular their geometry (i.e. narrow beam) and ejection speed (i.e. close to the speed of light) and other parameters.

1.3 Structure of this document

In the first part of this thesis, we provide a detailed examination of SS433, in order to highlight its unusual characteristics, and discuss whether its compact object is a black hole or a neutron star. Once done, we will undertake another survey that will take a deeper look at a neutron star's exotic properties. We will then be in a position to figure out how its magnetic dipole generates the required ultra-strong magnetic fields suitable for the formation of Landau states.

The second part of this document will present the core of this research. We will undertake a deep exploration of the Landau states. We will first take a look at how they

are created and how they behave in constant magnetic fields. Then, we will go a step further, by trying to determine how these same Landau states behave in varying magnetic fields, such as the ones found in the atmosphere of a neutron star: this is an issue that (surprisingly) does not seem to have been discussed in the literature. This will give an interesting novel result.

Capitalizing on this interesting discovery, two models will be proposed in the last part of this document: 1) a *Quasi-Realistic Astrophysical Jet Model* that will try to explain how an astrophysical jet could be formed in the atmosphere of a neutron star, and 2) a *Quasi-Realistic Jet Propulsion Mechanism* that will try to explain how photons could be emitted when the density in the Landau states changes in the vicinity of a neutron star's surface and propelled via the astrophysical jets formed in the atmosphere of the neutron star.

Although we outline the essentials of the technique and discuss general features, a realistic model is beyond the scope of this thesis as it would involve a complex computer model of the jet.

Part I

Surveys of Exotic Objects

Chapter 2

SS 433

2.1 Overall picture of the SS 433 system

SS 433 is the enigmatic binary system with a precessing, relativistic bipolar jet. Though it has been studied for more than twenty-five years since its discovery, some fundamental properties of the system still remain unknown. What is the nature of the compact object, *i.e.* is it a neutron star or a black hole? Which process governs the acceleration and the precession of the jets? In the following paragraph, we will highlight its unusual characteristics and possibly use them for testing the jet model via the Landau states developed in this thesis.

The first correct celestial coordinates of the source were published in 1977, in the Stephenson and Sanduleak catalogue of bright emission-line stars. The object was listed under the entry number 433 and this gave its name. Figure 2.1 shows the location of SS 433 in the constellation Aquila, the Eagle. More specifically, the optical counterpart of the system is located at $(\alpha, \delta) = (287.956°, 4.983°)_{2000}$ [28]. The corresponding galactic

coordinates are $(l, b) = (39.700°, -2.252°)$. The distance to the object was estimated to be 4.85 $\pm$ 0.2 kpc from the proper motion of the relativistic jet [38], *i.e.* at a distance of about 16,000 light-years. The radial velocity v_r of the SS 433 binary system itself is about 70 km/s. SS 433 is a 14(V) magnitude object which can be observed also with a small telescope.

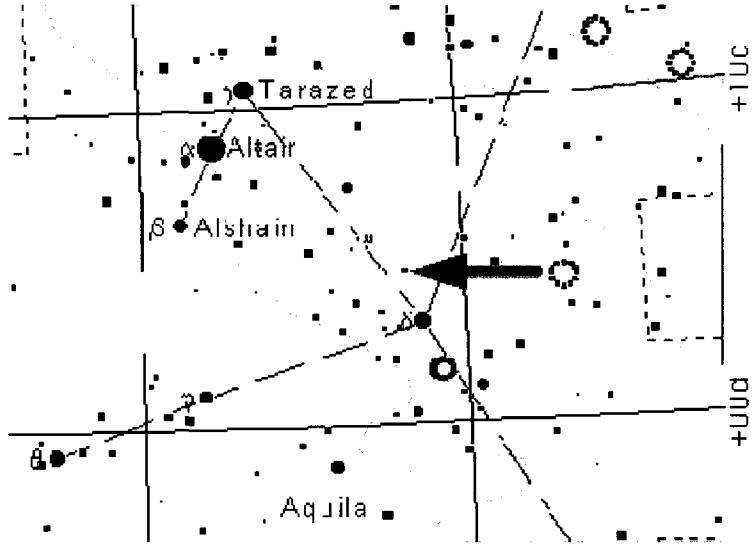

Figure 2.1: Location of SS 433 in constellation Aquila [39]

It was discovered in 1978 that this object was the common source of the emission in the optical, radio and X-ray band, previously identified in this area. Furthermore, it is now known that the position of SS 433 lies at the centre of a diffuse, elongated shell of gas known as W50, here shown in figure 2.2, which is probably a supernova remnant. W50 is at least 100,000 years old.

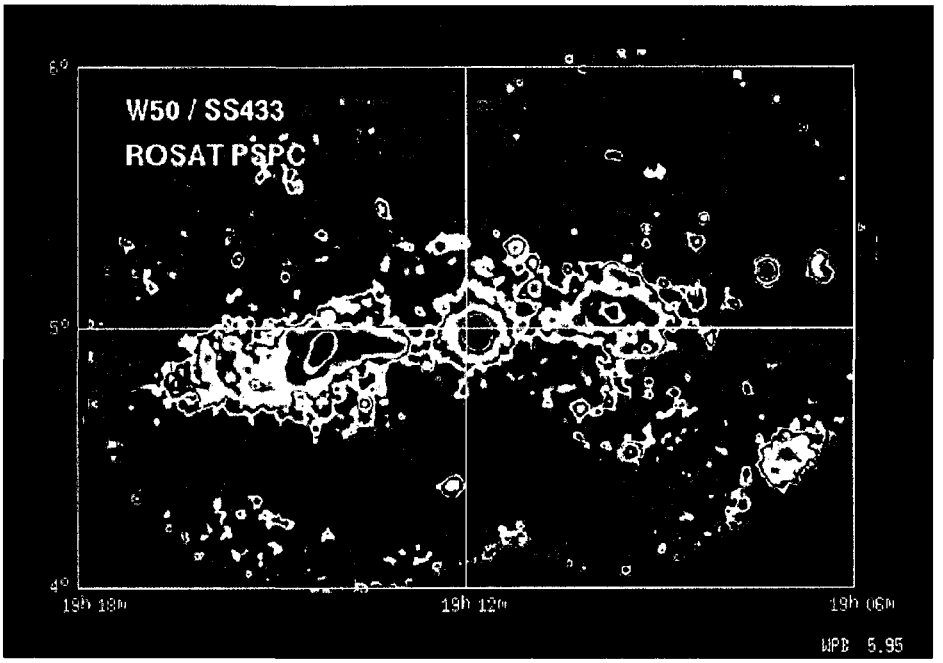

Figure 2.2: X-ray brightness distribution of the supernova remnant W 50 with its central object SS 433 [5].

It was also discovered in 1978 that this object displays three sets of emission lines [29]. One set of spectral lines was greatly "blue shifted", another set was greatly "red shifted", and a third set lacked a significant Doppler shift. Here was an object with 3 components: two were approaching and receding, respectively, at one-quarter the speed of light while the third stayed nearly still! This combination of very large Doppler shifts that vary (and even change sign) over a short period is quite unique amongst celestial objects. The wavelengths of the shifted lines vary with the period of 163 days, while the wavelengths of the nearly stationary lines show a smaller shift with a 13.1-day period.

There is now a broad agreement that SS 433 is a semidetached binary, illustrated here in figure 2.3. The secondary is a normal massive star, probably an OB star or a Wolf-

Rayet, which fills its Roche Lobe and loses mass to its companion, the primary star. The primary is a compact object, presumably a black hole or a neutron star.

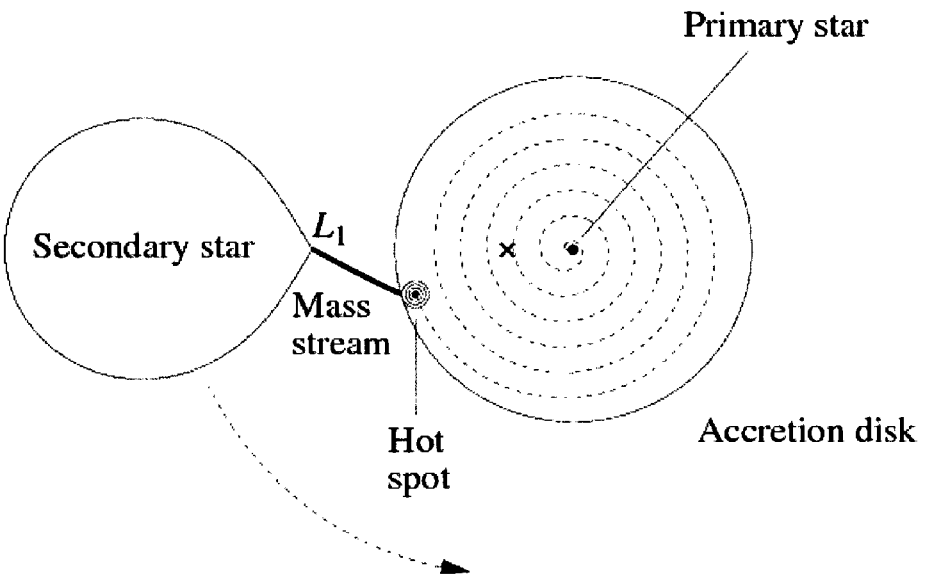

Figure 2.3: The semidetached binary SS 433 showing the accretion disk around the primary/compact star. [6]

The wavelengths of the above-mentioned nearly stationary lines suggest that the two objects follow circular orbits with a period of 13.1 days. The matter lost by the secondary forms an accretion disk around the compact object. The accretion disk contributes to the visible light from the system equally with the secondary.

The wavelengths of the above-mentioned "blue and red shifted" lines suggest that two oppositely aligned jets emerge from the vicinity of the compact object. A tidal interaction between the disk and the two stars could be responsible for a precessional wobble of the

disk that has a period of 163 days. This is a phenomenon analogous to Earth's 25,770-year precessional wobble.

Its optical continuum resembles a black body curve with color temperature of around 30,000 K and a bolometric luminosity of about 4.4 x 10^{39} erg/s. Using the Stefan-Boltzmann equation and assuming that the overall system is a spherical object of radius R and surface area $A = 4\pi R^2$, a rough order of magnitude of the size of SS 433 could be estimated as follows [6]

$$L = 4\pi R^2 \sigma T_e^4 \quad \Rightarrow \quad R = \sqrt{\frac{L}{4\pi\sigma T_e^4}} = 2.76 \text{ x } 10^{12} \text{ cm} \tag{2.1}$$

which is 39.7 $R_\odot$, where $R_\odot$ is the radius of the Sun, or 0.185 AU, where AU is the astronomical unit, i.e. the mean distance between the Earth and the Sun.

According to the Wien displacement law for a black body of temperature equal to 30,000 K, the continuous spectrum of SS 433 peaks at a wavelength of

$$\lambda_{max} = \frac{5000 \text{ Å } 5800 \text{ } K}{T} = \frac{5000 \text{ Å } 5800 \text{ } K}{30000 \text{ } K} = 966.67 \text{ Å}. \tag{2.2}$$

So the spectrum of SS 433 presumably peaks in the UV region. Unfortunately SS 433 lies close to the galactic plane where the UV absorption is know to be very strong ($\delta = 4.983°$). The X-ray observations of SS 433 from the Einstein Observatory show a central unresolved source ($\leq 10^{17}$ cm) and two extended, jet-like lobes of emission of size around 10^{20} cm, spatially aligned with the radio ears of the SNR W50 (see figure 2.4). The symmetric X-ray structure of SS 433s jet lobes is now believed to be formed by the jet activity of the past $10^4 \sim 10^5$ years. The luminosity of the X-ray binaries is about 10^{36} erg/s and accounts for about 90% of the total X-ray luminosity, while the remaining

10% is emitted in the extended lobes.

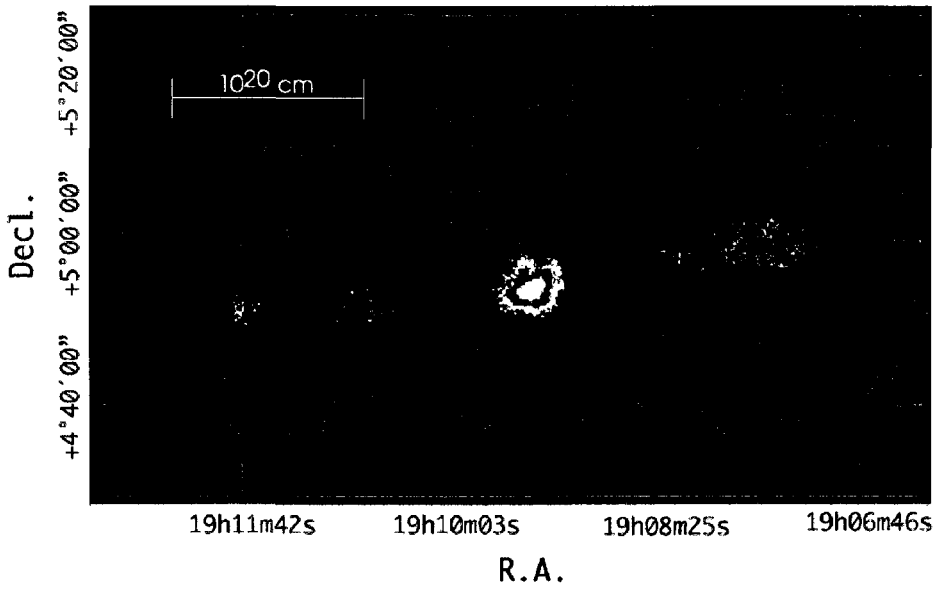

Figure 2.4: The X-ray lobes of SS 433 (W 50) [23].

2.2 The kinetic model for the relativistic Doppler shift measured for the emission lines in SS 433

A kinematic model describing the precessional motion of the jets has been developed by Hjellming and Johnston in 1981 [20]. It is summarized in table 2.1.

As illustrated in figure 2.5, this model suggests that the two oppositely directed jets precess with a precessional period P_{prec} tracing a precession cone with an half opening an-

Table 2.1: The five-parameter kinematic model of the jet in SS 433

The matter moves in two exactly oppositely aligned jets with constant relativistic velocity $\beta = 0.2601$, where β is the velocity of the jet in units of speed of light c.
Each jet changes direction with the velocity vector moving on the surface of a cone with an opening angle $\theta = 19.85°$. This is half of the opening angle of the precession cone traced out by the jet.
The period of this precessional motion or period is $P_{\rm prec} = 162.532$ days. For brevity, we refer to it as 163 days throughout.
The angle between the cone of symmetry axis and the line of sight is $i = 78.83°$. This is the inclination angle of the precessional axis.
The time at which the precessional phase $\Psi(t)$ equals zero is the precession time $t_{\rm prec}$, which equals to MJD 43561.87.

gle θ. The axis (precessional axis) of the precession cone has an inclination angle i. There are two instants during a precessional period when the jets of SS 433 are perpendicular to the line of sight.

2.3 SS 433: A neutron star or black hole candidate?

With the spectroscopic binary star system, if the period of the binary system is not prohibitively long and if the orbital motion has components along the line of sight, a periodic shift in the spectral lines will be observed. Assuming that the luminosities of each component are comparable, both spectra will be observed. However, if one star is much more luminous than the other, then the spectrum of the less luminous companion will be over-

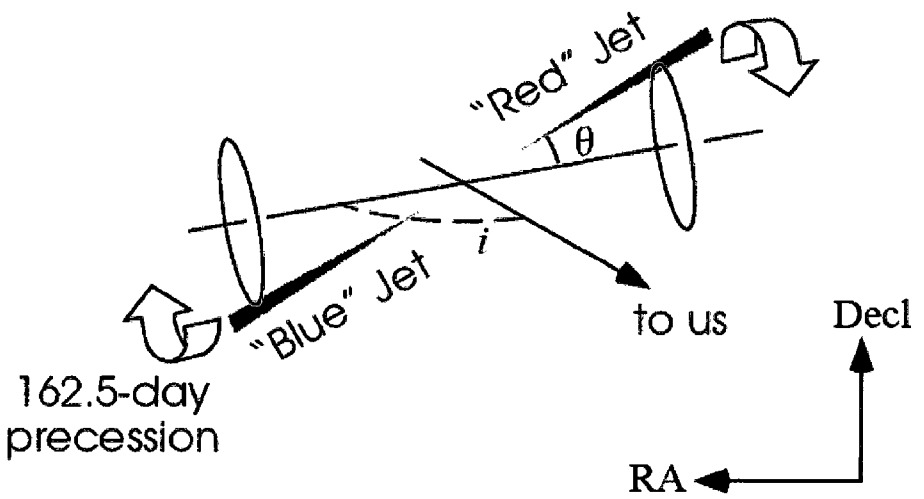

Figure 2.5: The precession geometry of SS 433 [23].

whelmed and only a single set of periodic lines will be seen. Such a system is referred to as a single-line spectroscopic binary. SS 433 is a single-line spectroscopic binary.

The mass function provides a theoretical estimate of the masses of individual stars in a spectroscopic binary star system. It is obtained assuming some very simple physics and geometry. Theoretically, it requires Kepler's Third Law and the definition of center of mass of a system, while observationally, it requires the measurement of the binary's period, and how fast the stars move about the center of mass. From the literature [6], one can then easily deduce that the mass function equation of the semidetached binary SS 433 is equal to

$$F = \frac{M_c^3}{(M_x + M_c)^2} = \frac{{K_{\text{obs}}}^3 P_{\text{obs}}}{2\pi G (\sin i)^3} \tag{2.3}$$

where M_x is the mass of the compact object or the primary star, presumably a black hole or a neutron star and M_c is the mass of its companion star, *i.e.* the normal massive star or the secondary, and i is the angle between the line of sight and the normal of the orbital

plane. As defined in the kinematic model shown in figure 2.5 and table 2.1, $i = 78.83°$. $P_{\rm obs}$ is the orbital period and $K_{\rm obs}$ is the observed velocity. Finally, G is the gravitational constant.

As previously mentioned, in SS 433 one component in the spectroscopic binary is so faint that its spectral lines cannot be observed; only $P_{\rm obs}$, $K_{\rm obs}$ and i are observed. Consequently, only the expression on the right-hand of the mass function (2.3) can be evaluated, but neither the individual masses of the components nor the total mass can be determined. As a result, the mass function is useful only if an estimate of the mass of at least one component of the system already exists by some indirect means.

The period in SS 433 is given by the stationary lines, such as the He II λ4686 line modulation. They are found, as the name implies, at their rest wavelengths. Usually, their strength is typically three times higher than the one of the corresponding moving lines. In the SS 433, all the stationary lines show periodic modulation, with a period $P_{\rm obs}$ close to 13.1 days.

Several values of He II λ4686 line Doppler modulation have been proposed from observations of optical stationary lines. Crampton and Hutchings (1981) [10] obtained $K_{\rm obs} = 195$km/s, and Fabrika and Bychkova (1990) [14] reported $K_{\rm obs} = 175$km/s, and D'Odorico et al. (1991) [33] derived $K_{\rm obs} = 112$km/s. These values are inconsistent with each other, and bring considerable uncertainties in mass determination. In this thesis, the value of $K_{\rm obs} = 195$ Km/s and $K_{\rm obs} = 112$ Km/s are adopted as the upper and lower limit of Doppler modulation. Putting all the just above-mentioned values into (2.3), one can

get (when using the observed orbital period $P_{\rm obs} = 13.1$ days)

$$F = \frac{M_c^3}{(M_x + M_c)^2} = \frac{M_x}{q(1+q)^2} = \frac{M_c}{(1+q)^2} = 10.6\ M_\odot\ (2.0\ M_\odot) \tag{2.4}$$

where $M_\odot$ is the mass of the Sun and q is the mass ratio $\frac{M_x}{M_c}$ of the stars. The value in brackets corresponds to the lowest value of K found, which is 112 km/s. Thus the resultant upper and lower limit of mass function are 10.6 $M_\odot$ and 2.0 $M_\odot$, respectively.

In order to obtain an estimation of the mass ratio q, the mass eclipses of the system components can provide the additional information needed. Different geometric model of the eclipse for binary system has been developed overtime. Altogether they are trying to fit several parameters simultaneously, in which the main outcome is trying to determine the system dimensions and mass ratio q. Once the mass ratio found, (2.4) could be used in order determine the individual mass of both stars. Several results have been published, all presenting different conclusions in term of individual mass of both stars. These examples can be summarized as follows.

- Zwitter and Calvani (1989) [37] have developed a very complex geometric model. They have then concluded that the compact object is a black hole with a mass of 10 $M_\odot$.

- D'Odorico et al. (1991) [33] derived a light compact object $M_x = 0.8\ M_\odot$ from the small Doppler modulation $K = 112$ km/s and the small mass ratio $q = 0.245$, and argued that this is evidence for a neutron star.

- Kotani et al. (1998) [23] obtained the mass ratio $q = 0.22$. Together with mass function, the masses of the compact system obtained were $M_x = 0.68\ M_\odot$ using

$K = 112$ km/s and $M_x = 3.6\ M_\odot$ using $K = 195$ km/s. Consequently, if the first value is adopted, the mass of the compact object would be below the standard mass of a neutron star of $M_{ns} = 1.4\ M_\odot$, while the second result obtained suggests that the system would be a massive binary, and that the compact object might be a black hole.

As we can see from above, there are some great uncertainties around the values of the mass ratio q and the line Doppler modulation $K_{\rm obs}$. It is now easy to understand in this context why it is so difficult to precisely determine M_x from the optical observation. Only improving the technique of measurement and improving the current model of the binary system will help us to unravel the puzzle.

However, it seems that the literature has recently revealed more evidence that the compact object in SS433 is a neutron star rather than a black hole. We will adopt this result for the rest of this work.

Chapter 3

Neutron Stars and their Magnetic Fields

3.1 Overall picture of the neutron star

In 1931 Chandrasekhar [8] showed that as a white dwarf, which is the last stage of evolution for all stars with less than 4 times the mass of the sun [6] and is in an equilibrium state between the force of gravity pulling inward, and the pressure from degenerate electrons pushing outward, became more massive, and the electrons that supported its weight became relativistic, there would be a point beyond which the degeneracy pressure would be insufficient to support the star. This mass is approximately 1.44 times the mass of the sun and is known as the "Chandrasekhar limit" ($M_{\rm Ch} = 1.44 M_{\odot}$). A little bit later, i.e. in 1934, Baade and Zwicky [3] proposed the existence of the neutron star, only two years after Chadwick's discovery of the neutron in 1932 [7]. In 1939, Oppenheimer and Volkoff [31] were the first to discuss the neutron star in the framework of general relativity.

The result is a condensed sphere of matter about 20 km across (or $R_{\rm ns} = 10^6$ cm), with a surface gravitational field approximately 2×10^{11} times stronger than that of Earth's. The density of a neutron star is so great that the protons and electrons making up the atoms fuse to form electrically neutral neutrons, the primary particles making up the neutron star ($\approx 10^{57}$ neutrons for a $1.4 M_\odot$ neutron star). Because they are electrically neutral, such particles can be packed very closely together, resulting in a celestial object with similar density to that of the atomic nucleus, i.e. $\approx 6.65 \times 10^{14}$ g/cm^3.

Chandrasekhar (1939) [9] was also the first to determine mass-radius relation of white dwarfs and the neutron stars. This latter may be found by setting the estimate of the central pressure, equal to the neutron degeneracy [6]. One can show that this relation is

$$R_{\rm ns} \approx \frac{(18\pi)^{2/3}}{10} \frac{\hbar^2}{G M_{\rm ns}^{1/3}} \left(\frac{1}{m_{\rm H}} \right)^{8/3} \tag{3.1}$$

where $m_{\rm H}$ is the mass of a hydrogen atom. The most important implication of (3.1) is that $M_{\rm ns} R_{\rm ns}^3 =$ constant, or

$$M_{\rm ns} V_{\rm ns} = \text{constant} \tag{3.2}$$

when assuming spherical symmetry. Consequently, the volume of a neutron star is inversely proportional to its mass; so more massive neutrons stars are actually smaller. The mass-volume relation is a result of the star deriving its support from neutron degeneracy pressure. The neutron star becomes smaller and denser with increasing mass.

According to the mass-volume relation (3.2), piling more and more mass onto a neutron star would eventually result in shrinking the star down to zero volume as its mass become infinite. However, if the neutron star exceeds a certain critical mass, there is a departure from this relation because there is a point beyond which neutron degeneracy pressure can

no longer support the star since the neutrons become relativistic. With the support of general relativity theory, one can show that the maximum mass possible for a neutron star cannot exceed about 3 $M_\odot$ [31]. This is less certain than the corresponding limit for white dwarf because the equation of state for a neutron matter is less well known. Over this limit, it will simply collapse and become a black hole.

If we assume that a typical neutron star is a rotating uniform sphere with a radius $R_{\rm ns} = 10^6$ cm and $M_{\rm ns} = 1.4M_\odot$, its moment of inertia, approximately given by $I_{\rm ns} = \frac{2}{5}M_{\rm ns}R_{\rm ns}^2$, is in the order of magnitude of 10^{45} g cm^2.

It is also anticipated that a neutron star must rotate very rapidly. Since it resulted of the sudden collapse of a relatively slowly rotating core of a supergiant star or white dwarf, conservation of the angular momentum of the collapsing core gives

$$I_f\Omega_f = I_i\Omega_i \ . \tag{3.3}$$

Using the above-defined moment of inertia and assuming that no mass will be lost during the collapsing process, i.e. $M_f = M_i$, (3.3) becomes

$$\Omega_f = \Omega_i \left(\frac{R_i}{R_f}\right)^2 \ or \ P_f = P_i \left(\frac{R_f}{R_i}\right)^2 \tag{3.4}$$

when written in terms of the rotation periods $P = 2\pi/\Omega$ as well.

From [6], one can estimate the ratio of the radii in 3.4 from Chandrasekhar's model to be

$$\frac{R_i}{R_f} = \frac{R_{\rm wd}}{R_{\rm ns}} \approx \frac{m_n}{m_e}\left(\frac{Z}{A}\right)^{5/3} \ . \tag{3.5}$$

where Z is the atomic number that denotes the number of protons in a nucleus. A is the

total number of protons and neutrons (together known as nucleons) in an atomic nucleus.

If we set $Z/A = 26/56$ for iron for the white dwarf in (3.5), the above-approximated ratio of the radii is around 512. If we now take the rotation period observed for the white dwarf 40 Eridani B, as $P_{\rm wd} = 1350$ s [6], and the just obtained approximated ratio of the radii, one can find that the resulting collapsed "neutron star" will be rotating very rapidly when they are formed, with rotation periods P_f on the order of a few milliseconds, e.g. 5.2 ms in the example above. In fact, the key observational confirms that neutron stars have period in the range 1.6 ms (PSR 1937+214) to 4.3 s (PSR 1845-19). Moreover, the enormous angular momentum of a rapidly rotating compact star would guarantee its precise clocklike behavior. Some pulsar periods have been measured to 13 significant digits, a measurement that challenges the accuracy of the best atomic clock.

3.2 Extremely strong magnetic fields

Another exotic property that can be predicted for neutron stars is that they should have extremely strong magnetic field, due to the conservation of the magnetic flux through the surface of a white dwarf as it collapses to form a neutron star. The flux of the magnetic field through a surface S is defined by the surface integral as follow

$$\Phi \equiv \int_S \mathbf{B} \cdot d\mathbf{A} \tag{3.6}$$

where $\mathbf{B}$ is the magnetic field vector. We could approximately say that the product of magnetic field strength and the area of the star's surface remain constant. Thus

$$B_f \, 4\pi R_f^2 = B_i \, 4\pi R_i^2 \;\Rightarrow\; B_f = B_i \left(\frac{R_i}{R_f}\right)^2 . \tag{3.7}$$

A typical white dwarf magnetic field is around $B \approx 10$ T (Tesla); the largest observed one is around $B \approx 5 \times 10^4$ T (huge compared with the Sun's global 2×10^{-4} T field). Using $\frac{R_{\rm wd}}{R_{\rm ns}} \approx 512$, the magnetic field of the neutron star $B_{\rm ns}$ would be between 10^6 T and 10^{10} T, which is compatible with observations [19].

The theoretical upper limit to the neutron star magnetic field strength is estimated by considering field strengths approaching the maximum "virial" value, i.e. obtained by setting a magnetic energy of the neutron star $\left(\frac{4\pi R_{\rm ns}^3}{3}\right)\left(\frac{B_{\rm max}^2}{8\pi}\right)$ less than its gravitational binding energy $\left(\frac{GM_{\rm ns}^2}{R_{\rm ns}}\right)$; this gives

$$B_{\rm max} < \sqrt{6G}\,\frac{M_{\rm ns}}{R_{\rm ns}^2}\,. \tag{3.8}$$

For a typical neutron star of $M_{\rm ns} = 1.4M_\odot$ and $R_{\rm ns} = 10^6$ cm, one finds that $B_{\rm max} \approx 10^{14}$ T [25].

3.3 Magnetic dipole model for rotating neutron stars

Rotating neutron stars or *pulsars* whose spin periods P (or spin frequencies $\Omega = 2\pi/P$) are observed to increase (decrease) with time are thought to lose rotational kinetic energy due to magnetic dipole braking. From the literature [35], one can find that the rate at which the star loses energy as it slows down can be found by taking a time derivative of the available rotational kinetic energy ($E = \frac{1}{2}I_{\rm ns}\Omega^2 = 2\pi^2 I_{\rm ns}P^{-2}$), which gives

$$\dot{E} = I_{\rm ns}\Omega\dot{\Omega} = -4\pi^2 I_{\rm ns}\,\frac{\dot{P}}{P^3} \tag{3.9}$$

where $I_{\rm ns}$ is the stars moment of inertia and $\dot{P}$ is the rate at which the period increases with time. The quantity $\dot{E}$ is referred to as the "spin-down luminosity" of the star. If we assume

that a neutron star is spherical with $M_{\rm ns} = 1.4M_{\odot}$, $R_{\rm ns} = 10^6$ cm and $I_{\rm ns} = 1.1 \times 10^{45}$ g cm^2 and inserting the period $P = 0.0333$ s and the period derivative $\dot{P} = 4.21 \times 10^{-13}$ for the Crab pulsar, then the rotational kinetic energy E and its time derivative $\dot{E}$ found in (3.9) give 2×10^{49} erg and -5×10^{38} erg/s respectively. Remarkably, this is the observed energy output of the Crab Nebula.

In general, this slowdown is caused by the loss of energy as magnetic dipole radiation [35]. The power radiated by a rotating magnetic dipole is given by

$$\dot{E} = -\frac{2}{3c^3} |\ddot{\mathbf{m}}|^2 = -\frac{B_s^2 R_{ns}^6 \Omega^4 \sin^2 \alpha}{6c^3} \tag{3.10}$$

where the dipole magnetic moment is given by $\dot{\mathbf{m}} = \frac{1}{2}\mu(-\mathbf{e}_{\perp}\Omega \sin\alpha \sin\Omega t + \mathbf{e}'_{\perp}\Omega \sin\alpha \cos\Omega t)$, for a dipole moment $\mu = B_s R_{ns}^3$, c is the speed of light in the vacuum and α is the angle between the rotation and magnetic axes, as shown in figure 3.1.

Following [35] and [19] and making the assumption that all of the observed pulsars spin-down luminosity is due to the magnetic dipole radiation, setting equations (3.9) and (3.10) equal to each other results in an expression for the stars surface magnetic field strength of

$$B_s = \left(\frac{3 I_{\rm ns} c^3 P \dot{P}}{2\pi^2 R_{ns}^6 \sin^2 \alpha} \right)^{1/2} . \tag{3.11}$$

Assuming $\alpha = 90^{\rm o}$, i.e. being at a neutron stars' magnetic pole and using the usual values for a standard neutron star (e.g. $I_{\rm ns} \approx 10^{45}$ g cm^2, etc.), B_s becomes 6.7×10^{15} $(P\dot{P})^{1/2}$ T/s$^{1/2}$, where $\dot{P}$ is in units of s s^{-1} and P is in units of second. This gives about 2×10^8 T for nominal parameters ($P \approx 1$ s; $\dot{P} \approx 10^{-15}$).

Inserting the period $P = 0.0333$ s and the period derivative $\dot{P} = 4.21 \times 10^{-13}$ for the

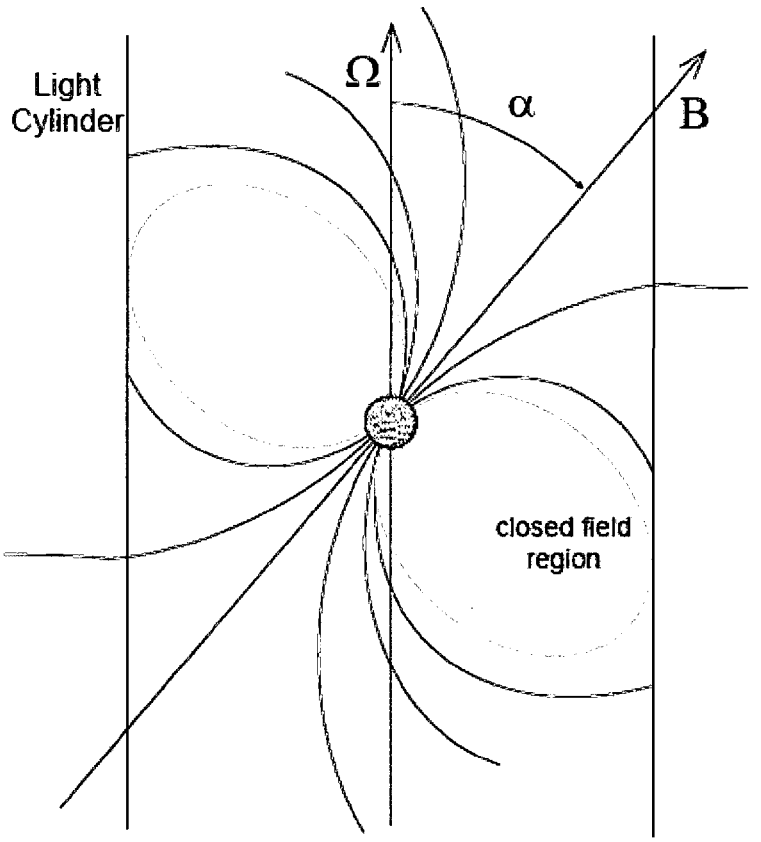

Figure 3.1: Rotating dipole model [35].

Crab pulsar, B_s is about 8 $\times$ 10^8 T. The periods and period derivatives of the various types of isolated pulsars are shown in the P and $\dot{P}$ diagram of figure 3.2. As one can see, these results agree with the range of the magnetic fields between 10^6 T and 10^{10} T, with a maximum of 10^{14} T previously estimated.

It is obvious that the external dipole field of the neutron star will decrease as the cube of the distance, giving

$$B(r) = B_s \left(\frac{R_{\rm ns}}{r}\right)^3 . \tag{3.12}$$

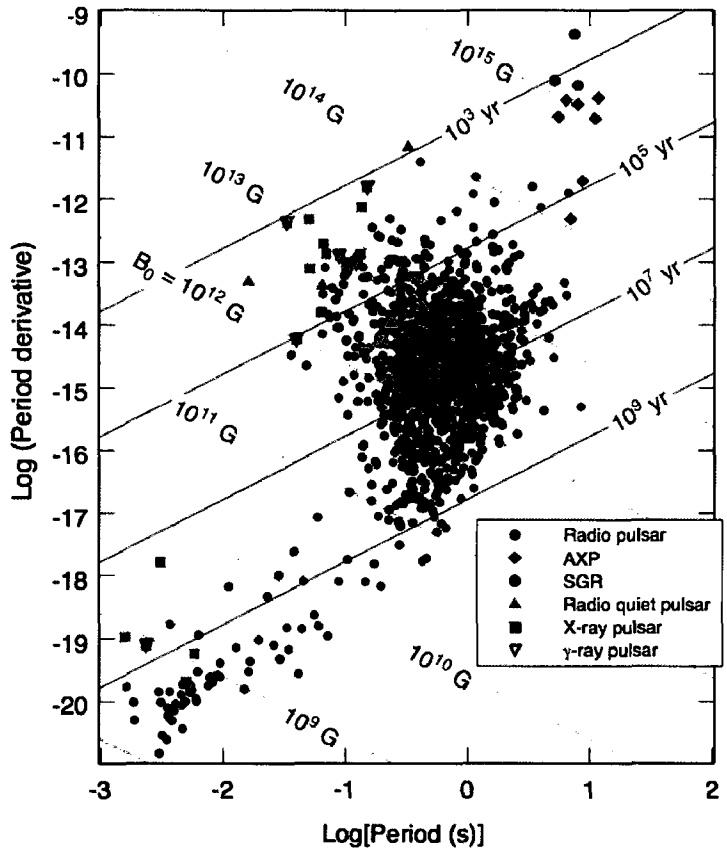

Figure 3.2: Plot of period derivative $\dot{P}$ versus the period P for the presently known rotation pulsars. (Green) lines of constant B_s found in (3.11) and (violet) lines of constant characteristic age of pulsars are illustrated as well [19].

This impact of the radial dependence of the magnetic dipole field will be explored in the next sections of this research topic. The magnetic field of a neutron star is sketched in figure 3.3.

Figure 3.3: Resulting magnetic fields of a neutron star [2].

Part II

Survey of the Landau States

Chapter 4

Landau States in Constant Magnetic Fields

Here come the Landau States! Landau states are the quantum analog of cyclotron motion: they are quantized in 2-D, but the charged particles are free to move along the direction of the **B** *field. As we will see in this chapter, they normally become important in some environments with extremely strong magnetic fields, such as previously discovered in neutron stars' sections 3.2 and 3.3.*

4.1 Non-Relativistic Solutions

Based upon a "differential approach" to classical mechanics [36], the Lagrangian is

$$L = T - V \tag{4.1}$$

where T and V are respectively the kinetic and potential energies. Since the force and the potential energy are related as follows

$$\mathbf{F} = -\nabla V \tag{4.2}$$

one can derive the Lagrangian for a charge q in an electromagnetic field. It suffices to start from the Lorentz equation, which gives the force applied on a charge when it is moving with velocity $\mathbf{v}$ in an electromagnetic field

$$\mathbf{F} = q\,(\mathbf{E} + \mathbf{v} \times \mathbf{B}) \tag{4.3}$$

and rewrite (4.3) in terms of the vector and scalar potentials $\mathbf{A}$ and ϕ rather than $\mathbf{E}$ and $\mathbf{B}$, i.e. using $\mathbf{E} = -\nabla\phi - \partial\mathbf{A}/\partial t$ and $\mathbf{B} = \nabla \times \mathbf{A}$. A bit of algebra then gives

$$V = q\phi - q\mathbf{A} \cdot \mathbf{v} \tag{4.4}$$

which is the potential energy of the interaction between a charge and the electromagnetic field. The Lagrangian (4.1) then becomes

$$L = T - q\phi + q\mathbf{A} \cdot \mathbf{v}\ . \tag{4.5}$$

In the Hamiltonian formalism, the generalized coordinates and momenta are used. The momenta are obtained from the Lagrangian by the equation $\mathbf{p_i} = \partial L/\partial \dot{\mathbf{q}}_\mathbf{i}$ and the Hamiltonian is

$$H = \sum_i \dot{\mathbf{q}}_\mathbf{i} \cdot \mathbf{p_i} - L = \sum_i \dot{\mathbf{q}}_\mathbf{i} \cdot \frac{\partial L}{\partial \dot{\mathbf{q}}_\mathbf{i}} - L\ . \tag{4.6}$$

In the non-relativistic limit ($v \ll c$), the kinetic energy T is $1/2\ mv^2$. Inserting T into (4.5) and using the resulting Lagrangian in (4.6), the non-relativistic Hamiltonian for a charged particle in an electromagnetic field is given by the following equation

$$H = \frac{1}{2m}(\mathbf{p} - q\mathbf{A})^2 + q\phi - \mu_\mathrm{s} \cdot \mathbf{B} \tag{4.7}$$

where $\mathbf{p} - q\mathbf{A}$ is the canonical momenta. The last term added in (4.7) represents the magnetic moment associated to the spin of a charged particle when interacting with a magnetic field. Here $\mu_\mathrm{s} = g\ \mu_\mathrm{B}\ \mathbf{S}/\hbar$, where $\mathbf{S}$ is the spin angular momentum of the particle, μ_B is

known as the Bohr magneton and has a value of $q\hbar/2m$ and g is the gyro-magnetic ratio that characterizes the particle. The constant g is very close to 2 for the electron, for the proton, g is 2.79.

To solve (4.7), we take the uniform magnetic field to be in the z-direction. Let us first use the following symmetric gauge for the vector potential

$$\mathbf{A} = -\frac{1}{2}\,\mathbf{r}\times\mathbf{B} = \frac{1}{2}B_z(-y,x,0),\ \phi = 0\ . \tag{4.8}$$

One can easily check the symmetric gauge (4.8) gives 1) $\mathbf{B} = \nabla\times\mathbf{A} = (0,0,B_z)$, i.e. an uniform magnetic field parallel to the z-axis, and 2) $\nabla\cdot\mathbf{A} = 0$, i.e. which constrains itself to the Coulomb gauge. Inserting the symmetric gauge (4.8) in the non-relativistic Hamiltonian (4.7) gives

$$H = \frac{1}{2m}\left(\left[p_x + \frac{qB_z y}{2}\right]^2 + \left[p_y - \frac{qB_z x}{2}\right]^2 + [p_z]^2\right) - \mu_s\cdot B_z\ . \tag{4.9}$$

Using the above-mentioned definition of μ_s and performing a bit of algebra then gives the Hamiltonian

$$H = \frac{1}{2m}\left(p_z^2\right) + \frac{1}{2m}\left(p_x^2 + p_y^2\right) + \frac{1}{8}m\omega_c^2\left(x^2+y^2\right) - \frac{1}{2}\hbar\omega_c(L_z + gS_z) \tag{4.10}$$

where the cyclotron frequency is $\omega_c = qB_z/m$, the angular momentum along $\mathbf{B}$ (in units of $\hbar$) is $L_z = \left(xp_y - yp_x\right)/\hbar$ and the spin angular momentum along $\mathbf{B}$ (in units of $\hbar$) is $S_z = \mathbf{S}/\hbar$.

The first kinetic-energy term in (4.10) corresponds to free, linear motion parallel to the z axis. The quadratic terms represent an isotropic two-dimensional harmonic oscillator of frequency $1/2\ \omega_c$. The linear term is a combined consequence of the orbital and rotational

angular momenta operators.

Now let us compare the magnitude of the linear and quadratic terms in (4.10) for an atom. We could say that $L_z + gS_z$ will be of order $\hbar$ and $\sqrt{(x^2+y^2)} \approx a_o = 0.53 \text{ x } 10^{-10}$ m, i.e. to be the order of the Bohr radius. Therefore, the ratio of the quadratic to linear terms will be approximatively

$$\frac{e^2B^2a_o^2/8m}{eB\hbar/2m} = \frac{eBa_o^2}{4\hbar} = \frac{(1.6 \text{ x } 10^{-19} \text{ C}) \ (0.53 \text{ x } 10^{-10} \text{ m})^2}{4 \ (1.05 \text{ x } 10^{-34} \text{ J s})} B \approx \frac{B\,(Tesla)}{10^6} \quad (4.11)$$

The quadratic term in (4.10), which is at the origin of the Landau states, becomes important when the magnetic field is very strong: in particular neutron stars (recall sections 3.2 and 3.3) could have fields in the range between 10^6 T and 10^{14} T.

The other condition under while the quadratic term becomes important is when its (x^2+y^2) term is of macroscopic size. This happens for the motion of an electron in a synchrotron. Here both the radius of the orbit and L_z are huge on an atomic scale.

We can observe that the coordinate z is missing from the Hamiltonian (4.10). It follows that $[p_z, H] = 0$, so that we can construct a function that is an eigenfunction of p_z, where we can write the eigenvalue of p_z as $\hbar k_z$, with an eigenenergy given by $E_z = \hbar^2 k_z^2/2m$. Clearly (4.10) commutes with L_z and S_z as well, so their eigenenergies are $1/2 \ \hbar\omega_c \ m_\ell$ and $1/2 \ \hbar\omega_c \ g m_s$ respectively. Put these considerations all together, the related eigenfunction then takes the form

$$\psi(x,y,z) = u(x) \ v(y) \ e^{ik_z z} \quad (4.12)$$

where $u(x)$ and $v(y)$ are some solutions of the time-independent Schrödinger equation

$H\ \psi(x,y,z) = E\ \psi(x,y,z)$, which becomes now

$$\left[\frac{p_{\rm x}^2}{2m} + \frac{1}{8}m\omega_{\rm c}^2 x^2 + \frac{p_{\rm y}^2}{2m} + \frac{1}{8}m\omega_{\rm c}^2 y^2\right] u(x)v(y) = \left(E - \frac{\hbar^2 k_{\rm z}^2}{2m} + \frac{1}{2}\hbar\omega_{\rm c}(m_\ell + g m_{\rm s})\right) u(x)v(y)$$
$$= (E_{\rm x} + E_{\rm y})\ u(x)\ v(y). \qquad (4.13)$$

The Schrödinger equation (4.13) is the same as that for an isotropic two-dimensional harmonic oscillator constrained to move along the x and y axis, with natural frequencies $1/2\ \omega_{\rm c}$. From the literature [36] or [26], one can find that the eigenenergies of this type of equation are

$$E_{n_\perp, m_\ell, m_{\rm s}} = \frac{1}{2}\ \hbar\omega_{\rm c}\ (n_\perp + 1 - m_\ell - g m_{\rm s}) + \frac{\hbar^2\ k_{\rm z}^2}{2m} \qquad (4.14)$$

where $n_\perp = n_{\rm x} + n_{\rm y}$. The energy levels (4.14) are commonly referred to as *Landau levels* or *Landau states*. Together with (4.12), the form of eigenfunctions $u(x)$ and $v(y)$ corresponding to the eigenenergy (4.14) gives the wavefunction

$$\psi_{n_{\rm x}, n_{\rm y}}(x,y,z) = \left(\frac{m\omega_{\rm c}}{2\hbar\pi}\right)^{1/2} \frac{1}{\sqrt{2^{n_{\rm x}} n_{\rm x}!}}\ \frac{1}{\sqrt{2^{n_{\rm y}} n_{\rm y}!}}\ H_{n_{\rm x}}\left(\sqrt{\frac{m\omega_{\rm c}}{2\hbar}}x\right)\ H_{n_{\rm y}}\left(\sqrt{\frac{m\omega_{\rm c}}{2\hbar}}y\right)\ e^{-\frac{m\omega_{\rm c}}{4\hbar}(x^2+y^2)\ +\ ik_z z} \qquad (4.15)$$

where the n-th order Hermite polynomials are written $H_{n_{\rm x}}$ and $H_{n_{\rm y}}$.

.

When (4.10) is solved instead in cylindrical coordinates with $\rho^2 = x^2 + y^2$ [15], one can find with a much harder calculation than the resulting non-normalized wavefunction takes the following form in the symmetric gauge

$$\psi_{n_r, m_\ell, k_z}(\rho, \phi, z) = \left(\sqrt{\frac{m\omega_{\rm c}}{2\hbar}}\rho\right)^{|m_\ell|} \left[L_{n_r}^{|m_\ell|}\left(\frac{m\omega_{\rm c}}{2\hbar}\rho^2\right)\right]\ e^{-\left(\frac{m\omega_{\rm c}}{4\hbar}\rho^2\right)\ +\ i(k_z z\ +\ m_\ell\phi)} \qquad (4.16)$$

where $L_{n_r}^{|m_\ell|}$ is the associated Laguerre polynomial: its general form can be found in any book dealing with special functions [43]. The principal quantum number $n_r = 0, 1, 2, 3, \ldots$. The associated energy eigenvalues are

$$E_{n_r, m_\ell, m_{\rm s}, k_z} = \frac{1}{2}\hbar\omega_{\rm c}\ (2n_r + 1 + |m_\ell| + m_\ell - \ g m_{\rm s}) + \frac{\hbar^2\ k_{\rm z}^2}{2m} \qquad (4.17)$$

where the spin effect has been reintroduced in (4.17). A simple look can quickly confirm that the above-found wavefunctions (4.15) and (4.16) and associated energy eigenvalues (4.14) and (4.17) have the same form.

Let us now use the following asymmetric gauge for the vector potential, called the *Landau Gauge*, for solving (4.7)

$$\mathbf{A} = B_z\ (-y, 0, 0),\ \phi = 0\ . \tag{4.18}$$

One can still easily check the *Landau Gauge* (4.18) gives 1) $\mathbf{B} = \nabla \times \mathbf{A} = (0, 0, B_z)$, i.e. an uniform magnetic field parallel to the z-axis, and 2) $\nabla \cdot \mathbf{A} = 0$, i.e. which satisfies the Coulomb gauge condition. Inserting the *Landau Gauge* (4.18) in the non-relativistic Hamiltonian (4.7) and putting the result into the time-independent Schrödinger equation $H\ \psi(x, y, z) = E\ \psi(x, y, z)$, give

$$\left[\frac{1}{2m}\left([p_x + qB_z y]^2 + [p_y]^2 + [p_z]^2\right) - \mu_s \cdot B_z\right] \psi(x, y, z) = E\ \psi(x, y, z)\ . \tag{4.19}$$

Now, if we put $p_x = -i\hbar\ \partial/\partial x$; $p_y = -i\hbar\ \partial/\partial y$, $p_z = -i\hbar\ \partial/\partial z$ and $p_x^2 = -\hbar^2\ \partial^2/\partial x^2$, $p_y^2 = -\hbar^2\ \partial^2/\partial y^2$, $p_z^2 = -\hbar^2\ \partial^2/\partial z^2$ into (4.19) and we reuse the above-mentioned definition of μ_s, it becomes

$$-\frac{\hbar^2}{2m}\left[\left(\frac{\partial^2}{\partial x^2} + \frac{2iqB_z y}{\hbar}\frac{\partial}{\partial x} - \frac{q^2 B_z^2 y^2}{\hbar^2}\right) + \frac{\partial^2}{\partial y^2} + \frac{\partial^2}{\partial z^2}\right] \psi(x, y, z) = \left(E + g\ \frac{q\hbar}{2m}\ S_z\right)\ \psi(x, y, z) \tag{4.20}$$

This time both the coordinates x and z are missing from from the Schrödinger equation (4.19). It follows that $[p_x, H] = [p_z, H] = 0$, so that we can construct a function that is an eigenfunction of p_x and p_z, where we can write their eigenvalues as $\hbar k_x$ and $\hbar k_z$. The related eigenfunction appears then as

$$\psi(x, y, z) = u(y)\ e^{ik_x x + ik_z z}. \tag{4.21}$$

Substituting (4.21) into (4.20) and taking into account once again that (4.19) commutes with S_z, so its eigenenergy is still $1/2\ \hbar\omega_c\ gm_s$, this gives

$$\frac{\partial^2 u(y)}{\partial y^2} + \left[-\frac{q^2 B_z^2}{\hbar^2}\left(y + \frac{\hbar k_x}{qB_z}\right)^2 + \left(\frac{2mE}{\hbar^2} - k_z^2 + \frac{qB_z}{\hbar}\, gm_s\right)\right] u(y) = 0. \tag{4.22}$$

Then if we define the following new parameters

$$\xi = \sqrt{\frac{qB_z}{\hbar}}\left(y + \frac{\hbar k_x}{qB_z}\right) \quad \Rightarrow \quad \frac{\partial^2}{\partial y^2} = \frac{qB_z}{\hbar}\,\frac{\partial^2}{\partial \xi^2} \tag{4.23}$$

We can rewrite (4.22) as

$$\frac{\partial^2 u(\xi)}{\partial \xi^2} + \left[-\xi^2 + \frac{\hbar}{qB_z}\left(\frac{2mE}{\hbar^2} - k_z^2 + \frac{qB_z}{\hbar}\, gm_s\right)\right] u(\xi) = 0 \tag{4.24}$$

Comparing (4.24) with the Schrödinger equation given by the Simple Harmonic Oscillator (SHO) [15] one deduces that

$$\epsilon = \frac{\hbar}{qB_z}\left(\frac{2mE_n}{\hbar^2} - k_z^2 + \frac{qB_z}{\hbar}\, gm_s\right) = 2n + 1 \tag{4.25}$$

i.e. the resulting eigenenergy is

$$E_n = \frac{1}{2}\hbar\omega_c\,(2n + 1 - gm_s) + \frac{\hbar^2 k_z^2}{2m} = \hbar\omega_c\left(n + \frac{1}{2} - \frac{gm_s}{2}\right) + \frac{\hbar^2 k_z^2}{2m} \tag{4.26}$$

where the previously defined cyclotron frequency has been reintroduced above. We are now quite familiar with the shape of the eigenenergy (recall (4.14) and (4.17)). The particle energy is quantized in the x-y plane, with the Landau energies characterized by the quantum number n as before, as well as the translational energy $\hbar^2 k_z^2/2m$ along the magnetic field. The corresponding wave function is the Simple Harmonic Oscillator (SHO) solution, as before: it can be written in terms of the cyclotron frequency,

$$\psi_n(x, y, z) = \left(\frac{m\omega_c}{\hbar\pi}\right)^{1/4} \frac{1}{\sqrt{2^n n!}} H_n\left(\sqrt{\frac{m\omega_c}{\hbar}}\,(y - y_0)\right) e^{-\frac{m\omega_c}{2\hbar}(y-y_0)^2}\, e^{ik_x x + ik_z z} \tag{4.27}$$

where the centre is at $y_0 = -\hbar k_x/qB_z$ and the n-th order Hermite polynomials are written H_n.

In the corresponding classical motion the charged particle moves in a helix of constant radius, energy, rotational frequency and z velocity. As illustrated in figure 4.1, the projection of the motion onto the x-y plane is a circle with a fixed center.

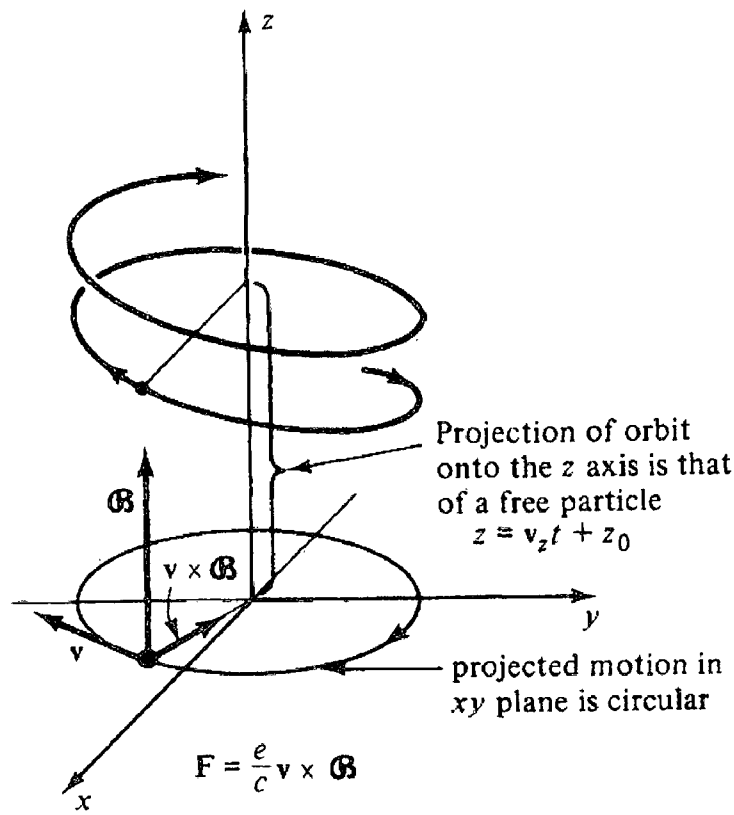

Figure 4.1: Classical Helical Motion of a positive charge in an uniform, constant magnetic field that points in the z direction [26].

In the present work, the one-dimensional Schrödinger equation (4.22) was solved ana-

lytically, via a java application written by the author that uses the Numerov method for converting the differential equation into a difference equation for the values of the wave function on each grid point. We can then observe in figure 4.2, in natural units, i.e. the numerical values of $\hbar$, m, q and ω are all equal to 1, the effect of varying the number of nodes n on the Schrödinger equation (4.22), when the Landau Gauge (4.18) and the parameters $B_z = 1$ and $k_x = 1$ have been used. We can see in figure 4.2 that the energy levels and the wave functions follow (4.26) and (4.27) respectively, as expected.

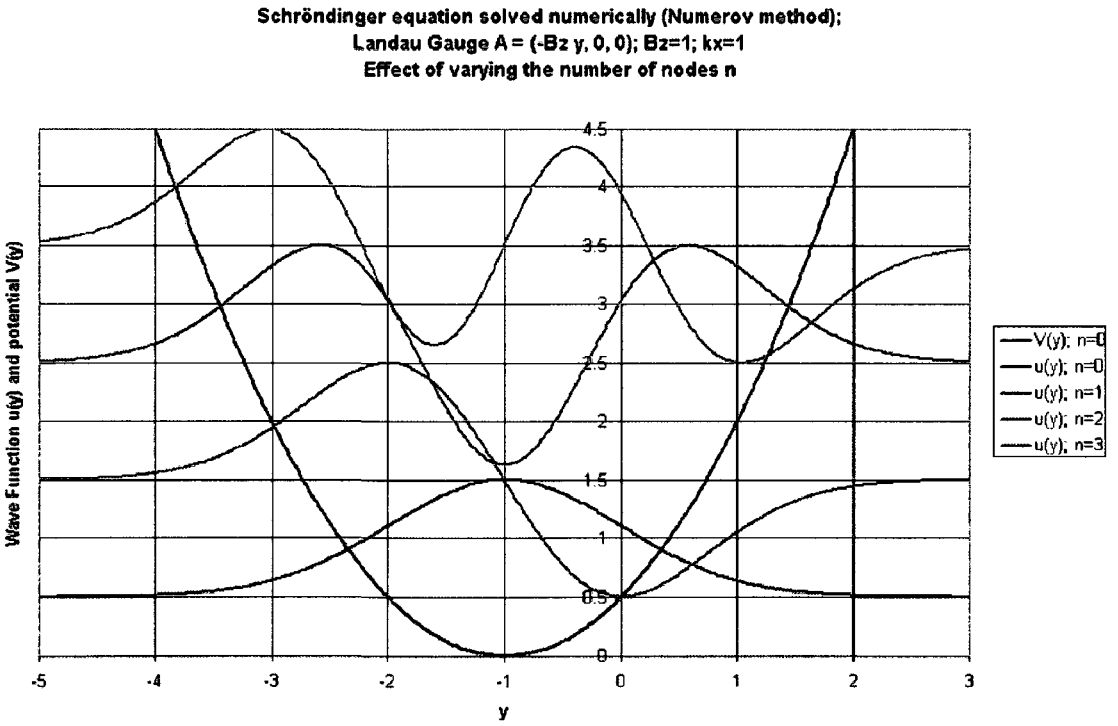

Figure 4.2: Effect of varying the number of nodes n in the Schrödinger equation, when the Landau Gauge is applied.

4.2 Relativistic Solutions

The derivation of the relativistic Landau states was first preformed by Johnson-Lippmann [21]: it is fairly complex and since it crucial for this work, we re-derive it below.

Hamilton's principle [40] states that the motion of a body (its trajectory and velocity at each instant) can be found by minimizing the action functional S

$$\delta S = 0 \tag{4.28}$$

where

$$S = \int_{t_1}^{t_2} L dt = \alpha \int_a^b ds \tag{4.29}$$

and L is the Lagrangian function for the system. In special relativity, the space-time interval ds is

$$ds = \sqrt{c^2 dt^2 - dx^2 - dy^2 - dz^2} \tag{4.30}$$

After pulling out cdt from the square root, and replacing $(dx^2 + dy^2 + dz^2)/dt^2$ by v^2, the action functional S becomes

$$S = \int_{t_1}^{t_2} L dt = \int_{t1}^{t2} \alpha c \sqrt{1 - \frac{v^2}{c^2}} dt \tag{4.31}$$

Therefore the relativistic Lagrangian for a free particle is

$$L = \alpha c \sqrt{1 - \frac{v^2}{c^2}} \tag{4.32}$$

We need now to determine the expression α. For small or non-relativistic velocities ($v \ll c$), the square root term in (4.32) can be approximated to

$$\sqrt{1 - \frac{v^2}{c^2}} \approx 1 - \frac{v^2}{2c^2} \tag{4.33}$$

Therefore, expanding (4.32) in the non-relativistic limit ($v \ll c$), we obtain

$$L \approx \alpha c - \frac{\alpha v^2}{2c} \tag{4.34}$$

The first term αc in (4.34) is a constant. Since it does not affect the equations of motion, we can ignore it. Comparing the second term above with the Lagrangian of a non-relativistic free particle $L = T = 1/2\ mv^2$ (recall (4.1) when $V = 0$), we obtain the following value for α

$$\alpha = -mc\ . \tag{4.35}$$

Therefore the relativistic Lagrangian for a free particle is

$$L = -mc^2\sqrt{1 - \frac{v^2}{c^2}}\ . \tag{4.36}$$

If we now reintroduce the generalized potential representing the interaction between the charge and the electromagnetic field obtained in (4.4), the relativistic Lagrangian for a charged particle in an electromagnetic field then becomes

$$L = -mc^2\sqrt{1 - \frac{v^2}{c^2}} + q\mathbf{A}\cdot\mathbf{v} - q\phi \tag{4.37}$$

Note that for small velocities ($v \ll c$), one can then recover (up to a constant) the non-relativistic Lagrangian

$$L \approx -mc^2 + \frac{1}{2}mv^2 + q\mathbf{A}\cdot\mathbf{v} - q\phi \tag{4.38}$$

We can now get the relativistic momenta by inserting (4.37) into $\mathbf{p_i} = \partial L/\partial\dot{\mathbf{q}}_\mathbf{i}$. This gives

$$\mathbf{p} - q\mathbf{A} = \frac{m\mathbf{v}}{\sqrt{1 - \frac{v^2}{c^2}}} \tag{4.39}$$

which can be rewritten

$$\frac{(\mathbf{p} - q\mathbf{A})^2 c^2}{v^2} = m^2c^2 + (\mathbf{p} - q\mathbf{A})^2 \tag{4.40}$$

Inserting now (4.37) into (4.6), the relativistic Hamiltonian for a charged particle in an electromagnetic field becomes

$$H = \frac{mc^2}{\sqrt{1-\frac{v^2}{c^2}}} + q\phi \,. \tag{4.41}$$

With the help of (4.39) and (4.40), the first term of (4.41) can be rewritten in term of the canonical momenta. Finally, one can then get the following relativistic Hamiltonian for a charged particle in an electromagnetic field, written in terms of $\mathbf{A}$, ϕ and $\mathbf{B}$

$$H = \sqrt{m^2c^4 + (\mathbf{p} - q\mathbf{A})^2 c^2} + q\phi \,. \tag{4.42}$$

Note once again that for small velocities ($v^2 \ll c^2$) found in (4.33), the relativistic Hamiltonian (4.42) becomes

$$H \approx mc^2 + \frac{(\mathbf{p} - q\mathbf{A})^2}{2m} + q\phi \tag{4.43}$$

which looks like (4.7) up to a constant, when we neglect the spin effect. Substituting (4.42) in the time-independent Schrödinger equation $H\ \Psi(t,x,y,z) = E\ \Psi(t,x,y,z)$ gives

$$\sqrt{m^2c^4 + (\mathbf{p} - q\mathbf{A})^2 c^2}\ \Psi = (E - q\phi)\ \Psi \tag{4.44}$$

In the interest of mathematical simplicity, we remove the square-root operator in (4.44) and rewriting Ψ^2 as ψ, this gives

$$\left(m^2c^4 + (\mathbf{p} - q\mathbf{A})^2 c^2\right)\ \psi = (E - q\phi)^2\ \psi \tag{4.45}$$

which is the *Klein-Gordon* equation. Unfortunately this equation fails to give a positive definite probability density $(i\hbar/2mc^2)\,(\psi^*\ \partial\psi/\partial t\ -\ \psi\ \partial\psi^*/\partial t)$. Following the historic path taken in 1928 by Dirac [12], we will use instead an equation in the form of the Schrödinger equation which is linear in the time and space derivatives. In the Dirac formalism, the

relativistic Hamiltonian (4.42) for a charged particle in an electromagnetic field, written in terms of $\mathbf{A}$, ϕ is replaced by

$$H = c \sum_{k=x,y,z} \alpha_k \cdot (\mathbf{p}_k - q\mathbf{A}_k) + \beta mc^2 + \ q\phi \tag{4.46}$$

For a relativistic spin 1/2 particle, the new elements in this equation are the following four 4×4 matrices α_x, α_y, α_z and β.

$$\alpha_x = \begin{pmatrix} 0 & 0 & 0 & 1 \\ 0 & 0 & 1 & 0 \\ 0 & 1 & 0 & 0 \\ 1 & 0 & 0 & 0 \end{pmatrix} \quad \alpha_y = \begin{pmatrix} 0 & 0 & 0 & -i \\ 0 & 0 & i & 0 \\ 0 & -i & 0 & 0 \\ i & 0 & 0 & 0 \end{pmatrix} \quad \alpha_z = \begin{pmatrix} 0 & 0 & 1 & 0 \\ 0 & 0 & 0 & -1 \\ 1 & 0 & 0 & 0 \\ 0 & -1 & 0 & 0 \end{pmatrix} \quad \beta = \begin{pmatrix} 1 & 0 & 0 & 0 \\ 0 & 1 & 0 & 0 \\ 0 & 0 & -1 & 0 \\ 0 & 0 & 0 & -1 \end{pmatrix} \tag{4.47}$$

These matrices are all Hermitian, i.e. some square matrices with complex entries which are equal to their own conjugate transpose; they have squares equal to the identity matrix, i.e. $\alpha_x^2 = \alpha_y^2 = \alpha_z^2 = \beta^2 = I$ and they all mutually anti-commute, i.e. $\{\alpha_i, \alpha_j\} = \alpha_i\alpha_j + \alpha_j\alpha_i = 0$ and $\{\alpha_i, \beta\} = \alpha_i\beta + \beta\alpha_i = 0$, where i and j are x, y or z. Once the "Dirac" relativistic Hamiltonian (4.46) is inserted into the time-independent Schrödinger equation $H\ \Psi = E\ \Psi$, this gives

$$\left[c\ \alpha_k \cdot (\mathbf{p}_k - q\mathbf{A}_k) + \beta mc^2 + \ q\phi\right] \psi = E\psi \tag{4.48}$$

This is the famous time independent Dirac equation, where $\alpha_k \cdot (\mathbf{p}_k - q\mathbf{A}_k)$ is a sum of three 4×4 matrices and the wavefunction ψ is a four-component column matrix or spinor

$$\psi = \begin{pmatrix} \psi_1 \\ \psi_2 \\ \psi_3 \\ \psi_4 \end{pmatrix} . \tag{4.49}$$

The simplest form of matrices that satisfy the requirements of Hermiticity, unitarity and anti-commutation are the Pauli matrices

$$\sigma_x = \begin{pmatrix} 0 & 1 \\ 1 & 0 \end{pmatrix}, \sigma_y = \begin{pmatrix} 0 & -i \\ i & 0 \end{pmatrix}, \sigma_z = \begin{pmatrix} 1 & 0 \\ 0 & -1 \end{pmatrix}. \tag{4.50}$$

The forms (4.47) may be then more concisely written

$$\alpha_{k=x,y,z} = \begin{pmatrix} 0 & \sigma_k \\ \sigma_k & 0 \end{pmatrix}, \beta = \begin{pmatrix} I_2 & 0 \\ 0 & -I_2 \end{pmatrix}, \tag{4.51}$$

where I is the 2×2 identity matrix.

A continuity equation may be obtained from the Dirac equation. For this: 1) we write (4.48) for ψ and for $\psi^\dagger$, 2) we then multiply the equation for ψ from the left by $\psi^\dagger$ and the equation for $\psi^\dagger$ from the right by ψ, 3) finally, we subtract the latter results from the former. The result is nothing but

$$\frac{\partial}{\partial t}\left(\underbrace{\psi^\dagger\psi}_{\rho}\right) + \nabla_k \cdot \left(\underbrace{c\psi^\dagger\alpha_k\psi}_{\mathbf{J}}\right) = 0 \tag{4.52}$$

Thus we can interpret ρ and $\mathbf{J}$ as the probability density and the probability current density respectively. The form of ρ is nonnegative and may be consistently identified as a position probability density. Thus Dirac equation has a positive-definite probability density.

The off-diagonal, symmetry property of α (4.51) leads to separation of the Dirac equation (4.48) into the coupled two-component spinors equations

$$\left(E - q\phi - mc^2\right)\varphi_1 - \left[c\,\sigma_k \cdot (\mathbf{p}_k - q\mathbf{A}_k)\right]\varphi_2 = 0 \tag{4.53}$$

$$\left(E - q\phi + mc^2\right)\varphi_2 - \left[c\,\sigma_k \cdot (\mathbf{p}_k - q\mathbf{A}_k)\right]\varphi_1 = 0 \tag{4.54}$$

where

$$\varphi_1 = \begin{pmatrix} \psi_1 \\ \psi_2 \end{pmatrix} \ , \ \varphi_2 = \begin{pmatrix} \psi_3 \\ \psi_4 \end{pmatrix} \tag{4.55}$$

and $\sigma_k \cdot (\mathbf{p}_k - q\mathbf{A}_k)$ is a sum of three 2×2 matrices. Solving φ_2 in (4.54) in terms of φ_1 gives

$$\varphi_2 = \frac{[c\ \sigma_k \cdot (\mathbf{p}_k - q\mathbf{A}_k)]}{(E - \ q\phi + mc^2)}\ \varphi_1 \tag{4.56}$$

Inserting (4.56) into (4.53)

$$\left[c^2\ \left(\sigma_k \cdot (\mathbf{p}_k - q\mathbf{A}_k)\ \left(E - \ q\phi + mc^2\right)^{-1}\ \sigma_k \cdot (\mathbf{p}_k - q\mathbf{A}_k)\right) - \left(E - \ q\phi - mc^2\right)\right]\ \varphi_1 \ = \ 0 \tag{4.57}$$

In the above equation (4.57), we have to be very careful with the term ϕ inserted between the two canonical momenta operators (e.g. recalls that $\mathbf{p}_k = -i\hbar\nabla_k$). This constraint may be easily avoided by using either the symmetric (4.8) or the Landau (4.18) gauge, since both set $\phi = 0$. Using these gauge conditions and assuming that the energy E is constant, (4.57) can be rewritten as follows

$$\left[c^2\ (\sigma_k \cdot (\mathbf{p}_k - q\mathbf{A}_k)\ \sigma_k \cdot (\mathbf{p}_k - q\mathbf{A}_k)) - \left(E^2 - m^2c^4\right)\right]\ \varphi_1 \ = \ 0. \tag{4.58}$$

Using the general identity $(\sigma \cdot \mathbf{a})(\sigma \cdot \mathbf{b}) = (\mathbf{a} \cdot \mathbf{b})\ I + i\sigma \cdot (\mathbf{a} \times \mathbf{b})$ (as long as the operators $\mathbf{a}$ and $\mathbf{b}$ commute with the pauli matrices) [15], one can then find that the first term in (4.58) is

$$[\sigma_k \cdot (\mathbf{p}_k - q\mathbf{A}_k)] \cdot [\sigma_k \cdot (\mathbf{p}_k - q\mathbf{A}_k)] = (\mathbf{p}_k - q\mathbf{A}_k)^2 \ + \ i\sigma_k \cdot [(\mathbf{p}_k - q\mathbf{A}_k) \times (\mathbf{p}_k - q\mathbf{A}_k)] \tag{4.59}$$

in which the last term in (4.59) is

$$(\mathbf{p}_k - q\mathbf{A}_k) \times (\mathbf{p}_k - q\mathbf{A}_k) = -q\ (\mathbf{p}_k \times \mathbf{A}_k + \mathbf{A}_k \times \mathbf{p}_k) = iq\hbar\ \nabla_k \times \mathbf{A}_k = iq\hbar\ \mathbf{B}_k \tag{4.60}$$

where $\mathbf{B}_k = \nabla_k \times \mathbf{A}_k$ is the magnetic field and $iq\hbar\ \nabla_k \times \mathbf{A}_k$ is an operator. The trick is when it operates on the wavefunction φ_1 we have

$$\begin{aligned} i\hbar\ \nabla_k \times \mathbf{A}_k\ \varphi_1 &= i\hbar\ \nabla_k \times \varphi_1 \mathbf{A}_k - i\hbar\ \varphi_1 \nabla_k \times \mathbf{A}_k \\ &= -i\hbar\ \varphi_1 \mathbf{A}_k \times \nabla_k + i\hbar\ \varphi_1 \mathbf{A}_k \times \nabla_k \\ &= i\hbar\ \varphi_1 \nabla_k \times \mathbf{A}_k + i\hbar\ \varphi_1 \mathbf{A}_k \times \nabla_k \\ &= -\ \varphi_1\ (\mathbf{p}_k \times \mathbf{A}_k + \mathbf{A}_k \times \mathbf{p}_k) \end{aligned} \tag{4.61}$$

which corresponds to the second term in (4.60) when the charge q is reintroduced. Therefore, if we put all together the new terms found in (4.60) and (4.59) into (4.58), it becomes

$$\left[c^2\ \left((\mathbf{p}_k - q\mathbf{A}_k)^2\ -\ q\hbar\ \sigma_k \cdot \mathbf{B}_k\right) - \left(E^2 - m^2c^4\right)\right]\ \varphi_1\ =\ 0 \tag{4.62}$$

The $q\hbar\ \sigma_k \cdot \mathbf{B}_k$ term of (4.62), when divided by the factor $2m$, can be regarded as the magnetic moment of the charged spinning particle. The g-factor can be introduced into (4.62) as well by multiplying the magnetic moment term by a factor $g/2$. It then finally becomes

$$\left[c^2\ \left((\mathbf{p}_k - q\mathbf{A}_k)^2\ -(g/2)\ q\ \hbar\ \sigma_k \cdot \mathbf{B}_k\right) - \left(E^2 - m^2c^4\right)\right]\ \varphi_1\ =\ 0. \tag{4.63}$$

Let us now use the Landau gauge (4.18) for solving (4.63). We have

$$\left[c^2\ \left([p_{\mathrm{x}} + qB_z y]^2 + [p_{\mathrm{y}}]^2 + [p_{\mathrm{z}}]^2\right) - \left(E^2 - m^2c^4 + c^2\ (g/2)\ q\ \hbar\ \sigma_z \cdot \mathbf{B}_z\right)\right]\ \varphi_1\ =\ 0. \tag{4.64}$$

Now putting $p_{\mathrm{k\,=\,x,y,z}} = -i\hbar\ \partial/\partial k$ and $p^2_{\mathrm{k\,=\,x,y,z}} = -\hbar^2\ \partial^2/\partial k^2$ into (4.64), this gives

$$\left[\left(-\hbar^2\frac{\partial^2}{\partial x^2} - 2i\hbar q B_z y\frac{\partial}{\partial x} + q^2B_z^2y^2 - \hbar^2\frac{\partial^2}{\partial y^2} - \hbar^2\frac{\partial^2}{\partial z^2}\right) - \left(\frac{E^2 - m^2c^4 + c^2\,(g/2)\,q\hbar\sigma_z \cdot \mathbf{B}_z}{c^2}\right)\right]\varphi_1 = 0 \tag{4.65}$$

It is seen that the equation (4.65) manifestly depends only on the coordinate y. The same conditions have already been met when building the eigenfunction (4.21). We can

then mimic it here and one can present the solution of the equation (4.65) with positive energy, i.e. $(E, \mathbf{p})$, of the charge q in the form

$$\varphi_1(x, y, z) = f(y)\ e^{ik_x x + ik_z z} = f(y)\ e^{i(p_x x + p_z z)/\hbar} \tag{4.66}$$

where $f(y)$ is a two-component matrix, which depends only on the y-coordinate and the particle spin momentum. There will be two independent solutions for $f(y)$, which are the eigenstates of σ_z with eigenvalues $s = \pm 1$. This means that we choose the two independent solutions in the form

$$f_+(y) = \begin{pmatrix} F_+(y) \\ 0 \end{pmatrix}, \quad f_-(y) = \begin{pmatrix} 0 \\ F_-(y) \end{pmatrix} . \tag{4.67}$$

Since $\sigma_z f_s = s f_s$, substituting (4.66) and (4.67) into (4.65) gives

$$\left[\frac{\partial^2}{\partial y^2} - \frac{1}{\hbar^2}(p_x + qB_z y)^2 + \left(\frac{E^2 - m^2c^4 - p_z^2c^2 + c^2\ (g/2)\ q\ \hbar\ \mathbf{B}_z\ s}{\hbar^2 c^2}\right)\right] F_s(y) = 0 \tag{4.68}$$

Then if we define the following new parameters

$$\xi = \sqrt{\frac{|q|B_z}{\hbar}}\left(y + \frac{p_x}{qB_z}\right) \Rightarrow \frac{\partial}{\partial y} = \sqrt{\frac{|q|B_z}{\hbar}}\frac{\partial}{\partial \xi} \Rightarrow \frac{\partial^2}{\partial y^2} = \frac{|q|B_z}{\hbar}\frac{\partial^2}{\partial \xi^2} \tag{4.69}$$

Inserting now (4.69) into (4.68) gives

$$\left[\frac{\partial^2}{\partial \xi^2} - \xi^2 + \underbrace{\left(\frac{E_\nu^2 - m^2c^4 - p_z^2c^2 + c^2\ (g/2)\ q\ \hbar\ \mathbf{B}_z\ s}{\hbar|q|\mathbf{B}_z c^2}\right)}_{\epsilon_\nu}\right] F_s(\xi) = 0 \tag{4.70}$$

This is still a special form of Hermite's equation (4.24) and the solutions exist provided $\epsilon_\nu = 2\nu + 1$ for $\nu = 0, 1, 2, \cdots$. This provides the relativistic energy eigenvalues

$$E_n^2 = m^2c^4 + p_z^2c^2 + c^2|q|\hbar\mathbf{B}_z 2n \tag{4.71}$$

where $n = \nu + (1/2)\,[1 - (g\ \zeta\ s/2)]$ is the quantum number numerating the energy levels of a charge particle in a magnetic field (Landau levels), $n = 0, 1, 2, \cdots$, $\zeta = q/|q|$ is the sign

of the particle charge. The solutions can have positive or negative energies. Thus negative energy solutions are still present in the Dirac equation, as in the Klein-Gordon case.

As previously mentioned, we are interested about the solution of the equation (4.65) with positive energy, which it is denoted here by the positive square root of the right side of E_n.

The wave function is still a Simple Harmonic Oscillator (SHO) solution. The eigenwave function defined in (4.66) then becomes, once normalized and rewritten in term of the cyclotron frequency

$$\varphi_{1,\nu}(x,y,z) = \underbrace{\left(\frac{m\omega_c}{\hbar\pi}\right)^{1/4} \frac{1}{\sqrt{2^\nu \nu!}} H_\nu\left(\sqrt{\frac{m\omega_c}{\hbar}}\,(y-y_0)\right) e^{-\frac{m\omega_c}{2\hbar}(y-y_0)^2}}_{I_\nu(\xi)}\; e^{i(p_x x + p_z z)/\hbar} \tag{4.72}$$

where and the ν-th order Hermite polynomials are written H_ν, p_z is the kinetic momentum along the z axis and p_x is the generalized momentum, which determines the position of the center of the Gaussian packet on the y axis via the relation $y_0 = -p_x/q\mathbf{B}_z$.

It should be noted that the solutions of the relativistic energy eigenvalues (4.71) are two fold degenerate for $s = 1$ and $s = -1$. For an electron ($\zeta = -1$, $g \approx 2$), we have $\nu = n - 1$ for $s = 1$ and $\nu = n$ for $s = -1$. In the case of the lowest energy state ($n = 0$), the solution for $s = 1$ doesn't exist since ν cannot be negative. Thus the $n = 0$ state for an electron is not degenerate and only the solution for $s = -1$ exists. All the other states ($n > 0$) are pairwise degenerate. For a proton ($\zeta = 1$, $g = 2.79$), both solutions for $s = \pm 1$ can exist. Therefore the two lowest states have spin 1/2 and the states are not degenerate.

Representing the solution corresponding to this n-th Landau level by a superscript n

(instead of ν), we can then write for the positive energy solutions

$$\varphi_{1,n}^{s=+1} = \begin{pmatrix} I_{n-1}(\xi) \\ 0 \end{pmatrix} e^{i(p_x x + p_z z)/\hbar}, \quad \varphi_{1,n}^{s=-1} = \begin{pmatrix} 0 \\ I_n(\xi) \end{pmatrix} e^{i(p_x x + p_z z)/\hbar} \tag{4.73}$$

As previously seen for an electron, the solution $\varphi_{1,n}^{s=+1}$ does not exist for $n = 0$. We will consistently incorporate this fact by defining $I_{-1} = 0$.

The solutions in (4.73) determine the upper components of the spinors through (4.66). The lower components, denoted previously by φ_2, can be solved using (4.56) as follows

$$\varphi_2 = \frac{[c\,\sigma_k \cdot (\mathbf{p}_k - q\mathbf{A}_k)]}{(E_n + mc^2)}\,\varphi_1 = \frac{c\left[\begin{pmatrix} \mathbf{p}_z & (\mathbf{p}_x + q\mathbf{B}_z y) - i\mathbf{p}_y \\ (\mathbf{p}_x + q\mathbf{B}_z y) + i\mathbf{p}_y & -\mathbf{p}_z \end{pmatrix}\right]}{(E_n + mc^2)}\,\varphi_1. \tag{4.74}$$

One can deduce from (4.69) these following important terms

$$(\mathbf{p}_x + q\mathbf{B}_z y) \mp i\mathbf{p}_y = \sqrt{\hbar|q|B_z}\left(\xi \mp \frac{\partial}{\partial \xi}\right) \tag{4.75}$$

These are operating on the harmonic oscillator wave functions $I_{n-1}(\xi)$ and $I_n(\xi)$ used in (4.73) and defined in (4.72). We can then use [17]

$$\left(\frac{\partial}{\partial \xi} + \xi\right) I_n = \sqrt{2n}\, I_{n-1}, \quad \left(\xi - \frac{\partial}{\partial \xi}\right) I_n = \sqrt{2(n+1)}\, I_{n+1}. \tag{4.76}$$

Since we now specialize to the case of electrons, for which $\zeta = -1$ or $q = -e$, (4.75) becomes

$$(\mathbf{p}_x - e\mathbf{B}_z y) \mp i\mathbf{p}_y = -\sqrt{\hbar|e|B_z}\left(\xi_- \pm \frac{\partial}{\partial \xi_-}\right) \tag{4.77}$$

where the dimensionless parameter ξ is now defined by

$$\xi_\pm = \sqrt{\frac{|e|B_z}{\hbar}}\left(y \pm \frac{p_x}{eB_z}\right) \Rightarrow \frac{\partial}{\partial y} = \sqrt{\frac{|e|B_z}{\hbar}}\,\frac{\partial}{\partial \xi_\pm} \tag{4.78}$$

when we are taking account of charge of the particle. Using a negative charge here in (4.75) has then the effect of switching the raising and lowering operators. Putting all together (4.77), (4.76) and (4.73) into (4.74), the full wave functions for the positive energy solutions of the Dirac equation can be written as

$$\varphi_n^{s=+1} = \begin{pmatrix} I_{n-1}(\xi_-) \\ 0 \\ \frac{c\ \mathbf{p}_z}{(E_n+mc^2)}\ I_{n-1}(\xi_-) \\ \frac{-c\ \sqrt{2n\hbar|e|B_z}}{(E_n+mc^2)}\ I_n(\xi_-) \end{pmatrix} e^{i(p_x x+p_z z)/\hbar},\ \varphi_n^{s=-1} = \begin{pmatrix} 0 \\ I_n(\xi_-) \\ \frac{-c\ \sqrt{2n\hbar|e|B_z}}{(E_n+mc^2)}\ I_{n-1}(\xi_-) \\ \frac{-c\ \mathbf{p}_z}{(E_n+mc^2)}\ I_n(\xi_-) \end{pmatrix} e^{i(p_x x+p_z z)/\hbar} \tag{4.79}$$

where the matrix terms are so-called the "Dirac bi-spinors". For the lowest Landau level solutions ($n = 0$) we have only

$$\varphi_{n=0}^{s=-1} = \begin{pmatrix} 0 \\ 1 \\ 0 \\ \frac{-c\ \mathbf{p}_z}{(E_0+mc^2)} \end{pmatrix} I_0(\xi_-)\ e^{i(p_x x+p_z z)/\hbar} \tag{4.80}$$

We can now make a last interesting observation from the relativistic energy eigenvalues relation (4.71). The validity of the non-relativistic approximation requires not only that the momentum must be small compared to the mass, but also to the magnetic field B_z. In these conditions, the square root of (4.71) becomes, when imposing $p_z \to 0$ and $n = 1$

$$E_n \approx \pm\, mc^2\sqrt{1+\frac{2|q|\hbar\mathbf{B}_z}{m^2c^2}} \approx \pm\, mc^2\left(1+\frac{|q|\hbar\mathbf{B}_z}{m^2c^2}\right) \Rightarrow \frac{|q|\hbar\mathbf{B}_z}{m^2c^2} \ll 1 \Rightarrow \mathbf{B}_z^Q \ll \frac{m^2c^2}{|q|\hbar} \tag{4.81}$$

We can then introduce the critical magnetic field $\mathbf{B}_z^Q$, when the magnetic energy becomes equal to the rest energy. Since the lightest charged particle is the electron, the ratio $\mathbf{B}_z^Q = m_e^2\ c^2/|e|\hbar = 4.4 \times 10^9\ T$ can be taken as a benchmark value for the magnetic field

beyond which relativistic effects cannot be ignored.

As previously noted sections 3.2 and 3.3, neutron stars can have magnetic fields comparable to $\mathbf{B}_z^Q$. In these extreme conditions, we must use the relativistic formulas when dealing with electrons or positrons. This is not the same story for the much more heavier proton, which has the critical magnetic field $\mathbf{B}_z^Q$ around $1.5 \times 10^{16}\ T$. It is then adequate to use the non-relativistic approximation, since the theoretical upper limit of magnetic field strength has been estimated around $10^{14}\ T$ for a typical neutron star.

Chapter 5

Landau States in Varying Magnetic Fields

We have so far considered Landau states in constant magnetic fields. This is obviously inconsistent with the reality of the dipole fields of a neutron star, which decrease as the cube of the distance. This chapter considers Landau states in a (rapidly) varying magnetic field.

5.1 Magnetic Dipole

At the end of the section 3.3, we discovered in (3.12) that a neutron star, which is a sphere of radius $R_{\rm ns}$, has a surface magnetic field strength given by (3.11). We have also affirmed via (3.12) that, at large distances r compared to $R_{\rm ns}$, a neutron star has an external dipole field that declines as the third power of distance. But we haven't really deduced it yet. It is now time to figure out the exact shape of the magnetic field prevailing in the atmosphere of a neutron star.

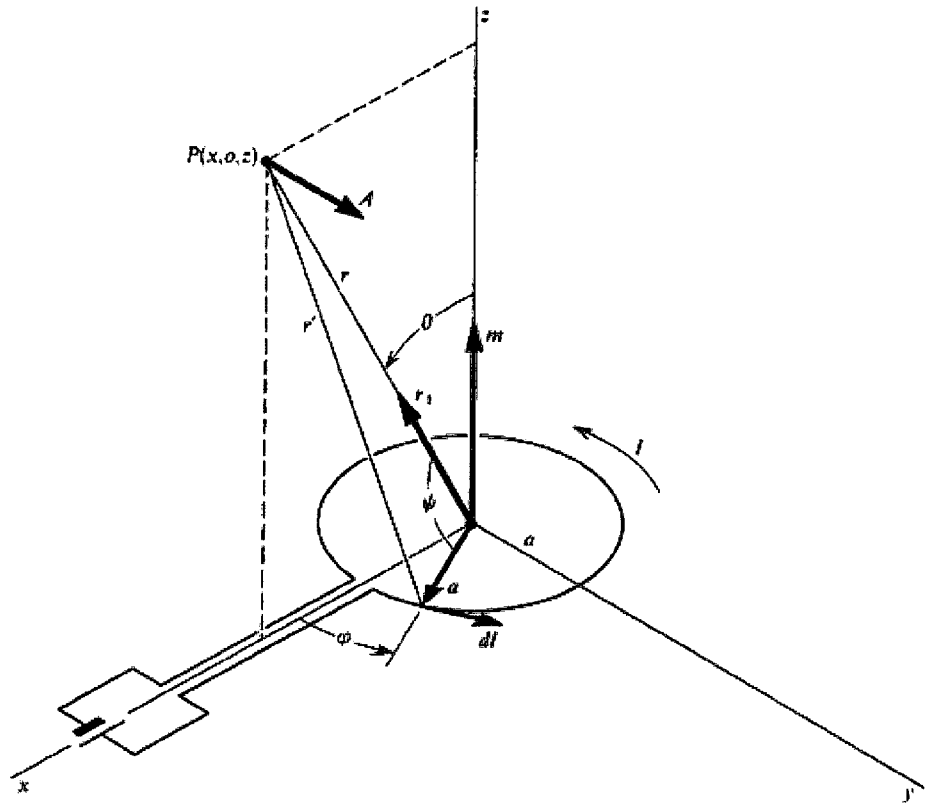

Figure 5.1: Magnetic dipole moment created by a loop of wire (area S, current I) [27].

Let us then start with the figure 5.1, where a loop of wire of radius a and an area S, situated at the origin in a plane perpendicular to the z-axis is carrying a current I. Here $\mathbf{m} = I \times \mathbf{S}$ is called the magnetic dipole moment of the loop. We are now considering the magnetic potential $\mathbf{A}$ at a point P, where it is directed in an azimuthal direction. The vector potential is then in the direction of the current element. One calculates

$$\mathbf{A} = \frac{\mu_0 I}{4\pi} \oint \frac{d\mathbf{l}}{r'} \tag{5.1}$$

where dl is a small element of loop and r' is the distance from dl to P. It can be shown that far from the dipole (or near the axis), the vector potential takes a simple form in

spherical polar coordinates:

$$\mathbf{A} = \frac{\mu_0}{4\pi}\frac{\mathbf{m}\times\mathbf{r}}{r^2}\ , \text{i.e.}\quad A_r = 0,\ A_\theta = 0,\ A_\varphi = \frac{\mu_0}{4\pi}\frac{m}{r^2}\sin\theta = \frac{\mu_0}{4\pi}\frac{m}{r^3}\sqrt{x^2+y^2} \tag{5.2}$$

where the identity $\sin\theta = \sqrt{x^2+y^2}/r$ has been used. To find $\mathbf{B}$, we simply compute $\nabla\times\mathbf{A}$ using (5.2), so we do find that

$$B_r = \frac{\mu_0}{4\pi}\frac{2m}{r^3}\cos\theta,\ B_\theta = \frac{\mu_0}{4\pi}\frac{m}{r^3}\sin\theta,\ B_\varphi = 0 \tag{5.3}$$

with the following length

$$|B| = \sqrt{B_r^2 + B_\theta^2 + B_\varphi^2} = \frac{\mu_0}{4\pi}\frac{m}{r^3}\sqrt{3\cos^2\theta + 1}. \tag{5.4}$$

In cartesian coordinates, the dipole field can be written in these equivalent forms

$$\begin{aligned} B_x &= \frac{\mu_0}{4\pi}\frac{3m}{r^5}xz \\ B_y &= \frac{\mu_0}{4\pi}\frac{3m}{r^5}yz \\ B_z &= \frac{\mu_0}{4\pi}\frac{m}{r^5}\left(3\,z^2 - r^2\right) \\ B_\perp &= \frac{\mu_0}{4\pi}\frac{3m}{r^5}z\sqrt{x^2+y^2} \end{aligned} \tag{5.5}$$

where $B_\perp = \sqrt{B_x^2 + B_y^2}$ and $r^2 = x^2 + y^2 + z^2$. One can use the identities $\cos\theta = z/r$ and $\sin\theta = \sqrt{x^2+y^2}/r$ (once again) for rewriting B_z and $B_\perp$ as follows

$$\begin{aligned} B_z &= \frac{\mu_0}{4\pi}\frac{m}{r^3}\left(3\,\cos^2\theta - 1\right) \\ B_\perp &= \frac{\mu_0}{4\pi}\frac{3m}{r^3}\sin\theta\cos\theta \end{aligned} \tag{5.6}$$

The last step is to determine the magnetic dipole moment m presents in the the neutron star environment. In section 3.3, we found that independent of the internal field geometry, B_s is related to $\mathbf{m}$ by [35]

$$\mathbf{m} = \frac{4\pi}{\mu_0}\frac{1}{2}B_s R_{ns}^3(\mathbf{e}_\parallel\cos\alpha + \mathbf{e}_\perp\sin\alpha\ \cos\Omega t + \mathbf{e}_\perp'\sin\alpha\ \sin\Omega t) \tag{5.7}$$

where α is angle between the magnetic dipole moment and the rotation axis (ref. to figure 3.1), $\mathbf{e}_{\|}$ is a unit vector parallel to the rotation axis and $\mathbf{e}_{\perp}$ and $\mathbf{e}'_{\perp}$ are fixed mutually orthogonal unit vectors perpendicular to $\mathbf{e}_{\|}$. With the help of the following identities

$$\mathbf{e}_{\perp} \cdot \mathbf{e}_{\perp} = \mathbf{e}'_{\perp} \cdot \mathbf{e}'_{\perp} = 1 \; ; \; \mathbf{e}_{\perp} \cdot \mathbf{e}'_{\perp} = \mathbf{e}'_{\perp} \cdot \mathbf{e}_{\perp} = 0 \tag{5.8}$$

one can find that

$$m = |\mathbf{m}| = \sqrt{\mathbf{m} \cdot \mathbf{m}} = \frac{4\pi}{\mu_0} \frac{1}{2} B_s R_{ns}^3. \tag{5.9}$$

putting m into (5.4) gives

$$|B| = B_s \left(\frac{R_{ns}}{r}\right)^3 \frac{1}{2} \sqrt{3\cos^2\theta + 1} \tag{5.10}$$

This confirms the statement that the external dipole field falls off as as the third power of the distance. This is especially true when $\theta = 0$. In this small θ limit: (5.10) becomes (3.12). This is the condition in which the Landau States equations in varying magnetic fields can be used, as we will figure out in the next section.

To conclude this section, let us perform three checks. Does the vector potential for a dipole field satisfy $\nabla \cdot \mathbf{A} = 0$ and does the resulting field $\mathbf{B}$ satisfy $\nabla \times \mathbf{B} = 0$ and $\nabla \cdot \mathbf{B} = 0$?

$$\nabla \cdot \mathbf{A} = \frac{1}{r^2}\frac{\partial (r^2 A_r)}{\partial r} + \frac{1}{r\sin\theta}\frac{\partial}{\partial\theta}(A_\theta \sin\theta) + \frac{1}{r\sin\theta}\frac{\partial A_\phi}{\partial\phi} = \frac{1}{r\sin\theta}\frac{\partial}{\partial\varphi}\left(\frac{\mu_0}{4\pi}\frac{m}{r^2}\sin\theta\right) = 0, \tag{5.11}$$

$$\nabla \times \mathbf{B} = \frac{\mu_0}{4\pi}\frac{m}{r^2\sin\theta}\begin{vmatrix} \mathbf{r} & r\theta & r\sin\theta\varphi \\ \frac{\partial}{\partial r} & \frac{\partial}{\partial\theta} & \frac{\partial}{\partial\varphi} \\ \frac{2\cos\theta}{r^3} & r\left(\frac{\sin\theta}{r^3}\right) & 0 \end{vmatrix} = \left[-\frac{\mu_0}{4\pi}\frac{2m}{r^4}\sin\theta + \frac{\mu_0}{4\pi}\frac{2m}{r^4}\sin\theta\right]\varphi = 0, \tag{5.12}$$

$$\nabla \cdot \mathbf{B} = \frac{1}{r^2}\frac{\partial (r^2 B_r)}{\partial r} + \frac{1}{r\sin\theta}\frac{\partial}{\partial\theta}(B_\theta \sin\theta) + \frac{1}{r\sin\theta}\frac{\partial B_\phi}{\partial\phi} = \frac{\mu_0}{4\pi}\left(-\frac{2\cos\theta}{r^4} + \frac{2\cos\theta}{r^4}\right) = 0. \tag{5.13}$$

So all the conditions are satisfied. Hence our dipole field can then be used in the Schrödinger equation to determine how charged particles behave close to the surface of the neutron star.

5.2 Non-Relativistic Solutions

Rather than consider a general magnetic field, we considered in the previous section just the magnetic dipole fields given by (5.2). This, of course, satisfies the Coulomb gauge condition (recall (5.11)), as well as gives the correct form of $\mathbf{B}$ (recall (5.3) and (5.5)), satisfying $\nabla \cdot \mathbf{B} = 0$ (recall (5.13)) and $\nabla \times \mathbf{B} = \mathbf{0}$ (recall (5.12)) as (of course) it must.

However this is not a convenient form for using in the Schrödinger equation. Since we are only concerned with solutions close to the z-axis, we can assume that $z \gg x, y$. We can then write $\mathbf{B}$ given by (5.5) in cartesian coordinates as

$$\mathbf{B} \approx \left(0, 0, \underbrace{\frac{\mu_0}{4\pi}\frac{2m}{z^3}}_{B_z(z)}\right) \text{ ; when } z \gg x, y \tag{5.14}$$

and then rewrite (5.2) in cartesian coordinates as

$$\mathbf{A} \approx \left(-\frac{\mu_0}{4\pi}\frac{my}{z^3}, \frac{\mu_0}{4\pi}\frac{mx}{z^3}, 0\right) \approx \frac{1}{2}B_z(z)(-y, x, 0) \tag{5.15}$$

This approximate vector potential for the magnetic dipole fields looks like the symmetric gauge defined in (4.8) when $\phi = 0$. We can then check that this gives rise to the correct $\mathbf{B}$ to leading order, and in turn satises $\nabla \cdot \mathbf{B} = 0, \nabla \times \mathbf{B} = 0$ and $\nabla \cdot \mathbf{A} = 0$ to leading order.

$$\mathbf{B} = \nabla \times \mathbf{A} = \frac{\mu_0}{4\pi}\left(\frac{3mx}{z^4}, \frac{3my}{z^4}, \frac{2m}{z^3}\right) \approx \left(0, 0, \underbrace{\frac{\mu_0}{4\pi}\frac{2m}{z^3}}_{B_z(z)}\right) \text{ ; when } z \gg x, y \tag{5.16}$$

$$\nabla \cdot \mathbf{B} = \frac{\mu_0}{4\pi}\left(\frac{3m}{z^4} + \frac{3m}{z^4} - \frac{6m}{z^3}\right) = 0 \tag{5.17}$$

$$\nabla \times \mathbf{B} = \frac{\mu_0}{4\pi}\left(\frac{12my}{z^5}, -\frac{12mx}{z^5}, 0\right) \approx 0; \text{ when } z \gg x, y \tag{5.18}$$

$$\nabla \times \mathbf{A} = \frac{\mu_0}{4\pi}\left(-\frac{\partial}{\partial x}\left(\frac{my}{z^3}\right) + \frac{\partial}{\partial y}\left(\frac{mx}{z^3}\right)\right) = 0 \tag{5.19}$$

We can easily extend this approximation to the confining magnetic-bottle solution we discuss below.

The symmetric and Landau gauges leads to the same magnetic field since they differ by a simple gauge transformation [15]. Let us then rebuild a new *Landau gauge* from (5.15) as follows

$$\begin{aligned}
\mathbf{A_L} &\approx \left(-\frac{\mu_0}{4\pi}\frac{my}{z^3}, \frac{\mu_0}{4\pi}\frac{mx}{z^3}, 0\right) - \left(\frac{\partial}{\partial x}, \frac{\partial}{\partial y}, \frac{\partial}{\partial z}\right)\left(\frac{xy}{2}\underbrace{\frac{\mu_0}{4\pi}\frac{2m}{z^3}}_{B_z(z)}\right) \\
&\approx \left(-\frac{\mu_0}{4\pi}\frac{2my}{z^3}, 0, -\frac{\mu_0}{4\pi}\frac{3mxy}{z^4}\right) = \left(-\frac{\mu_0}{4\pi}\frac{2my}{z^3}, 0, 0\right) \\
&\approx B_z(z)(-y, 0, 0); \text{ when } z \gg x, y.
\end{aligned} \tag{5.20}$$

We can still check if this gives rise to a $\mathbf{B}$ to leading order, and in turn satisfies $\nabla \cdot \mathbf{B} = 0, \nabla \times \mathbf{B} = 0$ to leading order as well as the Coulomb gauge condition $\nabla \cdot \mathbf{A_L} = 0$ to leading order. So

$$\mathbf{B} = \nabla \times \mathbf{A_L} = \frac{\mu_0}{4\pi}\left(0, \frac{6my}{z^4}, \frac{2m}{z^3}\right) \approx \left(0, 0, \underbrace{\frac{\mu_0}{4\pi}\frac{2m}{z^3}}_{B_z(z)}\right); \text{ when } z \gg x, y, \tag{5.21}$$

$$\nabla \cdot \mathbf{B} = \frac{\mu_0}{4\pi}\left(\frac{6m}{z^4} - \frac{6m}{z^4} = 0\right) = 0, \tag{5.22}$$

$$\nabla \times \mathbf{B} = \frac{\mu_0}{4\pi}\left(\frac{24my}{z^5}, 0, 0\right) \approx 0; \text{ when } z \gg x, y, \tag{5.23}$$

$$\nabla \times \mathbf{A_L} = \frac{\mu_0}{4\pi}\left(-\frac{\partial}{\partial x}\left(\frac{-2my}{z^3}\right)\right) = 0. \tag{5.24}$$

Since it does to leading order, we can still easily extend this to the confining magnetic bottle solution we discuss below. From now on, we will use only the revisited *Landau gauge* found by (5.20) up to the end of this research.

Let us now insert (5.20) into the non-relativistic Hamiltonian (4.7). Neglecting the spin-dependent terms, the time-independent Schrödinger equation $H\ \psi(x,y,z) = E\ \psi(x,y,z)$ then becomes

$$-\frac{\hbar^2}{2m}\left[\left(\frac{\partial^2}{\partial x^2}+\frac{2iqB_z(z)y}{\hbar}\frac{\partial}{\partial x}-\frac{q^2B_z^2(z)y^2}{\hbar^2}\right)+\frac{\partial^2}{\partial y^2}+\frac{\partial^2}{\partial z^2}\right]\psi(x,y,z) = E\ \psi(x,y,z) \tag{5.25}$$

This time only the coordinate x is missing from the Schrödinger equation (5.25). It follows that $[p_x, H] = 0$, so that we can construct a function that is an eigenfunction of p_x, where we can write their eigenvalue as $\hbar k_x$. The related eigenfunction appears then as

$$\psi(x,y,z) = e^{ik_x x}\ u(y)\ v(z). \tag{5.26}$$

Inserting it into (5.25) gives (once reorganized)

$$\frac{1}{u(y)}\frac{\partial^2 u(y)}{\partial y^2}-\left(k_x^2+\frac{2qB_z(z)k_x y}{\hbar}+\frac{q^2B_z^2(z)y^2}{\hbar^2}\right) = -\left(\frac{1}{v(z)}\frac{\partial^2 v(z)}{\partial z^2}+\frac{2mE}{\hbar^2}\right) \tag{5.27}$$

Since the right side of the equation above depends on z only, we can separate it as follows

$$\frac{1}{v(z)}\frac{\partial^2 v(z)}{\partial z^2}+\frac{2mE}{\hbar^2} = \frac{2mE'(z)}{\hbar^2} \tag{5.28}$$

The left side of (5.27) is then equal to

$$\frac{\partial^2 u(y)}{\partial y^2}-\left(k_x^2+\frac{2qB_z(z)k_x y}{\hbar}+\frac{q^2B_z^2(z)y^2}{\hbar^2}\right)u(y) = -\frac{2mE'(z)}{\hbar^2}\ u(y) \tag{5.29}$$

which could be rewritten as

$$\frac{\partial^2 u(y)}{\partial y^2}+\left[-\frac{q^2B_z^2(z)}{\hbar^2}\left(y+\frac{\hbar k_x}{qB_z(z)}\right)^2+\left(\frac{2mE'(z)}{\hbar^2}\right)\right]\ u(y) = 0. \tag{5.30}$$

Amazingly, we know how to solve the above equation, in which z is just a constant (recall (4.22)). Comparing to Landau levels in constant magnetic field B_z results obtained previously in (4.26), the non-relativistic energy is

$$E_n'(z) = \hbar\left(\frac{qB_z(z)}{m}\right)\left(n+\frac{1}{2}\right) = \hbar\omega_c(z)\left(n+\frac{1}{2}\right). \tag{5.31}$$

Note that (5.31) is dimensionally correct since

$$E_n'(z) = \underbrace{\left(\frac{[M][L]^2}{[T]^2}\,\frac{[T]}{1}\right)}_{\hbar}\ \underbrace{\frac{[C]}{1}}_{q}\ \underbrace{\frac{1}{[C]}\,\frac{[M][L]}{[T]^2}\,\frac{[T]}{[L]}}_{B}\ \underbrace{\frac{1}{[M]}}_{1/m} = \underbrace{\frac{[M][L]^2}{[T]^2}}_{E} \tag{5.32}$$

Thus, the right side (5.28) of the equation could be finally rewritten as

$$\frac{\partial^2 v(z)}{\partial z^2} + \frac{2m}{\hbar^2}\left[E - \underbrace{\left(\frac{\hbar qB_z(z)}{m}\right)\left(n+\frac{1}{2}\right)}_{V_{eff}(B_z(z),n)}\right] v(z) = 0\,. \tag{5.33}$$

which is just an ordinary differential equation... But what we have just found above is quite important and crucial for the rest of this research:

We could either have a discrete spectrum of Landau states if $B_z(z)$ is "confining" as a magnetic bottle or modified plane wave states if (say) it is decreasing as $1/r^3$.

Of course, this exciting outcome is only valid only close to the z-axis, i.e. where we can assume that $z \gg x, y$.

The most interesting results arising from above is that we could now use a *semi-classical* approach to link a new quantized force $\mathbf{F}\left(B_z(z), n\right)$ (with respect to the z-direction) that acts on a particle in a potential energy $V_{eff}\left(B_z(z), n\right)$ found in (5.33), via (4.2). Combining this with the fact that the external dipole field found in the atmosphere of the neutron star falls off as $1/r^3$ allows us to evaluate the exact form of the quantized force in chapter 6.

5.3 Relativistic Solutions

Could we get a similar result for a relativistic particle in a quasi uniform magnetic field $B_z(z)$ in the small θ limit condition? Inserting (5.20) into the relativistic coupled time-independent Dirac equation (4.65) and neglecting the spin term gives

$$\left[\left(-\hbar^2\frac{\partial^2}{\partial x^2} - 2i\hbar q B_z(z)\, y\frac{\partial}{\partial x} + q^2 B_z^2(z) y^2 - \hbar^2\frac{\partial^2}{\partial y^2} - \hbar^2\frac{\partial^2}{\partial z^2}\right) - \left(\frac{E^2 - m^2c^4}{c^2}\right)\right]\varphi_1 = 0\ . \tag{5.34}$$

Note that the last term of (5.34) can be reduced to $2mE$ in non-relativistic regime. It is then equivalent to the binding energy term found in the non-relativistic Schrödinger equation.

It is seen that the equation (5.34) manifestly depends this time on both the coordinates y and z. A similar condition has already been met when building the eigenfunction (5.26). We can then mimic it here and one can present the solution of the equation (5.34) with positive energy, i.e. $(E, \mathbf{p})$, of the charge q in the form

$$\varphi_1(x, y, z) = f(y)\ g(z)\ e^{ik_x x} = f(y)\ g(z)\ e^{i(p_x x)/\hbar} \tag{5.35}$$

where $f(y)$ is still a two-component matrix defined in (4.67), which depends only on the y-coordinate. Substituting (5.35) and (4.67) into (5.34) gives

$$\frac{1}{F_s(y)}\frac{\partial^2}{\partial y^2}F_s(y) - \frac{1}{\hbar^2}\left[p_x + qB_z(z)\, y\right]^2 = -\left[\frac{1}{g(z)}\frac{\partial^2}{\partial z^2}g(z) + \left(\frac{E^2 - m^2c^4}{\hbar^2c^2}\right)\right] \tag{5.36}$$

One can still notice that the right side of the equation above depends on z only, so it can be rewritten as follows

$$\frac{1}{g(z)}\frac{\partial^2}{\partial z^2}g(z) + \left(\frac{E^2 - m^2c^4}{\hbar^2c^2}\right) = \left(\frac{E'^2(z) - m^2c^4}{\hbar^2c^2}\right) \tag{5.37}$$

The left side of (5.36) is then equal to

$$\frac{\partial^2}{\partial y^2}F_s(y) - \frac{1}{\hbar^2}\left[p_x + qB_z\left(z\right)y\right]^2 \; F_s(y) = -\left(\frac{E^{'2}\left(z\right) - m^2c^4}{\hbar^2c^2}\right) \; F_s(y) \tag{5.38}$$

which could be rewritten as

$$\left[\frac{\partial^2}{\partial y^2} - \frac{1}{\hbar^2}\left(p_x + qB_z\left(z\right)y\right)^2 + \left(\frac{E^{'2}\left(z\right) - m^2c^4}{\hbar^2c^2}\right)\right] \; F_s(y) = 0 \tag{5.39}$$

Again, we know how to solve the above equation, in which z is a constant (recall (4.68)). Comparing to Landau levels in a constant magnetic field B_z results obtained previously in (4.71), the relativistic energy is

$$E^{'2}_{n}\left(z\right) = m^2c^4 + c^2|q|\hbar B_z\left(z\right)2n \tag{5.40}$$

where $n = \nu + (1/2)$ is the quantum number numerating the energy levels of a charge particle in a magnetic field (Landau levels), $n = 0, 1, 2, \cdots$. As already mentioned, the solutions can have positive or negative energies. Note that (5.40) is dimensionally correct since

$$E^{'2}_{n}\left(z\right) = \underbrace{[M]^2}_{m^2} \; \underbrace{\frac{[L]^4}{[T]^4}}_{c^4} + \underbrace{\frac{[L]^2}{[T]^2}}_{c^2} \; \underbrace{\frac{[C]}{1}}_{q} \; \underbrace{\left(\frac{[M][L]^2}{[T]^2} \; \frac{[T]}{1}\right)}_{\hbar} \; \underbrace{\frac{1}{[C]} \; \frac{[M][L]}{[T]^2} \; \frac{[T]}{[L]}}_{B} = \underbrace{\frac{[M]^2[L]^4}{[T]^4}}_{E^2} \tag{5.41}$$

Thus, the right side (5.37) of the equation could be rewritten as

$$\frac{\partial^2 g(z)}{\partial z^2} + \frac{1}{\hbar^2c^2}\left[E^2 - \left(m^2c^4 + c^2|q|\hbar B_z\left(z\right)2n\right)\right]g(z) = 0 \tag{5.42}$$

As obtained before, this results is a solution quantized in the z-direction as well. As usual, we must not forget that this is only valid close to the z-axis, i.e. where we can assume that $z \gg x, y$.

Let us rewrite (5.42) as follows

$$\left(p_z^2c^2 + m^2c^4\right) = \left(E^2 - c^2|q|\hbar B_z\left(z\right)2n\right) \tag{5.43}$$

Compare (5.43) to [16]

$$H = T + V = \frac{mc^2}{\sqrt{1 - \frac{v^2}{c^2}}} + V = E \tag{5.44}$$

$$\frac{mc^2}{\sqrt{1 - \frac{v^2}{c^2}}} = E - V \Rightarrow \frac{m^2c^4}{1 - \frac{v^2}{c^2}} = (E - V)^2 \tag{5.45}$$

We can use the relativistic momenta for a free particle

$$\mathbf{p}_z = \frac{m\mathbf{v}_z}{\sqrt{1 - \frac{v^2}{c^2}}} \Rightarrow \frac{\mathbf{p}_z}{\mathbf{v}_z} = \frac{m}{\sqrt{1 - \frac{v^2}{c^2}}} \Rightarrow \frac{p_z^2}{v_z^2} = \frac{m^2}{1 - \frac{v^2}{c^2}} \ . \tag{5.46}$$

Rewriting (5.55) with the help of (5.46) gives

$$\frac{p_z^2c^4}{v_z^2} = (E - V)^2 \ . \tag{5.47}$$

Now using the following relation for free particle

$$\frac{p_z^2c^4}{v_z^2} = m^2c^4 + p_z^2c^2 \tag{5.48}$$

(5.47) finally becomes

$$p_z^2c^2 + m^2c^4 = (E - V)^2 = E^2 - 2EV + V^2 \tag{5.49}$$

Combining now (5.49) and (5.43), one gets

$$V^2 - 2EV + c^2|q|\hbar B_z(z)\,2n = 0 \tag{5.50}$$

which gives for the effective potential V

$$V = E \pm \sqrt{E^2 - c^2|q|\hbar B_z(z)\,2n} \tag{5.51}$$

Now let us check if (5.51) can be reduced simply to the non-relativistic form found in (5.33). If $E^2 \gg c^2|q|\hbar B_z(z)\,2n$, which happens when B_z is low and $B_z \ll \mathbf{B}_z^Q$ in the non-relativistic regime (5.51) can be reduced to

$$V = E \pm E\sqrt{1 - \frac{c^2|q|\hbar B_z(z)\,2n}{E^2}} \approx E \pm E \mp \frac{c^2|q|\hbar B_z(z)\,2n}{2E} \ . \tag{5.52}$$

If we are now taking the negative solution, this gives

$$V \approx \frac{c^2|q|\hbar B_z(z)}{E}\, n\,. \tag{5.53}$$

If we are now allowed to replace E by mc^2, this becomes

$$V \approx \frac{|q|\hbar B_z(z)}{m}\, n = \frac{|q|\hbar B_z(z)}{m}\left(\nu + \frac{1}{2}\right)\,, \tag{5.54}$$

where we have neglected the spin term in the relation $n = \nu + (1/2)[1 - (g\,\zeta\,s/2)]$. Since (5.54) looks like the $V_{eff}(B_z(z), n)$ found in (5.33), it seems that (5.51) can be reduced simply to the non-relativistic form.

As noted at the end of the last section, the same *semi-classical* approach could used to find the quantized force $\mathbf{F}$ that acts on a relativistic particle arising from a potential energy $V(B_z(z), n)$ found in (5.51), via (4.2), where B_z represents the external dipole field found in the atmosphere of the neutron star that declines with the third power of distance (3.12). This should reveal the real nature of the new quantized relativistic force $\mathbf{F_z}$.

Just a last word for saying that, since it seems that the Force-Potential Energy relation in special relativity is rarely used, let us try another approach by rewriting (5.43) as follows

$$p_z^2c^2 = E^2 - \left(\underbrace{m^2c^4 + c^2|q|\hbar B_z(z)\,2n}_{E_n^2(z)}\right)\,. \tag{5.55}$$

Since E is constant hence

$$\frac{dz}{dt} = v_z = \frac{p_z c^2}{\hat{E}} = c\left(\frac{\sqrt{E^2 - E_n^2(z)}}{\hat{E}}\right) \tag{5.56}$$

where $\hat{E}$ is the total relativistic energy

$$\hat{E}^2 = p_z^2c^2 + m^2c^4 = \sqrt{E^2 - c^2|q|\hbar B_z(z)\,2n}. \tag{5.57}$$

Thus this approach is giving the relationship between the relativistic velocity v_z of the particles in the z-direction and the magnetic field $B_z(z)$, which is embedded into the energy $E_n^2(z)$. We will use this result in the next chapter as well.

Part III

Toward the Jet Model via Landau States

Chapter 6

The effective force in a varying magnetic field

Some interesting results have arisen from a study of Landau states. We have first developed the basic non-relativistic and relativistic standing wave equations for describing the behavior of a charged particle in a uniform magnetic field. Since a real neutron star's atmosphere contains a varying magnetic field, we have developed a new method, giving two equations: the usual one and a brand-new one! The latter describes the behavior of a charged particle trapped in an effective potential energy that is a function of a varying magnetic field.

6.1 From a classical approach to a quantized result

The most interesting results arising from the above is that we could now use a "semi-classical" approach to link the resulting "quantized" force $\mathbf{F}$ acting on a particle, and the potential energy U of that particle, via the relation (4.2), where ∇ is the gradient operator. In our situation, U is equal to $V_{eff}\left(B_z\left(z\right), n\right)$ found in (5.33). Therefore, the non relativistic "quantized" force $\mathbf{F}$ on Landau states due to a varying magnetic field that

acts on a particle far from the origin, near to the z-axis and in the direction of the magnetic field then becomes

$$\mathbf{F}\left(B_z(z),n\right) \;=\; -\nabla V_{eff}\left(B_z\left(z\right),n\right) \;=\; -\left(\frac{\hbar q}{m}\right)\left(n+\frac{1}{2}\right)\nabla\left|B_z\left(z\right)\right| \;. \tag{6.1}$$

Note the unusual form of this force. The corresponding relativistic force can be found by inserting the effective potential (5.51) into the following Force-Potential Energy relation [16]

$$F_z \;=\frac{d}{dt}\left(\frac{m\mathbf{v}_z}{\sqrt{1-\frac{v^2}{c^2}}}\right)=-\frac{dV}{dz}=-\frac{d}{dz}\left(E\pm\sqrt{E^2-c^2|q|\hbar\left|B_z\left(z\right)\right|2n}\right) \tag{6.2}$$

so

$$F_z=\pm\frac{1}{2}\,\frac{c^2|q|\hbar 2n}{\sqrt{E^2-c^2|q|\hbar\left|B_z\left(z\right)\right|2n}}\,\nabla\left|B_z\left(z\right)\right| \tag{6.3}$$

where $E^2 > c^2|q|\hbar B_z\left(z\right)2n$.

Now let us check if (6.3) can be reduced simply to the non-relativistic form found in (6.1). If $E^2 \gg c^2|q|\hbar B_z\left(z\right)2n$, which happens when B_z is low and $B_z \ll \mathbf{B}_z^Q$ in the non relativistic regime (6.3) can be reduced to

$$F_z\approx\pm\frac{1}{2}\,\frac{c^2|q|\hbar 2n}{E}\,\nabla\left|B_z\left(z\right)\right|\left(1+\frac{c^2|q|\hbar\left|B_z\left(z\right)\right|2n}{E^2}\right) \;. \tag{6.4}$$

If we are now still taking the negative solution and ignoring terms that vanish faster than $1/E$, this gives

$$F_z\approx-\frac{c^2|q|\hbar}{E}\;n\;\nabla\left|B_z\left(z\right)\right| \tag{6.5}$$

If we are now allowed to replace E by mc^2, this becomes

$$F_z\approx-\frac{|q|\hbar}{m}\;n\;\nabla\left|B_z\left(z\right)\right|=-\frac{|q|\hbar}{m}\left(\nu+\frac{1}{2}\right)\nabla\left|B_z\left(z\right)\right| \tag{6.6}$$

where we have neglected the spin term in the relation $n = \nu + (1/2)\left[1-(g\;\zeta\;s/2)\right]$. Since (6.6) looks like the $\mathbf{F}\left(B_z(z),n\right)$ found in (6.1), it seems that (6.3) can be reduced

simply to the non-relativistic form.

Since the Force-Potential Energy relation in special relativity is rarely used, we might use the second approach suggested at the end of the section 5.3 that has given us the relationship between the relativistic velocity v_z of the particles in the z-direction and the magnetic field $B_z(z)$ (embedded into the energy $E_n^2(z)$). If we take the derivative of equation (5.55) with respect to z, this gives

$$p_z c^2 \frac{dp_z}{dz} = -E_n(z) \frac{dE_n(z)}{dz} = -\frac{c^2|q|\hbar 2n}{2} \frac{dB_z(z)}{dz} \tag{6.7}$$

Since $p_z c^2 = v_z \hat{E}$ (recall (5.48) and (5.56) for a free particle), (6.7) can be rewritten as

$$F_z = \frac{dp_z}{dt} = \frac{dz}{dt}\frac{dp_z}{dz} = v_z \frac{dp_z}{dz} = -\frac{c^2|q|\hbar 2n}{2\hat{E}} \frac{dB_z(z)}{dz} = -\frac{m^2c^4}{\hat{E}} \frac{2n}{2\mathbf{B}_z^Q} \frac{dB_z(z)}{dz} \tag{6.8}$$

One can also retrieve the negative solution of (6.3) from (6.7) as follows

$$\begin{aligned} F_z &= -\frac{1}{2}\frac{c^2|q|\hbar 2n}{\hat{E}} \frac{dB_z(z)}{dz} \\ &= -\frac{1}{2}\frac{c^2|q|\hbar 2n}{\sqrt{p_z^2c^2 + m^2c^4}} \frac{dB_z(z)}{dz} \\ &= -\frac{1}{2}\frac{c^2|q|\hbar 2n}{\sqrt{E^2 - c^2|q|\hbar\,|B_z(z)|\,2n}} \frac{dB_z(z)}{dz} \end{aligned} \tag{6.9}$$

This confirms that both relativistic approaches used above are giving the same results.

We now insert the form of the magnetic dipole field that exists in the atmosphere of the neutron star in (6.1).

6.2 Motion of the charged particle given by the new force $\mathbf{F}(B_z(z), n)$

Since we know the nature of the magnetic field $|B|$ prevailing in the atmosphere of a neutron star, we can now find the equation of the motion of a particle determined by the *force-potential energy* relation expressed in (6.1).

Because we are forced to work in the small θ limit, i.e. the charged particle must remain near to the z-axis, we use spherical coordinates. In such a system, the grad of a scalar f, i.e. ∇f is

$$\frac{\partial f}{\partial r}\hat{\boldsymbol{r}} + \frac{1}{r}\frac{\partial f}{\partial \theta}\hat{\boldsymbol{\theta}} + \frac{1}{r\sin\theta}\frac{\partial f}{\partial \phi}\hat{\boldsymbol{\phi}} \tag{6.10}$$

Using the magnetic field given by a dipole field obtained in (5.4) into (6.10) above, the grad of a scalar $|B|$ in spherical coordinate becomes

$$\nabla|B| = -\frac{\mu_0}{4\pi}\left(\frac{3m}{r^4}\right)\frac{\left[(3\cos^2\theta+1)\ \hat{\boldsymbol{r}} + (\sin\theta\ \cos\theta)\,\hat{\boldsymbol{\theta}}\right]}{\sqrt{3\cos^2\theta+1}} \tag{6.11}$$

The non relativistic "quantized" force $\mathbf{F}$ (given by (6.1)) on a Landau state due to a varying magnetic field that acts on a particle far from the origin, near to the z-axis and in the direction of the magnetic field then becomes

$$\mathbf{F}(B_z(r,\theta),n) = \left(\frac{\mu_0}{4\pi}\right)\left(\frac{\hbar q}{m}\right)\left(n+\frac{1}{2}\right)\left(\frac{3\ \mu_d}{r^4}\right)\frac{\left[(3\cos^2\theta+1)\ \hat{\boldsymbol{r}} + (\sin\theta\ \cos\theta)\,\hat{\boldsymbol{\theta}}\right]}{\sqrt{3\cos^2\theta+1}} \tag{6.12}$$

Note that the μ_d above designates the dipole moment, not to be confused with the mass m of the particle. Since we are near the z-axis, i.e. $\theta \approx 0$, we could say that $\cos\theta \approx 1$. Consequently, the non relativistic "quantized" force $\mathbf{F}$ on a Landau state due to a varying magnetic field that acts on a particle far from the origin, near to the z-axis and in the

direction of the magnetic field could be approximated by

$$\mathbf{F}(B_z(r,\theta),n) \approx \left(\frac{\mu_0}{4\pi}\right)\left(\frac{\hbar q}{m}\right)\left(n+\frac{1}{2}\right)\left(\frac{3\,\mu_d}{2\,r^4}\right)\left[4\,\hat{\boldsymbol{r}}+\theta\,\hat{\boldsymbol{\theta}}\right] . \tag{6.13}$$

(6.12) and (6.13) are dimensionally correct since

$$\mathbf{F} \approx \underbrace{\left(\frac{[M][L]^2}{[T]^2}\,\frac{[T]}{1}\right)}_{\hbar}\underbrace{\frac{[C]}{1}}_{q}\underbrace{\frac{1}{[M]}}_{1/m}\underbrace{\frac{[M][L]}{[C]^2}}_{\mu_0}\underbrace{\frac{[C][L]^2}{[T]}}_{\mu_d}\underbrace{\frac{1}{[L]^4}}_{\frac{1}{r^4}} = \underbrace{\frac{[M][L]}{[T]^2}}_{F} \tag{6.14}$$

The properties of the *Landau states* are modified by the varying magnetic field. If the field is "confining" (for example, a magnetic bottle) then the states will be quantized in the z-direction as well as in the x-y plane.

In a neutron star's atmosphere, the direction and magnitude of the field (and hence the direction of the force in (6.13)) change continuously as we move away.

We will now try to capitalize on this result to develop a quasi-realistic model for the divergent flow (in spherical coordinates) that could exist on the atmosphere of the neutron star.

Chapter 7

The Quasi-Realistic Jet Model - preliminary version

We will now exploit the fact that in varying magnetic field, the Landau states are quantized with respect to the z-direction. This produces a non relativistic "quantized" force **F** *(6.13) that acts on a particle far from the origin, near to the z-axis on the atmosphere of the neutron star. We will then develop an innovative Quasi-Realistic Model for the Divergent flow (in Spherical Coordinates) that could exist on the atmosphere of the Neutron Star.*

The purpose of this exercise is to demonstrate in terms of an analytic model that we can satisfy the current conservation condition exactly, along with an approximate solution of the equation of motion. The first example is an unrealistic example with simple radial flow. The second is a more sophisticated example that provides a solution that has jet like features. Clearly any more realistic solution will need a much more sophisticated solution.

7.1 The current density conservation principle

In general, we will have a conserved current density

$$\vec{j} = n\, q\, \vec{v} \text{ and } \vec{\nabla} \cdot \vec{j} = 0 \tag{7.1}$$

$$\vec{\nabla} n \cdot \vec{v} + n\, \vec{\nabla} \cdot \vec{v} = 0 \tag{7.2}$$

where $\vec{j}$ is the current density (A/m^2), n is the number density, q is the charge (C) of the individual particles, so $\rho = nq$ is the charge density (C/m^3) and $\vec{v}$ is the velocity (m/s) of charged particles. Intuitively, the above conserved current suggests that

- when the number density n is big, e.g. close to the neutron star surface, the charge velocity $\vec{v}$ is small;
- when the number density n is small e.g. far from the neutron star surface, the charge velocity $\vec{v}$ is big.

This is exactly the expected properties of an astrophysical jet.

7.2 The 1-D kinematics of radial constant-acceleration

Many physical situations can be modeled as constant-acceleration processes, such as projectile motion. As a warm-up exercise for validating the current conservation principle described in section 7.1, let us then consider a beam accelerated radially at a constant rate $\vec{a_r}$. Here the radial constant-acceleration (with respect to time $t$and distance r) means: *radially outward from the centre.* In this case, the usual 1-D kinematic equations [41] state that

$$v_r = \sqrt{2\, a_r\, r} \quad \Rightarrow \quad \frac{dv_r}{dr} = \sqrt{\frac{a_r}{2\, r}}\,. \tag{7.3}$$

Putting (7.3) into (7.2), the conservation equation becomes

$$\frac{dn_r}{dr}\sqrt{2\,a_r\,r} + n_r\sqrt{\frac{a_r}{2\,r}} = 0 \quad \Rightarrow \quad \frac{dn_r}{n_r} = -\frac{1}{2}\frac{dr}{r} \tag{7.4}$$

with the solution

$$n_r = \frac{c}{r^{\frac{1}{2}}} \tag{7.5}$$

where c is a constant. To determine n_r we are posing the limit conditions: when $r = R \Rightarrow n_r = n_0$. The constant c then equals $n_0\sqrt{R}$. Putting all this together, the number density with respect to the position r becomes

$$n_r(r) = n_0\left(\frac{R}{r}\right)^{1/2}. \tag{7.6}$$

Finally, with the help of (7.3) and (7.6), the current density (7.1) becomes

$$j_r(r) = qn_0\sqrt{2a_rR} \tag{7.7}$$

which is independent of the position r, as illustrated in figure 7.1. So the conservation law (7.1) is trivially satisfied.

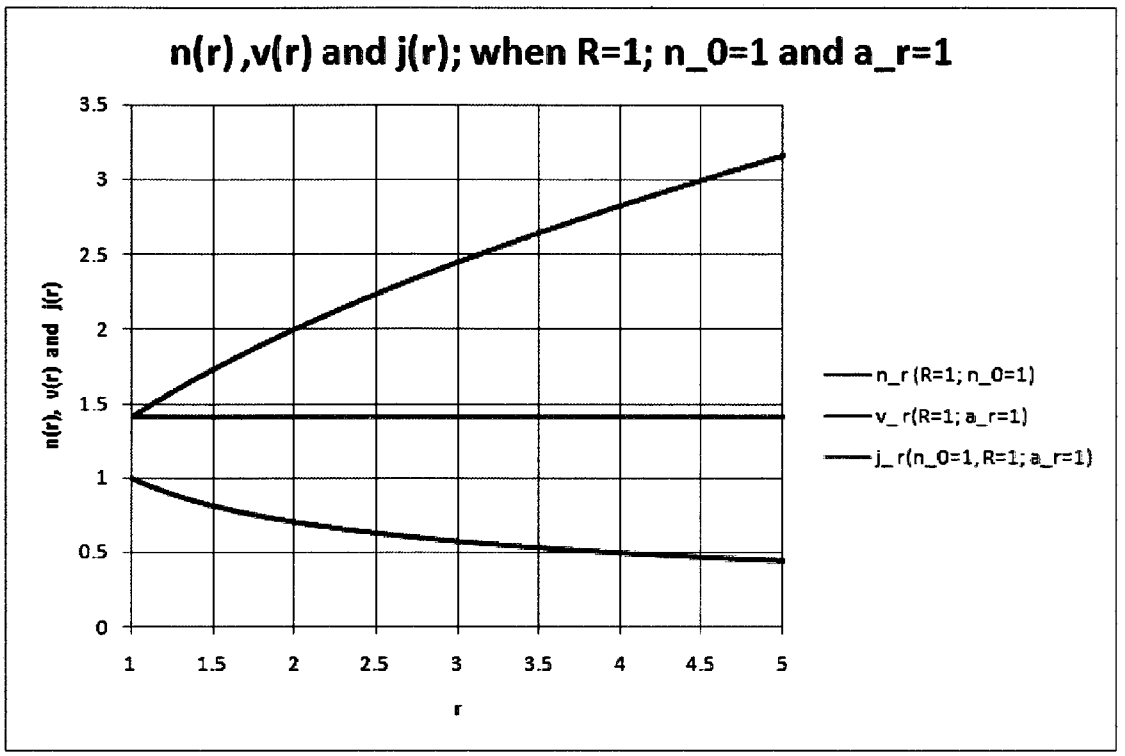

Figure 7.1: Evidence of the conserved current density when the particle is accelerated radially at a constant rate.

7.3 The quasi-realistic jet model in spherical coordinates - first version

To mimic the effects of dipole field that exists on a neutron star, it is better to consider the position, the velocity and acceleration fields in spherical coordinates $[r, \phi, \theta]$, as follows:

$$\begin{aligned}
\vec{r}(t) &= r\,\hat{\boldsymbol{r}} \\
\vec{v}(t) = \dot{\vec{r}}(t) = \frac{d\vec{r}(t)}{dt} &= \dot{r}\,\hat{\boldsymbol{r}} + r\,\sin\theta\,\dot{\phi}\,\hat{\boldsymbol{\phi}} + r\,\dot{\theta}\,\hat{\boldsymbol{\theta}} \\
\vec{a}(t) = \ddot{\vec{r}}(t) = \frac{d^2\vec{r}(t)}{dt^2} &= \left(\ddot{r} - r\,\dot{\theta}^2 - r\,\dot{\phi}^2\,\sin^2\theta\right)\,\hat{\boldsymbol{r}} + \\
&\quad \left(r\,\ddot{\phi}\,\sin\theta + 2\,\dot{r}\,\dot{\phi}\,\sin\theta + 2\,r\,\dot{\theta}\,\dot{\phi}\,\cos\theta\right)\,\hat{\boldsymbol{\phi}} + \\
&\quad \left(r\,\ddot{\theta} + 2\,\dot{r}\,\dot{\theta} - r\,\dot{\phi}^2\,\sin\theta\,\cos\theta\right)\,\hat{\boldsymbol{\theta}}
\end{aligned} \tag{7.8}$$

We can assume that there is no velocity component in the azimuthal direction, so $\dot{\phi} = \ddot{\phi} = 0$, and (7.8) becomes

$$\begin{aligned}
\vec{v}(t) &= v_r\,\hat{\boldsymbol{r}} + r\,v_\theta\,\hat{\boldsymbol{\theta}} \\
\vec{a}(t) = \frac{d\vec{v}(t)}{dt} &= \left(\frac{dv_r}{dt} - r\,v_\theta^2\right)\,\hat{\boldsymbol{r}} + \left(r\,\frac{dv_\theta}{dt} + 2\,v_r\,v_\theta\right)\,\hat{\boldsymbol{\theta}}
\end{aligned} \tag{7.9}$$

where $v_r = dr/dt$ and $v_\theta = d\theta/dt$. We can now find a semi-analytic approximation as follows. On the neutron star, if we have a dipole field causing the acceleration, we expect the flow at large distances to be radial, i.e.

$$v_r\,(r = \infty) = v_0, \quad v_\theta\,(r = \infty) = 0 \tag{7.10}$$

We would like to find a semi-analytic solution that satisfies these constraints to leading order. We can guess

$$v_r = v_0\left(1 - \left(\frac{r_1}{r}\right)^\alpha\right), \quad v_\theta = v_1\left(\frac{1}{r}\right)\sin\theta\left(\frac{r_1}{r}\right)^\beta. \tag{7.11}$$

So, $\vec{v}$ in (7.9) can be rewriten as

$$\vec{v}\,(t) = v_0 \left(1 - \left(\frac{r_1}{r}\right)^{\alpha}\right) \hat{\boldsymbol{r}} + v_1 \sin\theta \left(\frac{r_1}{r}\right)^{\beta} \hat{\boldsymbol{\theta}} \tag{7.12}$$

and the resulting acceleration $\vec{a}\,(t)$ can be deduced as follows

$$\vec{a}(t) = \frac{d\vec{v}(t)}{dt} = \left[\frac{dv_r}{dr}\underbrace{\frac{dr}{dt}}_{v_r} - r\,v_\theta^2\right]\hat{\boldsymbol{r}} + \left[r\left(\frac{dv_\theta}{dr}\underbrace{\frac{dr}{dt}}_{v_r} + \frac{dv_\theta}{d\theta}\underbrace{\frac{d\theta}{dt}}_{v_\theta}\right) + 2\,v_r\,v_\theta\right]\hat{\boldsymbol{\theta}}$$

which gives

$$\begin{aligned}\vec{a}(t) \;=\; & \left[v_0^2\,\alpha\left(\frac{r_1^{\alpha}}{r^{\alpha+1}}\right)\left(1-\left(\frac{r_1}{r}\right)^{\alpha}\right) - v_1^2\,(\sin\theta)^2\left(\frac{r_1^{2\beta}}{r^{2\beta+1}}\right)\right]\hat{\boldsymbol{r}} + \\ & \left[\left(-v_1\,v_0\,\sin\theta\left(\frac{r_1^{\beta}}{r^{\beta+1}}\right)(1+\beta)\right)\left(1-\left(\frac{r_1}{r}\right)^{\alpha}\right) + \right. \\ & v_1^2\,\cos\theta\,\sin\theta\left(\frac{r_1^{2\beta}}{r^{2\beta+1}}\right) + \\ & \left. 2\,v_0\,v_1\,\sin\theta\left(\frac{r_1^{\beta}}{r^{\beta+1}}\right)\left(1-\left(\frac{r_1}{r}\right)^{\alpha}\right)\right]\hat{\boldsymbol{\theta}}\,.\end{aligned} \tag{7.13}$$

Now let us see how the acceleration (7.13) looks like when we are dropping the terms that should vanish at $r = \infty$.

$$\vec{a}(t) \approx \left[v_0^2\,\alpha\left(\frac{r_1^{\alpha}}{r^{\alpha+1}}\right)\right]\hat{\boldsymbol{r}} + \left[v_1\,v_0\,\sin\theta\,(1-\beta)\left(\frac{r_1^{\beta}}{r^{\beta+1}}\right)\right]\hat{\boldsymbol{\theta}} \tag{7.14}$$

In the small θ limit, (7.14) finally becomes

$$\vec{a}(t) \approx \left[v_0^2\,\alpha\left(\frac{r_1^{\alpha}}{r^{\alpha+1}}\right)\right]\hat{\boldsymbol{r}} + \left[v_1\,v_0\,\theta\,(1-\beta)\left(\frac{r_1^{\beta}}{r^{\beta+1}}\right)\right]\hat{\boldsymbol{\theta}} \tag{7.15}$$

We want the above-obtained acceleration (7.14) (when r is big) to look like the embedded acceleration found in the non relativistic "quantized" force $\mathbf{F}$ (given by (6.13)) on Landau state due to a varying magnetic field that acts on a particle far from the origin, near to the z-axis and in the direction of the magnetic field, i.e.

$$\mathbf{F} = m\,\vec{a} \approx \underbrace{\left(\frac{\mu_0\,\mu_d}{4\pi}\right)\left(\frac{\hbar q}{m}\right)\left(n_L + \frac{1}{2}\right)}_{a_{n_L}}\left(\frac{3}{2\,r^4}\right)\left[4\,\hat{\boldsymbol{r}} + \theta\,\hat{\boldsymbol{\theta}}\right] \tag{7.16}$$

Note that the n_L above designates the quantum number that determined the *Landau levels or states*, not to be confused with the number density n. Thus giving in the $\hat{\boldsymbol{r}}$ direction

$$\left[m\, v_0^2\, \alpha \left(\frac{r_1^\alpha}{r^{\alpha+1}}\right)\right] = a_{n_L} \left(\frac{3 \cdot 2}{r^4}\right) \tag{7.17}$$

and in the $\hat{\boldsymbol{\theta}}$ direction

$$\left[m\, v_1\, v_0\, \theta\, (1-\beta) \left(\frac{r_1^\beta}{r^{\beta+1}}\right)\right] = a_{n_L} \left(\frac{3\,\theta}{2\, r^4}\right) . \tag{7.18}$$

We could then first conclude from (7.17) and (7.18) that $\alpha = \beta = 3$. Thus

$$a_{n_L} = \frac{m\, v_0\, v_0\, r_1^3}{2} = -\frac{m\, v_1\, v_0\, r_1^3\, 4}{3} \tag{7.19}$$

i.e.

$$v_1 = -\frac{3}{8}\, v_0 \quad where \quad v_0 = \left(\frac{2\, a_{n_L}}{m\, r_1^3}\right)^{1/2} . \tag{7.20}$$

Using $\alpha = \beta = 3$ and (7.20) above, the velocity fields in spherical coordinates (7.12) become

$$\vec{v}\,(t) = \vec{v}\,(r, \theta, n_L) = \underbrace{v_0 \left(1 - \left(\frac{r_1}{r}\right)^3\right)}_{v_r} \hat{\boldsymbol{r}} \quad \underbrace{- \left(\frac{3}{8}\right) v_0 \sin\theta \left(\frac{r_1}{r}\right)^3}_{v'_\theta} \hat{\boldsymbol{\theta}} . \tag{7.21}$$

This, of course, ignores terms that vanish faster than $1/r^3$. The resulting velocity above is then quantized through the n_L term embedded into the initial velocity v_0, as demonstrated in figure 7.2 and figure 7.3. Both figures confirm that our solutions satisfy the conditions $v_r\,(r = \infty) = v_0$ and $v_\theta\,(r = \infty) = 0$. In fact, both figures reveals that the θ dependence of the velocity $\vec{v}$ vanishes very quickly, again in agreement with our intuition.

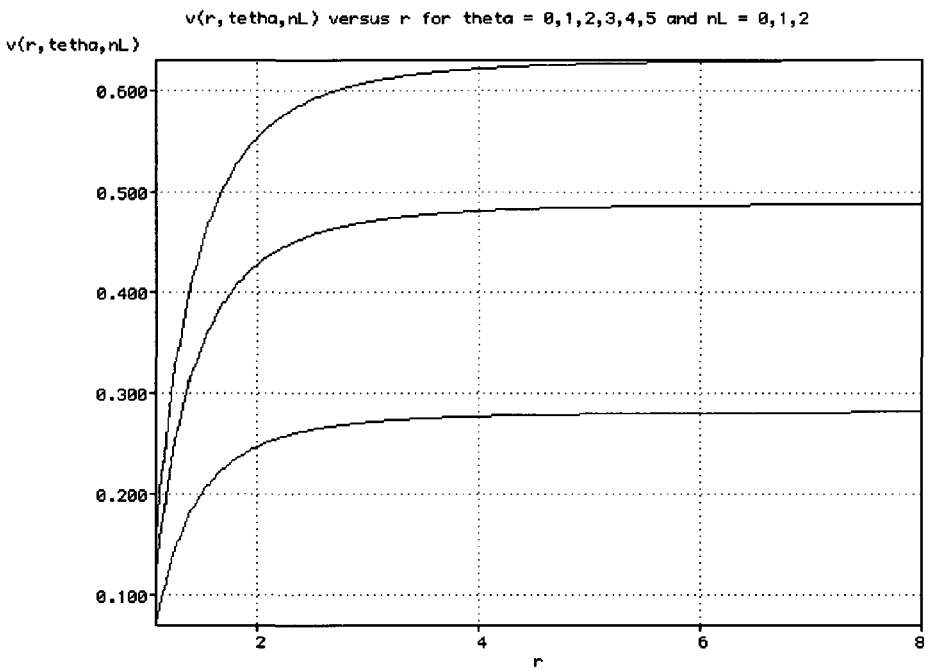

Figure 7.2: The particle velocity $\vec{v}(r, \theta, n_L)$ versus r for $\theta = 0°$ to $5°$ and for $n_L = 0$ (lowest red curve), $n_L = 1$ (blue curve), and $n_L = 2$ (highest red curve); when $m = q = \hbar = \mu = \mu_d = r_1 = 1$.

It is now time to verify the conservation equation (7.2). Let us start by calculating the divergence of $\vec{v}$ in spherical coordinates when we are imposing that $\dot{\phi} = \ddot{\phi} = 0$. So

$$\nabla \cdot \mathbf{v} = \frac{1}{r^2} \frac{\partial}{\partial r} \left(r^2 v_r\right) + \frac{1}{r \sin\theta} \frac{\partial}{\partial \theta} \left(v'_\theta \sin\theta\right) \tag{7.22}$$

Inserting now (7.21) into (7.22), we get

$$\nabla \cdot \mathbf{v} = v_0 \left[\left(\frac{2}{r} + \frac{r_1^3}{r^4}\right) - \left(\frac{3}{4} \frac{r_1^3}{r^4} \cos\theta\right)\right] . \tag{7.23}$$

In spherical coordinates, after imposing $\dot{\phi} = \ddot{\phi} = 0$, the gradient of the scalar density n in spherical coordinates is

$$\nabla n = \frac{\partial n}{\partial r} \hat{\boldsymbol{r}} + \frac{1}{r} \frac{\partial n}{\partial \theta} \hat{\boldsymbol{\theta}} \tag{7.24}$$

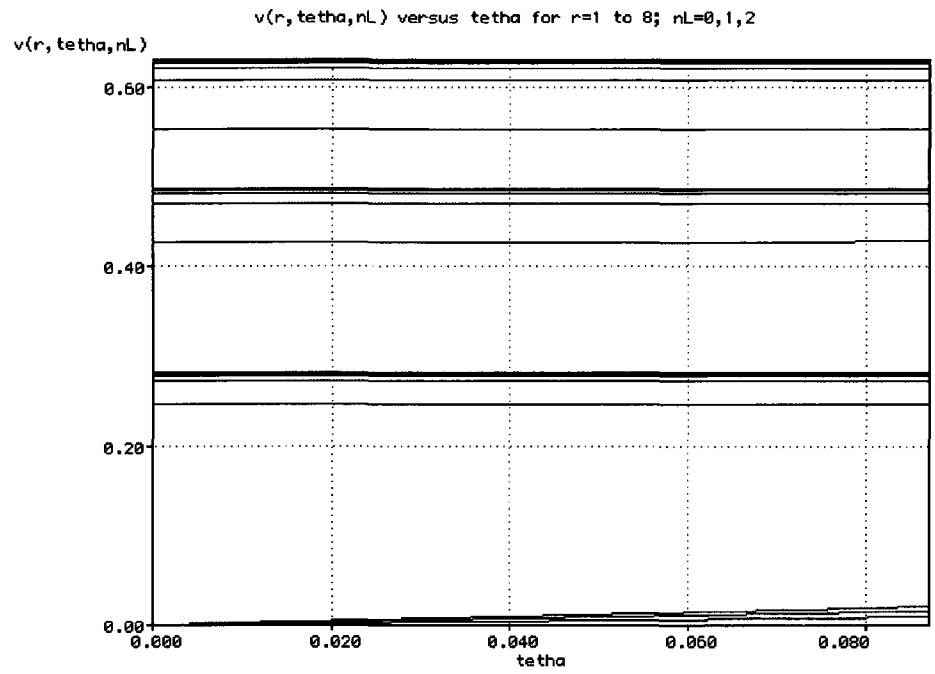

Figure 7.3: The particle velocity $\vec{v}(r,\theta,n_L)$ versus θ for $r = 1$ to 8, $n_L = 0$ (lowest red-to-blue series of curves), $n_L = 1$ (middle red-to-blue series of curves), $n_L = 2$ (highest red-to-violet series of curves); when $m = q = \hbar = \mu = \mu_d = r_1 = 1$.

The conservation equation (7.2) becomes with the help of (7.21), (7.23) and (7.24)

$$\underbrace{\left(\frac{\partial n}{\partial r}\hat{\boldsymbol{r}} + \frac{1}{r}\frac{\partial n}{\partial \theta}\hat{\boldsymbol{\theta}}\right)}_{\vec{\nabla}\, n} \cdot \underbrace{\left[v_0\left(1-\left(\frac{r_1}{r}\right)^3\right)\hat{\boldsymbol{r}} - \left(\frac{3}{8}\right)v_0 \sin\theta \left(\frac{r_1}{r}\right)^3 \hat{\boldsymbol{\theta}}\right]}_{\vec{v}} + n \underbrace{v_0\left[\left(\frac{2}{r}+\frac{r_1^3}{r^4}\right) - \left(\frac{3}{4}\frac{r_1^3}{r^4}\cos\theta\right)\right]}_{\vec{\nabla}\cdot\vec{v}} = 0 \quad (7.25)$$

which is reorganized and simplified by multipling it by r^4/r_1^3. This gives

$$\frac{\partial n}{\partial r}\, r\left(\frac{r^3}{r_1^3}-1\right) + n\left(\frac{2\,r^3}{r_1^3}+1\right) - \frac{\partial n}{\partial \theta}\left(\frac{3}{8}\right)\sin\theta - n\left(\frac{3}{4}\cos\theta\right) = 0 \quad (7.26)$$

which is obviously separable. Putting

$$n(r,\theta) = \rho(r)\,\Theta(\theta) \quad (7.27)$$

we obtain

$$\frac{1}{\rho}\frac{\partial \rho}{\partial r}\, r\left(\frac{r^3}{r_1^3}-1\right)+\left(\frac{2\,r^3}{r_1^3}+1\right)=\frac{1}{\Theta}\frac{\partial \Theta}{\partial \theta}\left(\frac{3}{8}\right)\sin\theta+\left(\frac{3}{4}\,\cos\theta\right)=k \tag{7.28}$$

or

$$\frac{\partial \rho}{\rho}\;=\;\frac{k\;-\;\left(\frac{2\,r^3}{r_1^3}+1\right)}{r\left(\frac{r^3}{r_1^3}-1\right)}\,\partial r\;=\;\frac{(k-1)\;r_1^3\;-\;2\,r^3}{r\,(r^3\;-\;r_1^3)}\,\partial r \tag{7.29}$$

and

$$\frac{\partial \Theta}{\Theta}\;=\;2\,\left(\frac{4\,k}{3\,\sin\theta}\;-\;\cot\theta\right)\,\partial\theta\;. \tag{7.30}$$

In the small θ limit, (7.30) becomes

$$\frac{\partial \Theta}{\Theta}\;=\;\left(\frac{8\,k}{3}\;-\;2\right)\,\frac{\partial\theta}{\theta} \tag{7.31}$$

Both logarithmic derivatives above can be evaluated exactly. For Θ, one gets (always in the small θ limit) from above

$$\Theta_k\,(\theta)\;=\;\theta^{\left(\frac{8\,k}{3}\;-\;2\right)}\;=\;\theta^{\eta}\;=\;\Theta_\eta\,(\theta) \tag{7.32}$$

As far as $\rho(r)$ is concerned, it becomes

$$\ln\rho\;=\;(k-1)\;r_1^3\int\frac{dr}{r\;(r^3\;-\;r_1^3)}\;-\;2\int\frac{r^2\;dr}{(r^3\;-\;r_1^3)} \tag{7.33}$$

and

$$\ln\rho\;=\;(k-1)\;r_1^3\,\left(\frac{-1}{3\,r_1^3}\right)\,ln\left(\frac{r^3}{r^3\;-\;r_1^3}\right)\;+c_1\;-\;2\,\left(\frac{1}{3}\right)\,ln\left(r^3\;-\;r_1^3\right)\;+c_2 \tag{7.34}$$

which finally gives

$$\rho_k(r)=\frac{\left(r^3\;-\;r_1^3\right)^{\frac{k-3}{3}}}{r^{k-1}}=\frac{1}{r^2}\left(1-\left(\frac{r_1}{r}\right)^3\right)^{\frac{k-3}{3}}=\frac{1}{r^2}\left(1-\left(\frac{r_1}{r}\right)^3\right)^{\frac{\eta-6}{8}}=\rho_\eta(r) \tag{7.35}$$

note that $r^3 > r_1^3$ so there are no singularities. One also notices that $\Theta_k\,(\theta)$ and $\rho_k(r)$ were rewritten as $\Theta_\eta\,(\theta)$ and $\rho_\eta(r)$ in (7.32) and (7.35) respectively. The general solutions for

the number density (7.27) then becomes (when we superpose different solutions for specic value of η)

$$n(r,\theta)_\eta = \rho_\eta(r)\ \Theta_\eta(\theta) = \frac{1}{r^2}\left(1-\left(\frac{r_1}{r}\right)^3\right)^{-\frac{3}{4}} \sum_\eta A_\eta \left[\left(1-\left(\frac{r_1}{r}\right)^3\right)^{\frac{1}{8}}\theta\right]^\eta . \qquad (7.36)$$

We want that (7.36) have a finite solution. This could be achieved by using a judicious choice: $A_\eta = D(-1)^\eta/\eta!$, where η is an integer. Thus we can sum the series explicitly since $e^{-x} = \sum_{\eta=0}(-1)^\eta x^\eta/\eta!$. The number density (7.36) can be rewritten as

$$n(r,\theta) = D\,\frac{1}{r^2}\left(1-\left(\frac{r_1}{r}\right)^3\right)^{-\frac{3}{4}} e^{-\left(1-\left(\frac{r_1}{r}\right)^3\right)^{\frac{1}{8}}\theta} \qquad (7.37)$$

To determine $n(r,\theta)$, we can start from an explicit distribution at the surface of the star. We choose a constant density at the surface $r = r_0$ then $n(r_0,\theta) = n_0$. The constant D in (7.37) can first be determined. Finally, the number density becomes

$$n(r,\theta) = n_0\left(\frac{r}{r_0}\right)^{\frac{1}{4}}\left(\frac{r_0^3-r_1^3}{r^3-r_1^3}\right)^{\frac{3}{4}} e^{\left(\left(\frac{\left(r_0^3-r_1^3\right)}{r_0^3}\right)^{\frac{1}{8}}-\left(\frac{\left(r^3-r_1^3\right)}{r^3}\right)^{\frac{1}{8}}\right)\theta} . \qquad (7.38)$$

The figures 7.4 and 7.5 illustrate the behavior of the number density $n(r,\theta)$ versus r and θ respectively. Both figures confirm that the number density n decreases with r. They also reveal that θ has no influence on the resulting number density n when r is growing.

Finally, putting the velocity fields (7.21) and the number density (7.38) in spherical coordinates into the current density relation (7.1); the "quantized" current density becomes

$$\begin{aligned}\vec{j}(r,\theta,n_L) &= qn_0v_0\left(\frac{r}{r_0}\right)^{\frac{1}{4}}\left(\frac{r_0^3-r_1^3}{r^3-r_1^3}\right)^{\frac{3}{4}} e^{\left(\left(\frac{\left(r_0^3-r_1^3\right)}{r_0^3}\right)^{\frac{1}{8}}-\left(\frac{\left(r^3-r_1^3\right)}{r^3}\right)^{\frac{1}{8}}\right)\theta} \times \\ &\left[\left(1-\left(\frac{r_1}{r}\right)^3\right)\hat{\boldsymbol{r}} - \left(\frac{3}{8}\right)\sin\theta\left(\frac{r_1}{r}\right)^3\hat{\boldsymbol{\theta}}\right] . \qquad (7.39)\end{aligned}$$

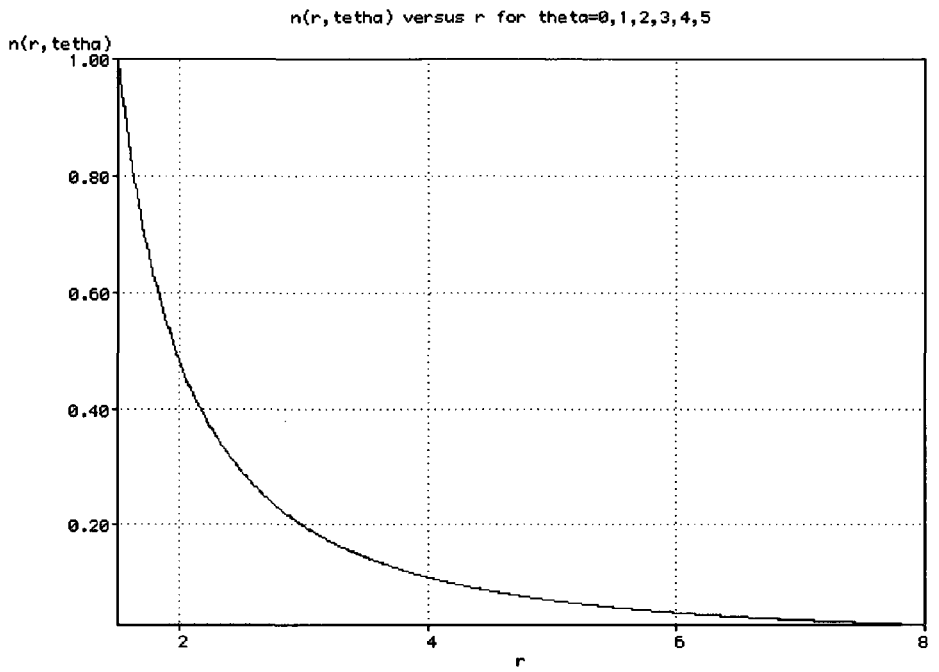

Figure 7.4: The number density $n(r, \theta)$ versus r for $\theta = 0°$ to $5°$; when $n_0 = r_1 = 1$ and $r_0 = 1.5\ r_1$.

The figures 7.6 and 7.7 illustrate the behavior of the current density versus r, θ and n_L. These have the expected form: *near the z-axis (i.e. when $\theta \approx 0$); the current density falls off rapidly with r, and the particle speed firstly increases and is asymptotically constant as $r \to \infty$.* These are exactly the expected features of an astrophysical jet!

Through the particle velocity (7.21), which is now quantized through the n_L term embedded into the initial velocity v_0, we can determine the jet velocity for each *Landau state.* Now the challenge is to determine the initial number density n_0 present in the relations (7.38) and (7.39) for each *Landau state.* This will be achieved in the next chapter.

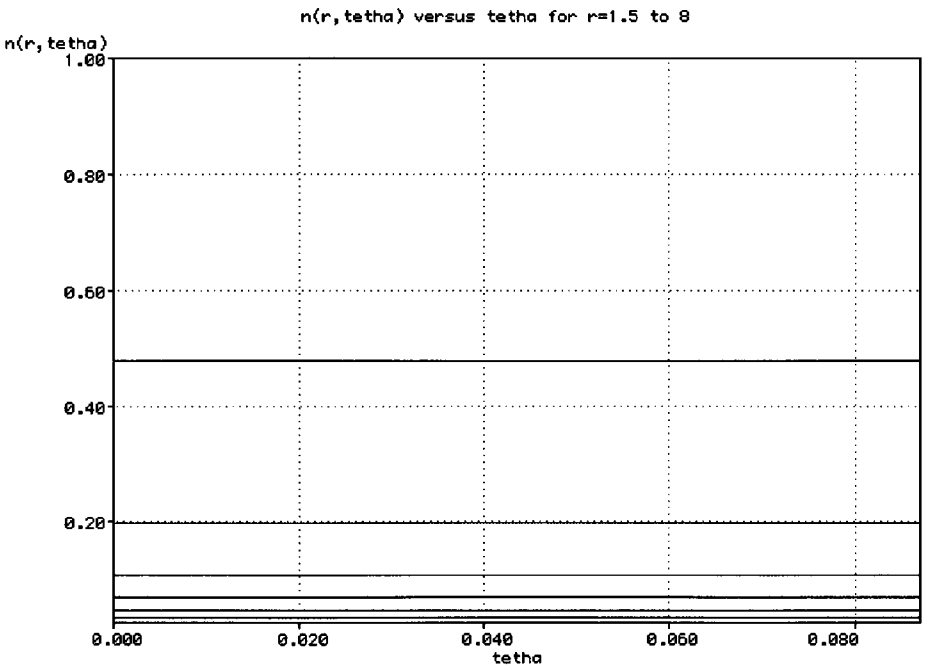

Figure 7.5: The number density $n(r, \theta)$ versus θ for $r = 1.5$ (highest curve) to 8 (lowest curve); when $n_0 = r_1 = 1$ and $r_0 = 1.5\ r_1$.

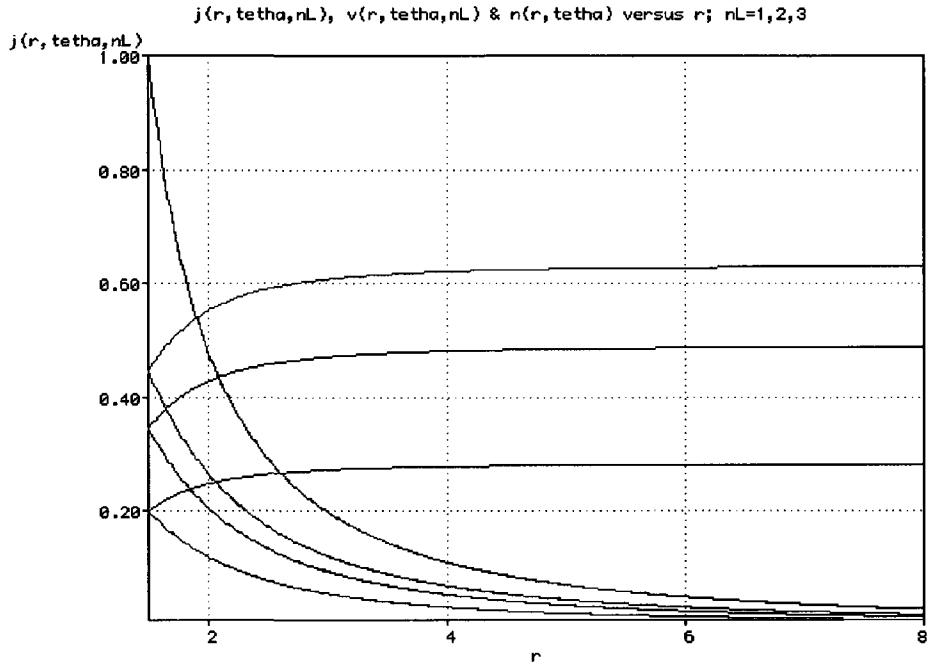

Figure 7.6: The particle velocity $\vec{v}(r, \theta, n_L)$, the number density $n(r, \theta)$ and the current density $j(r, \theta)$ versus r for $\theta = 0°$ to $5°$ and for $n_L = 0$ (lowest 2 red curves), $n_L = 1$ (middle 2 blue curves), and $n_L = 2$ (highest 2 red curves); when $m = q = \hbar = \mu = \mu_d = r_1 = n_0 = r_1 = 1$ and $r_0 = 1.5\ r_1$.

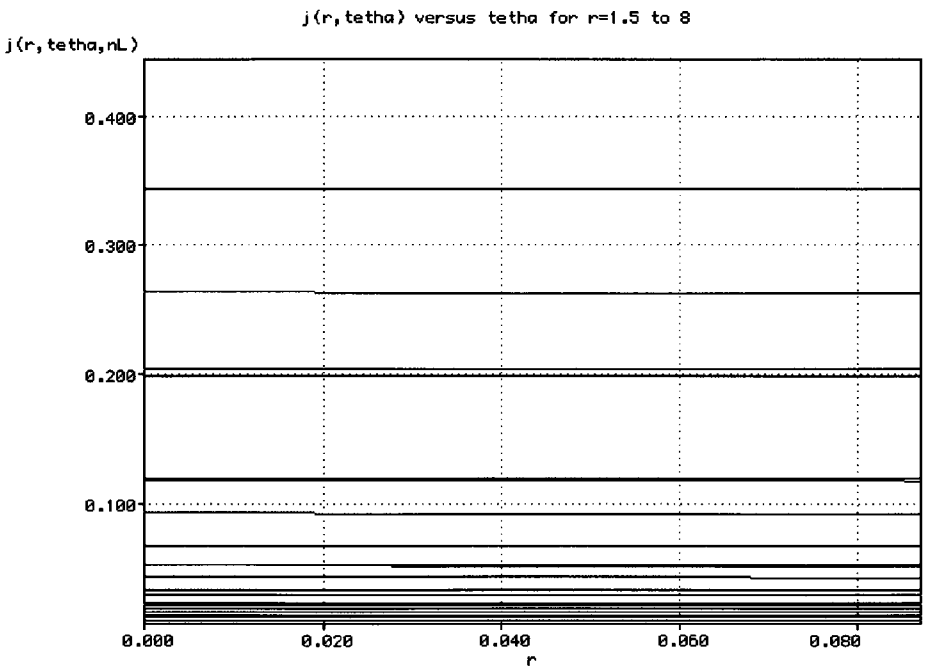

Figure 7.7: The current density $j(r, \theta)$ versus θ for $r = 1.5$ to 8 and and for $n_L = 0, 1$ and 2; when $m = q = \hbar = \mu = \mu_d = r_1 = n_0 = r_1 = 1$ and $r_0 = 1.5\ r_1$.

Chapter 8

The Quasi-Realistic Jet Propulsion Mechanism

It is now time to determine the initial number density n_0 introduced in the previous chapter for different values of n_L and see its impact once reintroduced into the current density relation. It is also time to propose the Jet Propulsion Mechanism based on Landau states. *We have up to now considered a single particle. However we know that if an electron is in an excited Landau state, it will decay very rapidly to the ground state, with a rate given approximately by the cyclotron frequency [25]. In practice, there will be a high density of electrons, and so this decay will be "Pauli-blocked", i.e. there will be no vacant states for the electron to decay to and so the acceleration will be ongoing.*

8.1 Degeneracy of Landau Levels

Our work using the *Landau gauge* in a uniform magnetic field revealed that the solution of the Schrödinger equation was just the solution for a simple harmonic oscillator whose equilibrium point is shifted from $y = 0$ to $y = y_0$ where $y_0 = -\hbar k_x/qB_z$. In the corresponding

classical motion the charged particles moves in an helix of constant radius, constant energy (recall (4.26)), constant rotation frequency (namely the cyclotron frequency $\omega_c = qB_z/m$) and constant z velocity, as illustrated in figure 4.1.

The following discussion follows that in Singh [36]. If the charged particle is confined to an area whose x-length is L_x and y-length is L_y, then the boundary condition in the x-direction,

$$\psi(x) = \psi(x + L_x) \ . \tag{8.1}$$

As the *Landau states* given by (4.26) are obviously degenerate in k_x, we will focus on this wavenumber for the free-particle motion decribed by $e^{ik_x x}$. The periodic boundary conditions expressed in (8.1) implies that k_x cannot be continuous, but must satisfy $e^{ik_x L_x} = 1$, which means that

$$k_x = \frac{2\pi n_x}{L_x}; \text{ where } n_x = 0, \pm 1, \pm 2, \ldots \tag{8.2}$$

The presence of a uniform magnetic field, the motion of the charged particle becomes a helical motion where y_0 is associated with the center of the corresponding classical circular motion. In such a situation, n_x values are positive numbers and we may take y_0 to lie in

$$0 \leq |y_0| \leq L_y \tag{8.3}$$

Putting now $|y_0|$, (8.2) and (8.3), one can deduce

$$0 \leq n_x \leq \frac{qB_z}{\hbar}\left(\frac{L_x L_y}{2\pi}\right) = \frac{L_x L_y}{2\pi l_B^2}; \text{ where } n_x = 0, 1, 2, \ldots \tag{8.4}$$

where $l_B = \sqrt{\hbar/qB_z}$, whose value is 2.567 x 10^{-8} m $/\sqrt{B_z(\text{tesla})}$, represents the magnetic length.

Since the area of the sample is $L_x\ L_y$, the maximum number of states per unit area of a full Landau level is therefore

$$\bar{n}_x = \frac{qB_z}{2\pi\hbar} = \frac{1}{2\pi l_B^2} \equiv \tilde{g} \tag{8.5}$$

where $\bar{n}_x$ represents the desired expression for the degeneracy $\tilde{g}$ of a *Landau States*. From (4.26), we can now deduce that the energy spacing between two adjacent Landau levels is proportional to

$$\triangle E = E_{n+1} - E_n = \hbar\omega_c = \frac{\hbar q B_z}{m} = \frac{\hbar^2}{m l_B^2}\ . \tag{8.6}$$

Finally, the number of states in the presence of magnetic field per unit area can then be determined when combining (8.5) and (8.6) by

$$\frac{d\bar{n}_x}{dE} = \frac{\bar{n}_x}{\hbar\omega_c} = \frac{m}{2\pi\hbar^2} \tag{8.7}$$

This is the same result as the two-dimensional density of state in the $x-y$ plane for a free particle [36]. Thus, on the macroscopic energy scale, the density of states is unaffected by the presence of a magnetic field.

In the one-dimensional k_z-space, the relation E versus k_z relation found in (4.26) gives the band-structure and the density of states. The density of states is then (for a particular Landau level with energy starting at E_n, and taking account this time the spin degeneracy) [36]

$$g_{1D}(E) = \frac{2}{L_z}\frac{dn}{dE} = \frac{2}{L_z}\frac{dn}{dk}\frac{dk}{dE} = \frac{2^{1/2}m^{1/2}}{\pi\hbar}\sum_n \frac{1}{\sqrt{E-E_n}}\ . \tag{8.8}$$

The density of states of the three-dimensional system in the presence of magnetic field is essentially given by an "one-dimensional density of states" given by (8.8), weighted by the two-dimensional degeneracy factor found in (8.5). The three-dimensional density becomes

(upon summing the contribution from all Landau levels with starting energies less than E):

$$g_{3D}(E) = g_{1D}(E)\,\frac{1}{L_x L_y}\frac{dn_x}{dE}\,\hbar\omega_c = \frac{1}{4\pi^2}\left(\frac{2m}{\hbar^2}\right)^{\frac{3}{2}}\hbar\omega_c \sum_n \frac{1}{\sqrt{E-\hbar\omega_c\left(n+\frac{1}{2}\right)}}\,. \tag{8.9}$$

The three-dimensional non relativistic density of states is shown in figure 8.1.

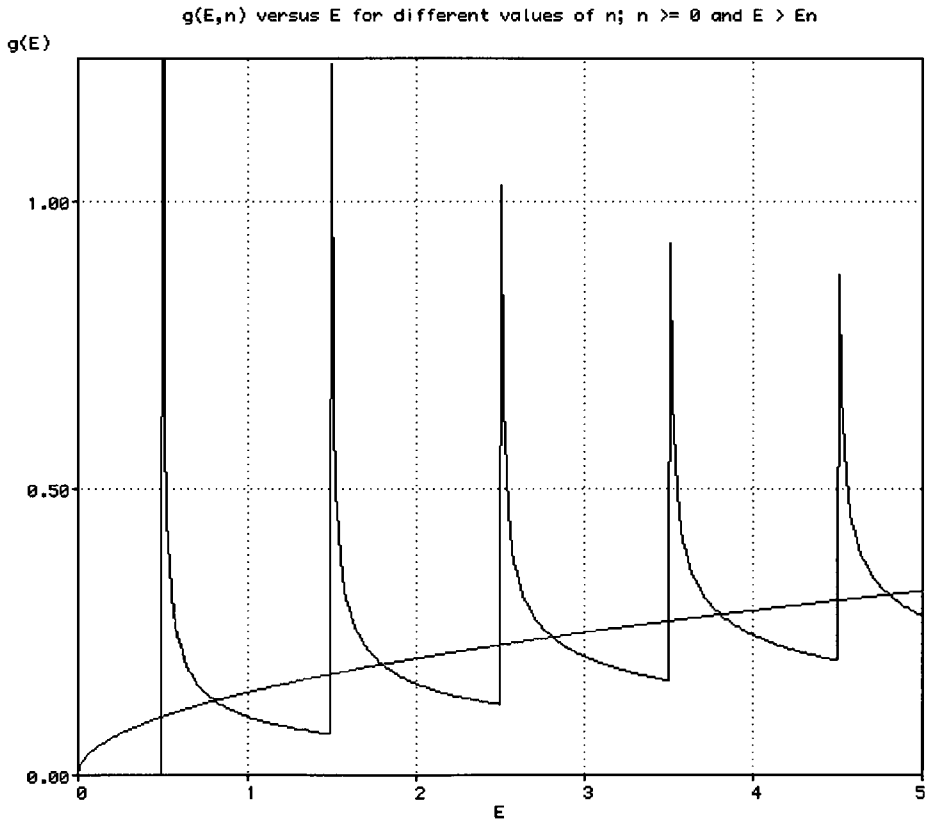

Figure 8.1: Non-relativistic 3D density of states in presence of magnetic field (black curve showing some singularities) compared to the continuous 3D density of states in zero field (red curve); for $\hbar = m = B = q = 1$

For finding the "one-dimensional relativistic density of states", we simply need to re-

place the non relativistic E_n versus k_z relation found in by (4.26) by the relativistic one deduced in (4.71), i.e.

$$E = \underbrace{\hbar\omega_c\left(n+\frac{1}{2}-\frac{gm_s}{2}\right)}_{E_n}+\frac{\hbar^2k_z^2}{2m} \;\Rightarrow\; \hat{E}^2 = \underbrace{c^2|q|\hbar\mathbf{B}_z 2n}_{\hat{E_n}^2}+\hbar^2k_z^2c^2+m^2c^4 \tag{8.10}$$

where $\hat{E}$ and $\hat{E}_n$ are the relativistic energies. The density of states is then (for a particular Landau level with energy starting at E_n and not taking account the spin degeneracy yet)

$$g_{1D}(E) = \frac{1}{L_z}\frac{dn}{dk}\frac{dk}{dE} = \frac{1}{\pi\hbar c}\sum_n \frac{\hat{E}}{\sqrt{\hat{E}^2-\left(\hat{E_n}^2+m^2c^4\right)}} = \frac{1}{\pi\hbar c}\sum_n \frac{\hat{E}}{\sqrt{\hat{E}^2-(c^2|q|\hbar\mathbf{B}_z 2n+m^2c^4)}} \tag{8.11}$$

As we derived before, the relativistic density of states of the three-dimensional system in the presence of magnetic field is essentially given by an "one-dimensional density of states" given by (8.11), weighted by the two-dimensional degeneracy factor found in (8.5). The three-dimensional relativistic density becomes, once we add the contribution from all Landau levels with starting energies less than E and not taking account the spin degeneracy yet:

$$g_{3D}(E) = \frac{qB_z}{2\pi^2\hbar^2c}\sum_n \frac{\hat{E}}{\sqrt{\hat{E}^2-(c^2|q|\hbar\mathbf{B}_z 2n+m^2c^4)}}\,. \tag{8.12}$$

We can now take account the spin degeneracy. We have already said in section 4.2 that for the positive energy solutions, the $n=0$ state for an electron is not degenerate and only the solution for $s=-1$ exists. All the other states ($n>0$) are pairwise degenerate. Once applied on (8.12), this latter becomes

$$g_{3D}(E) = \frac{qB_z}{2\pi^2\hbar^2c}\left(\frac{\hat{E}}{\sqrt{\hat{E}^2-m^2c^4}}+2\sum_{n>0}\frac{\hat{E}}{\sqrt{\hat{E}^2-(c^2|q|\hbar\mathbf{B}_z 2n+m^2c^4)}}\right)\,. \tag{8.13}$$

The factor of 2 in the second term in (8.12) comes from the fact that all the levels (except the first) have two degenerate spin states. The three-dimensional relativistic density of states is shown in figure 8.2.

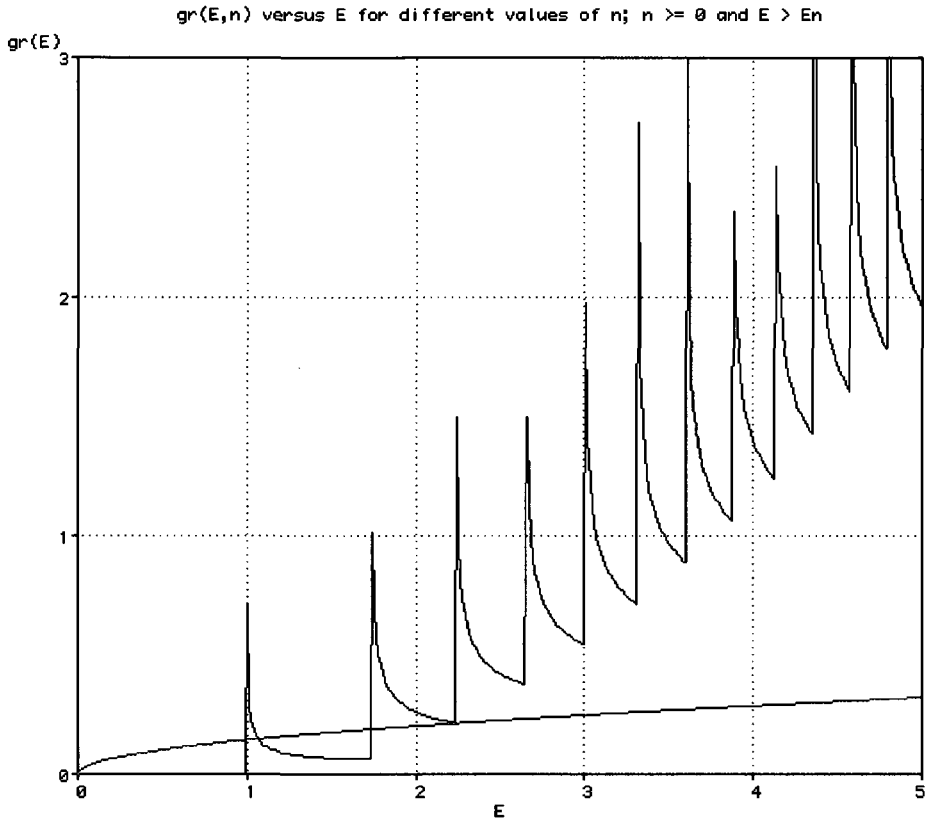

Figure 8.2: Relativistic 3D density of states in presence of magnetic field (black curve showing some singularities) compared to the continuous 3D density of states in zero field (red curve); for $\hbar = m = B = q = c = 1$.

8.2 The Landau-Fermi decay mechanism

Since we know now how to determine the non relativistic and relativistic densities of states of the three-dimensional system in the presence of a magnetic field, we have then all the components for determining the initial number density n_0 present in the relations (7.38) and (7.39) for each *Landau state*. The number density of charged particles n is obtained

by integrating the following product [26]

$$n(E) = \int g_{3D}(E)\ f(E)\ dE \tag{8.14}$$

The term $f(E)$ in (8.14) represents the Fermi-Dirac distribution.

$$f(E) = \frac{1}{1 + e^{\left(\frac{E-E_F}{k_B T}\right)}} \tag{8.15}$$

where $f(E)$ is the probability of occupancy of an electron with respect to the energy of state E at the absolute temperature T, E_F is the Fermi energy, k_B is Boltzmann's constant. At $T = 0$, we see on figure 8.3 that $f(E) = 1$ for $E < E_F$ and $f(E) = 0$ for $E > E_F$. At $T = 0K$, all levels are occupied up to the Fermi level. On the x-axis, i.e. at $f(E) = 0$, the exceeding of the curve after $E = E_F$ is equal to KT at finite temperatures. A good indicator of having a step function curve is then given by calculating the ratio $(E_F + kT)/E_F$. Should the result be as close as possible to 1, so a step function curve you get as Fermi-Dirac distribution.

Inserting the density of states of the three-dimensional system in the presence of a magnetic field (8.9) and the Fermi-Dirac distribution (8.15) into (8.14), one finds

$$n_0(E, n_L) = \frac{1}{4\pi^2}\left(\frac{2m}{\hbar^2}\right)^{\frac{3}{2}} \hbar\omega_c \sum_{n_L} \int_{E_{n_L}}^{\infty} \frac{1}{\sqrt{E - \hbar\omega_c\left(n_L + \frac{1}{2}\right)}} \left(\frac{1}{1 + e^{\left(\frac{E-E_F}{k_B T}\right)}}\right) dE. \tag{8.16}$$

Note that the n_L above designates the quantum number that determined the *Landau levels or states*, not to be confused with the number density n.

Let us now determine if the real condition $E - E_F \gg k_B T$ for the energies that transforms the Fermi-Dirac distribution curve into a step function (i.e. equal 1 when $E \leq E_F$ and 0 when $E > E_F$) at the surface of the neutron star are satisfied.

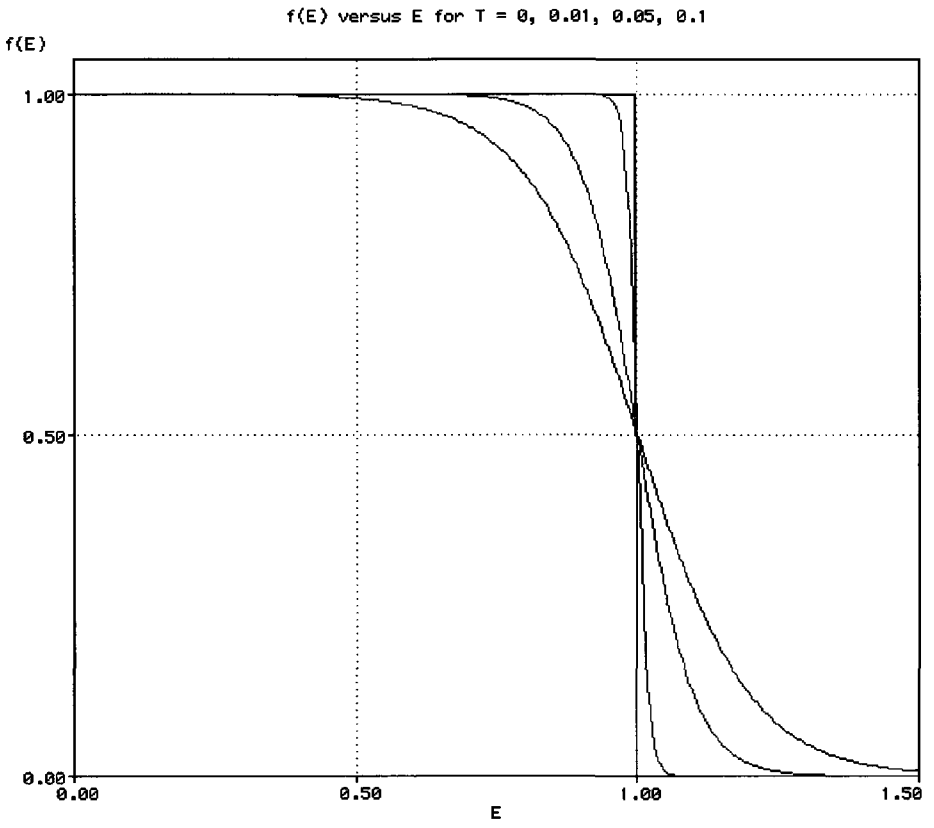

Figure 8.3: The Fermi-Dirac distribution $f(E)$ versus E for $T = 0$ (black), $T = 0.01$ (red), $T = 0.05$ (green) and $T = 0.1$ (blue); and for $E_F = k_B = 1$.

The effective surface temperature prevailing on the atmosphere of a hot neutron star is $T_s \approx 3 \times 10^6 K$ to $T_s \approx 3 \times 10^5 K$ for a cold one [18], which correspond to some $k_B T$ of 259 eV and 25.9 eV respectively.

Let us get some basic numbers about the Fermi energy of the electrons found in the atmosphere of a neutron star. If the energy and momentum are low, then the Fermi energy E_F is related to the Fermi momentum $p_F \approx \hbar/\triangle x$[1] by $E_F \approx p^2/2m$. Since $\triangle x \approx n^{-1/3}$,

[1]Here $\triangle x$ represents the size of a region where a particle is localized.

in this non relativistic regime $E_F \approx n^{2/3}$. At some point, however, $E_F > mc^2$. Then $E_F \approx p_F c$, so $E_F \approx n^{1/3}$ in the relativistic regime. For electrons, the crossover to relativistic Fermi energy, i.e. $E_F \approx mc^2 \approx 0.5MeV$, happens at a density $\rho \approx 10^6\ g/cm^3$, assuming a fully ionized plasma with two nucleons per electron. Consequently:

1. Each increase of the density of a factor ten in the non relativistic regime ($\rho \approx 10^6 < g/cm^3$) approximately quadruples the Fermi energy since $E_F \approx n^{2/3}$.

2. Each increase of the density of a factor ten in the relativistic regime ($\rho \approx 10^6 > g/cm^3$) approximately doubles the Fermi energy since $E_F \approx n^{1/3}$.

What that means is that the energetic "cost" of adding another electron to the system is not just mc^2, as it would be normally, but is $mc^2 + E_F$ in the relativistic regime. It therefore becomes less and less favorable to have electrons around as the density increases.

The table 8.1 gives the estimated Fermi energy with respect to the electron density from the neutron star atmosphere upper to the bottom boundaries, based on the simple rules enumerated above. Having in our hands the order of magnitude of the Fermi energy at different electron densities and the atmosphere surface temperature, the resulting ratio $(E_F + kT)/E_F$ has been presented in table 8.1 as well.

This confirms that the condition $E - E_F \gg k_B T$ is satisfied for the electron density greater than $10^3\ g/cm^3$: in other words we can treat the neutron star as "*cold*". We can then replace the Fermi-Dirac distribution relation in (8.16) by the desired step function. Moreover, the non relativistic density of states equations of the three-dimensional system in the presence of a magnetic field can be used for the electron densities from $10^3\ g/cm^3$

Table 8.1: Estimated Fermi energy with respect to the electron density from the neutron star's upper atmosphere to the bottom boundaries; for $T_s \approx 3 \times 10^6 K$ and $k_B T_s \approx 259\ eV$.

Regime	$\rho\ (\frac{g}{cm^3})$	E_F		$\frac{E_F+kT}{E_F}$
Non-relativistic	10^1	232	eV	2.12
	10^2	1.1	keV	1.24
	10^3	5.0	keV	1.05
	10^4	23.2	keV	1.01
	10^5	0.1077	MeV	1.00
Transition	10^6	0.5000	MeV	1.00
Relativistic	10^7	1.0772	MeV	1.00
	10^8	2.3208	MeV	1.00
	10^9	5.0000	MeV	1.00

up to $10^6\ g/cm^3$. The relativistic regime must be used for the electron density higher than $10^6\ g/cm^3$. Having said that, (8.16) becomes

$$n_0(E, n_L) = \frac{1}{4\pi^2}\left(\frac{2m}{\hbar^2}\right)^{\frac{3}{2}} \hbar\omega_c \sum_{n_L} \int_{E_{n_L}}^{E_F} \frac{dE}{\sqrt{E - \hbar\omega_c\left(n_L + \frac{1}{2}\right)}} \tag{8.17}$$

which finally gives

$$n_0(E_F, n_L) = \frac{1}{4\pi^2}\left(\frac{2m}{\hbar^2}\right)^{\frac{3}{2}} 4\ E_0 \sum_{n_L} \sqrt{E_F - E_0\,(2\ n_L + 1)} \tag{8.18}$$

once rewritten in term of $E_0 = \hbar\omega_c/2$. The figure 8.4 shows the non relativistic number density of the charged particles $n_0(E_F, n_L)$ versus the Fermi energy E_F.

Now let us assume that the transitions are instantaneous, i.e. if there is a vacancy in the $(n_L - 1)$ state, an electron in the n_L state will make an instant transition. Then

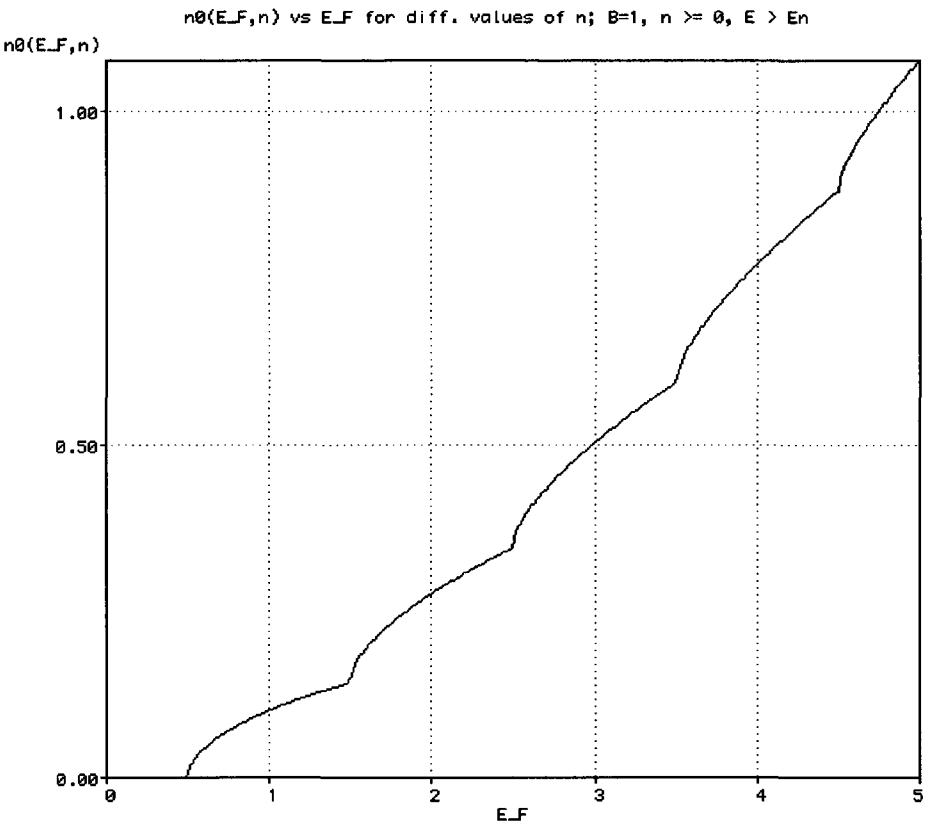

Figure 8.4: Non-relativistic $n_0(E_{\rm F}, n_L))$ versus $E_{\rm F}$ for different values of n, $n >= 0$, $E_F > E_n$ when $B = 1$.

electrons will decay to lowest *Landau state*. Now suppose we specialize to the system where only the lowest 1 or 2 states are occupied

$$n_0(E_{\rm F}, n_L = 0, 1) = \underbrace{\frac{1}{4\pi^2}\left(\frac{2m}{\hbar^2}\right)^{\frac{3}{2}} 4\ E_0\ \sqrt{E_{\rm F} - E_0}}_{n_0(E_{\rm F}, n_L=0)} + \underbrace{\frac{1}{4\pi^2}\left(\frac{2m}{\hbar^2}\right)^{\frac{3}{2}} 4\ E_0\ \sqrt{E_{\rm F} - 3\ E_0}}_{n_0(E_{\rm F}, n_L=0,1)} . \tag{8.19}$$

(8.19) now determines the initial number densities $n_0(E_{\rm F}, n_L = 0)$ and $n_0(E_{\rm F}, n_L = 1)$ present in the relation (7.38) defined in the previous chapter.

In relativistic regime, we insert the relativistic density of states of the three-dimensional system in the presence of magnetic field (8.12) and the Fermi-Dirac distribution (8.15) into (8.14), one finds

$$n_0(E,n_L)=\frac{qB_z}{2\pi^2\hbar^2c}\sum_{n_L}\int_{\hat{E}_{n_L}}^{\infty}\frac{\hat{E}}{\sqrt{\hat{E}^2-(c^2|q|\hbar\mathbf{B}_z2n_L+m^2c^4)}}\left(\frac{1}{1+e^{\left(\frac{E-E_F}{k_BT}\right)}}\right)d\hat{E}\ . \quad (8.20)$$

without spin degeneracy. Since table 8.16 confirms that the condition $E-E_F\gg k_BT$ is well met for the electron density greater than $10^6\ g/cm^3$ on the bottom atmosphere of the neutron star, we can still replace the Fermi-Dirac distribution relation in (8.16) by the desired step function. Thus

$$n_0(E,n_L)=\frac{qB_z}{2\pi^2\hbar^2c}\sum_{n_L}\int_{\hat{E}_{n_L}}^{\hat{E}_F}\frac{\hat{E}}{\sqrt{\hat{E}^2-(c^2|q|\hbar\mathbf{B}_z2n_L+m^2c^4)}}\,d\hat{E} \quad (8.21)$$

which finally gives

$$n_0(E,n_L)=\frac{qB_z}{2\pi^2\hbar^2c}\sum_{n_L}\sqrt{\hat{E}^2-(c^2|q|\hbar\mathbf{B}_z2n_L+m^2c^4)}\ . \quad (8.22)$$

Since for the positive energy solutions, the $n=0$ state for an electron is not degenerate and only the solution for $s=-1$ exists, and all the other states ($n>0$) are pairwise degenerate, (8.23) can be rewritten as

$$n_0(E,n_L)=\frac{qB_z}{2\pi^2\hbar^2c}\left(\sqrt{\hat{E}_F^2-m^2c^4}+2\sum_{n_L>0}\sqrt{\hat{E}_F^2-(c^2|q|\hbar\mathbf{B}_z2n_L+m^2c^4)}\right) \quad (8.23)$$

where $\hat{E}_F$ is the relativistic Fermi energy, and the sum is over values of n_L such that the square root is real. The factor of 2 comes from the fact that all the levels except the first have 2 degenerate spin states. The figure 8.5 shows the relativistic and non relativistic number density of the charged particles $n_0(E_F,n_L)$ versus the Fermi energy E_F.

We have then now all the required components for completing the Quasi-Realistic Jet Model. This will be achieved in the final chapter.

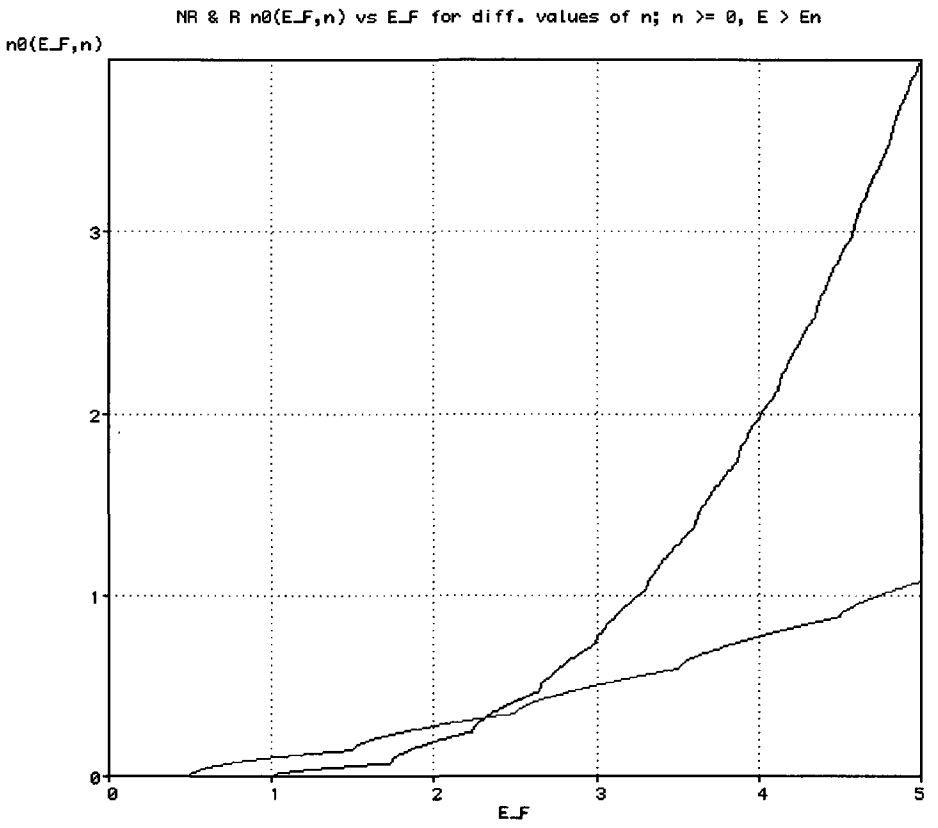

Figure 8.5: Relativistic (black curve) and Non-relativistic (red curve) $n_0(E_{\mathrm{F}}, n_L))$ versus E_{F} for different values of n, $n >= 0$, $E_F > E_n$ when $B = 1$.

8.3 First Quasi-Realistic Jet Propulsion Mechanism

Before concluding this chapter, we propose a potential Quasi-Realistic Jet Propulsion Mechanism that explains how the photons could be emitted when the density in the Landau states changes in the vicinity of a neutron star's surface and propelled via the astrophysical jets formed in the atmosphere of the neutron star.

We have previously learned that the spacing between Landau levels is determined by

the relation $\triangle E = \hbar\omega_c = \hbar q B_z/m$ (recall (8.6)). We have also learned that the dipole fields of a neutron star decrease as the cube of the distance. Consequently, in the upper atmosphere of the neutron star, where the magnetic field is relatively weak, the spacing between equal Landau levels are low. The highest energy states occupied is that the Fermi energy E_F. Because the Landau levels are close to each other in a such environment, it is easy to imagine that there are several levels below the "Fermi" level, where the occupancy rate for each levels (the Fermi level included) is given by (8.18).

A totally different situation happens at the bottom of the atmosphere of the neutron star, where the magnetic field is very strong: the spacing between equal Landau levels are huge. This change of the spacing between equal Landau levels in weak and strong magnetic field is illustrated in figure 8.6.

As a result, a low number of levels fall below the Fermi level, whose value E_F hasn't changed significantly compared with the one found in the upper atmosphere of the neutron star (recall that $E_F \approx n^{1/3}$ versus $B_z \approx 1/z^3$). We can also note that, through the de *Haas-van Alphen* effect [26], E_F exhibits a periodicity with respect of $1/B_z$ when B_z is increased, but its average amplitude remains the same.

Therefore, in the very strong magnetic field that exists close to the surface of the neutron star, only the lowest levels, say the ground state $n_L = 0$ and the first excited level $n_L = 1$, are occupied, with the occupancy rates given by (8.18).

However we know that if an electron is in an excited Landau state, it will decay very

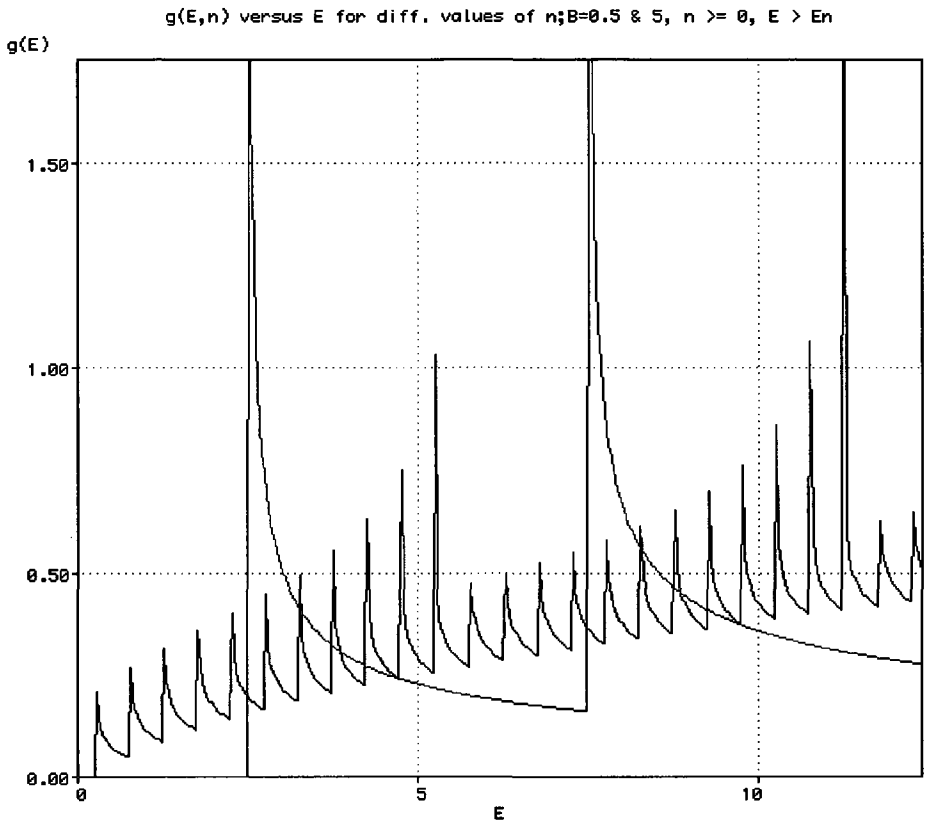

Figure 8.6: $g(E, n)$ versus E for different values of n, $n >= 0$, $E > E_n$ when $B = 1$ (black curve) and $B = 5$ (red curve).

rapidly to the ground state, with a rate given approximately by the cyclotron frequency [25]. Because of the very high density (or occupancy rate) of electrons at the ground state, this decay will be "Pauli-blocked", i.e. there will be no vacant states for the electron to decay, and so the acceleration will be ongoing. *It will then be propelled via the astrophysical jets formed in the atmosphere of the neutron star* we described in chapter 7.

Chapter 9

The Quasi-Realistic Jet Model - final version

9.1 The quasi-realistic jet model in spherical coordinates - final version

Since we learned how to determine the number density for different states, let us now put (8.19) into the relation (7.38)

$$n\left(r,\theta,n_L=0\right) = \underbrace{\frac{1}{4\pi^2}\left(\frac{2m}{\hbar^2}\right)^{\frac{3}{2}} 4\,E_0\,\sqrt{E_{\mathrm{F}}-E_0}}_{n_0(E_{\mathrm{F}},n_L=0)} \times \left(\frac{r}{r_0}\right)^{\frac{1}{4}} \left(\frac{r_0^3-r_1^3}{r^3-r_1^3}\right)^{\frac{3}{4}} e^{\left(\left(\frac{\left(r_0^3-r_1^3\right)}{r_0^3}\right)^{\frac{1}{8}}-\left(\frac{\left(r^3-r_1^3\right)}{r^3}\right)^{\frac{1}{8}}\right)\theta} \tag{9.1}$$

for the ground state. As far as the first excited state is concerned, it becomes

$$n\left(r,\theta,n_L=1\right) = \underbrace{\frac{1}{4\pi^2}\left(\frac{2m}{\hbar^2}\right)^{\frac{3}{2}} 4\,E_0\,\sqrt{E_{\rm F}-3\,E_0}}_{n_0(E_{\rm F},n_L=0,1)} \times \left(\frac{r}{r_0}\right)^{\frac{1}{4}}\left(\frac{r_0^3-r_1^3}{r^3-r_1^3}\right)^{\frac{3}{4}} e^{\left(\left(\frac{\left(r_0^3-r_1^3\right)}{r_0^3}\right)^{\frac{1}{8}}-\left(\frac{\left(r^3-r_1^3\right)}{r^3}\right)^{\frac{1}{8}}\right)\theta} \tag{9.2}$$

$n\left(r,\theta,n_L=0\right)$ and $n\left(r,\theta,n_L=1\right)$ are drawn in figure (9.1) for $E_F = 4\,E_0$, i.e. $n\left(r,\theta,n_L=0\right) = \sqrt{3}\,n\left(r,\theta,n_L=1\right)$.

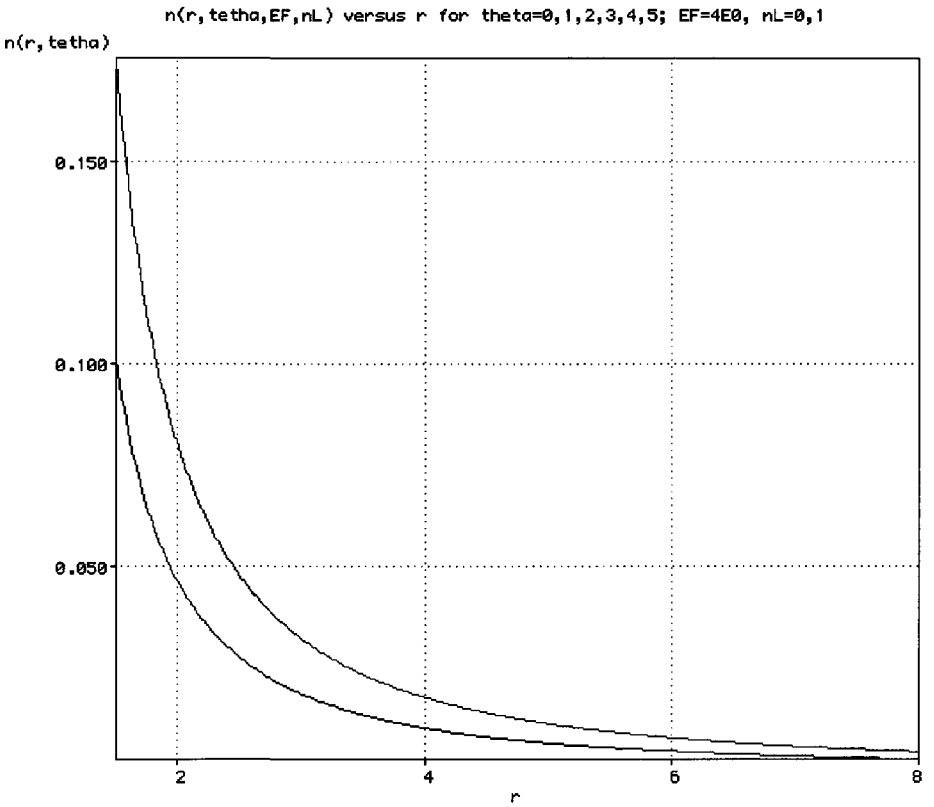

Figure 9.1: The number density $n\left(r,\theta,n_L\right)$ versus r for $\theta = 0°$ to $5°$, $n_L = 0$ (the red curve), $n_L = 1$ (the blue curve); when $E_F = 4E_0$, $r_1 = 1$ and $r_0 = 1.5\,r_1$.

We could determine the jet currents $\vec{j}\,(r,\theta,n_L)$ for each state by now just inserting the jet velocities for each state given by (7.21) in the small θ limit and the initial charge density for each state given by (9.1) and (9.2) into the quantized jet current relation expressed in (7.39). This gives for the ground state

$$\begin{aligned}\vec{j}\,(r,\theta,n_L=0) \;=\; & q\underbrace{\left(\frac{1}{m\,r_1^3}\right)^{1/2}\left(\frac{\mu_0\,\mu_d}{4\pi}\right)^{1/2}\left(\frac{\hbar q}{m}\right)^{1/2}}_{v_0(n_L=0)}\underbrace{\frac{1}{4\pi^2}\left(\frac{2m}{\hbar^2}\right)^{\frac{3}{2}}\,4\,E_0\,\sqrt{E_{\rm F}-E_0}}_{n_0(E_{\rm F},n_L=0)}\;\times \\ & \left(\frac{r}{r_0}\right)^{\frac{1}{4}}\left(\frac{r_0^3-r_1^3}{r^3-r_1^3}\right)^{\frac{3}{4}} e^{\left(\left(\frac{\left(r_0^3-r_1^3\right)}{r_0^3}\right)^{\frac{1}{8}}-\left(\frac{\left(r^3-r_1^3\right)}{r^3}\right)^{\frac{1}{8}}\right)\theta}\;\times \\ & \left[\left(1-\left(\frac{r_1}{r}\right)^3\right)\hat{\boldsymbol{r}}\;-\;\left(\frac{3}{8}\right)\theta\left(\frac{r_1}{r}\right)^3\hat{\boldsymbol{\theta}}\right]\;. \end{aligned} \tag{9.3}$$

For the first excited state, the jet current becomes

$$\begin{aligned}\vec{j}\,(r,\theta,n_L=1) \;=\; & q\underbrace{\left(\frac{3}{m\,r_1^3}\right)^{1/2}\left(\frac{\mu_0\,\mu_d}{4\pi}\right)^{1/2}\left(\frac{\hbar q}{m}\right)^{1/2}}_{v_0(n_L=1)}\underbrace{\frac{1}{4\pi^2}\left(\frac{2m}{\hbar^2}\right)^{\frac{3}{2}}\,4\,E_0\,\sqrt{E_{\rm F}-3\,E_0}}_{n_0(E_{\rm F},n_L=0,1)}\;\times \\ & \left(\frac{r}{r_0}\right)^{\frac{1}{4}}\left(\frac{r_0^3-r_1^3}{r^3-r_1^3}\right)^{\frac{3}{4}} e^{\left(\left(\frac{\left(r_0^3-r_1^3\right)}{r_0^3}\right)^{\frac{1}{8}}-\left(\frac{\left(r^3-r_1^3\right)}{r^3}\right)^{\frac{1}{8}}\right)\theta}\;\times \\ & \left[\left(1-\left(\frac{r_1}{r}\right)^3\right)\hat{\boldsymbol{r}}\;-\;\left(\frac{3}{8}\right)\theta\left(\frac{r_1}{r}\right)^3\hat{\boldsymbol{\theta}}\right]\;. \end{aligned} \tag{9.4}$$

The resulting jet current versus r for different values of Fermi Energy E_F, each for the ground state $n_L = 0$ and the first excited state $n_L = 1$ is displayed in figure (9.2).

The figure (9.2) reveals a new behavior for the current density: for low values of E_F, the current density decreases with n_L (lowest black and red curves in figure (9.2); for a high values of E_F, current density increases with n_L (highest black and red curves in figure (9.2). In between, there are certain values of E_F where the current density is totally independent of n_L (blue curve in figure (9.2)!

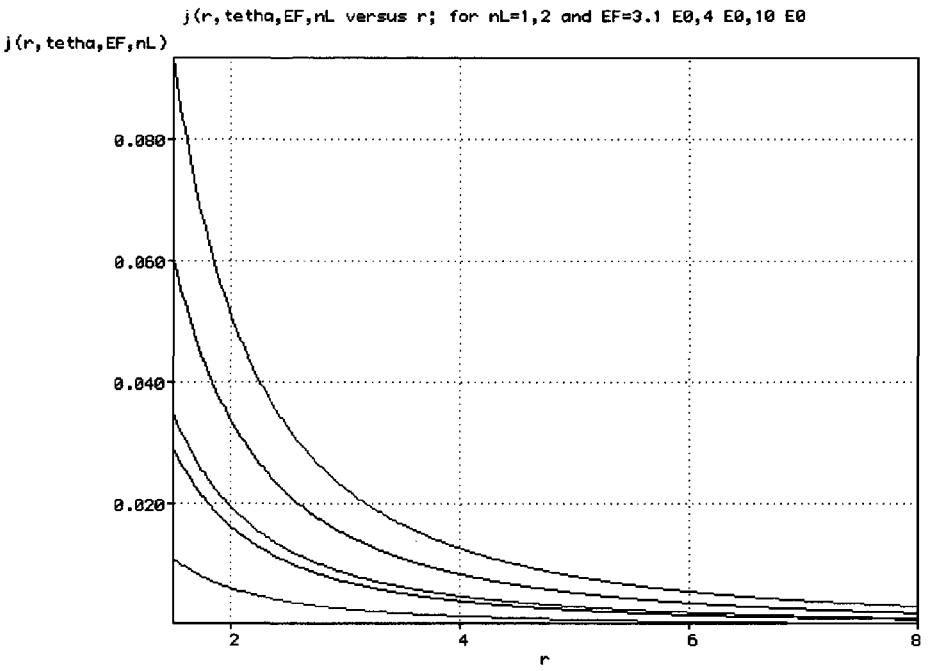

Figure 9.2: the jet currents $j\,(r,\theta,n_L)$ versus r; for $E_F = 3.1E_0$ and $n_L = 0$ (lowest black), 1 (lowest red); for $E_F = 4E_0$ and $n_L = 0$ and 1 (blue); for $E_F = 10E_0$ and $n_L = 0$ (hightest black), 1 (highest red).

This can be explained as follows. We found previously that the v_0 term in (7.1) goes with the square root of n_L (recall (7.20)) and (7.16)). We also recently found that the initial number density (8.18) goes with the square root of $(E_F - n_L)$. Once considered all together, the order of magnitude of the initial current can be written as

$$j_0\,(n_L, E_F) \propto v_0\; n_0 \approx \left(\left(n_L + \frac{1}{2}\right)\left(\frac{M-1}{2} - n_L\right)\right)^{\frac{1}{2}} \tag{9.5}$$

where $M > 2n_L + 1$ and M represents the linear factor between the Fermi energy and E_0, i.e. $E_F = ME_0 = M\hbar\omega_c/2$. We can then deduce from (9.5) that when M is big, j_0 goes with $\sqrt{Mn}$. When M is infinitesimal (say $M > 2n_L+1+\epsilon$, where $\epsilon \to 0$), j_0 goes with $\sqrt{n\epsilon}$.

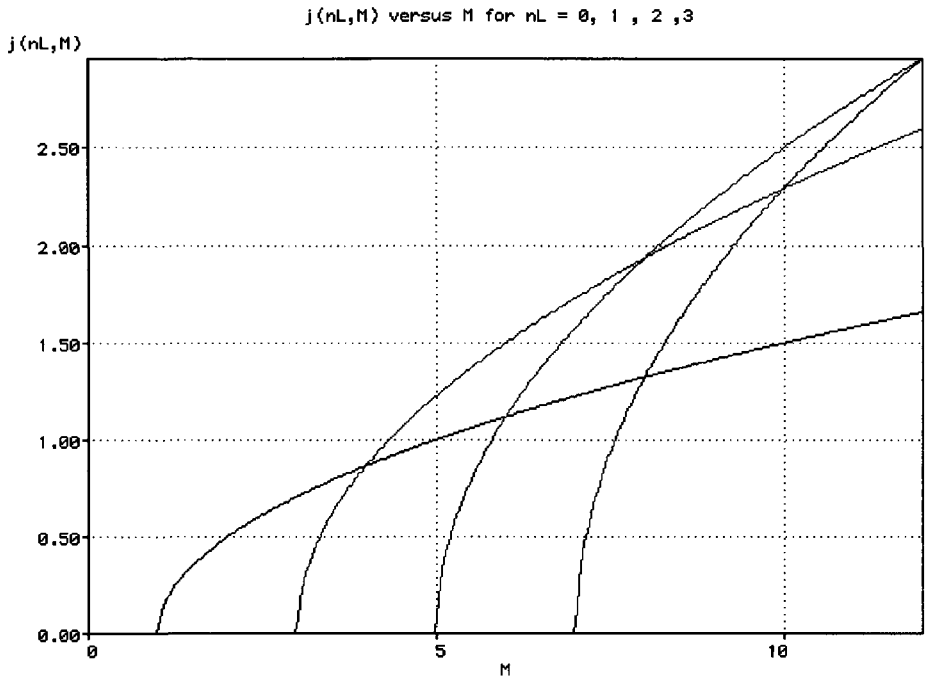

Figure 9.3: the jet currents $j(r, \theta, n_L)$ versus M for $n_L = 0$ (black), 1 (red), 2 (green), 3 (blue).

Figure 9.3 confirms that some initial current densities can be identical for two different values of n_L, at a specific value of E_F. This result is also summarized in table 9.1.

This new-observed initial current density behavior suggests that in the upper atmosphere of the neutron star, where E_F is lower since it scales with $n^{1/3}$ in relativistic regime, the initial current density increases with n_L. At the bottom of the atmosphere of the neutron star, where E_F is bigger, the initial current density increase with n_L. This could tentatively confirm the assertion that we made at the end of the section 9, namely:

Table 9.1: E_F and related pairs of n_L that give some identical initial current densities

$E_F = ME_0$	(pairs of n_L)		
4 E_0	(0,1)		
6 E_0	(0,2)		
8 E_0	(0,3)	(1,2)	
10 E_0	(0,4)	(1,3)	
12 E_0	(0,5)	(1,4)	(2,3)

Because of the very high density (or occupancy rate) of electrons at the ground state, this decay will be "Pauli-blocked", i.e. there will be no vacant states for the electron to decay, and so the acceleration will be ongoing. It will then be propelled via the astrophysical jets formed in the atmosphere of the neutron star.

This suggests that, because they cannot decay to the ground state, the electrons in excited states are propelled via the astrophysical jets, hence a higher current density for $n_L = 2$ than $n_L = 1$ at the bottom of the atmosphere of the neutron star.

Let us now conclude this chapter by saying that the final version of the Quasi-Realistic Jet Model developed is now ripe to be tested. This is the subject of the next section.

9.2 Jet Model via the Landau States and SS 433

Since we have a Quasi-Realistic Jet Model in place, the logical step now is to give it a try, using real objects' properties, such as the astrophysical jets observed in SS 433.

Let us see if we can get some reasonable figures when combining certain equations derived in the thesis with real SS433's properties. For instance, let us find an answer to the following question: *Assuming that SS433's compact object is a neutron star, what is the order of magnitude of its magnetic field?*

According to (4.71), the relativistic Landau energy for a particle mass m and charge q is

$$E_n^2 = m^2c^4 + p_z^2c^2 + c^2|q|\hbar\mathbf{B}_z 2n \tag{9.6}$$

where $n = \nu + (1/2)\left[1 - (g\ \zeta\ s/2)\right]$ is the quantum number numerating the energy levels of a charge particle in a magnetic field (Landau levels), $n = 0, 1, 2, \cdots$, $\zeta = q/|q|$ is the sign of the particle charge.

Hence if we put both a proton and a electron in the field, we would have a total relativistic energy

$$E_{n_e,n_p}^2 = \left(m_e^2 + m_p^2\right)c^4 + \left(p_{z_e}^2 + p_{z_p}^2\right)c^2 + c^2|q|\hbar\mathbf{B}_z 2\left(n_e + n_p\right) \tag{9.7}$$

close to the surface of the star.

Consistent with the Quasi-Realistic Jet Propulsion Mechanism described in section 8.3, we can imagine that the "Pauli-blocked" particles will be propelled via the astrophysical jets formed in the atmosphere of the neutron star in reason of the very high density (or occupancy rate) of particles at the ground state when located at the bottom of the atmosphere of the neutron star.

From the optical spectrum of SS433 illustrated in figure 1.4, we can observe the moving

lines that lie at unfamiliar wavelengths, which reveal the observational evidences of jets in SS433 [29]. The blue shifted and red shifted lines are denoted by the prefixes + and − respectively. The most predominant of these lines is H_α from the Balmer series. Other spectral lines from the Balmer, Paschen and Brackett series of hydrogen are observed as well and produced the jets.

From these observations, we can then believe that at large distance from a neutron star we have a beam of neutral hydrogen with asymptotic constant velocity v_0, as obtained in figure 7.2. So far from the neutron star, close to the dipole or z-axis (i.e. $z \gg x, y$) and where the effect of the magnetic dipole has negligible (recall (5.10)), the final total relativistic energy is (from now on ignoring the electron mass)

$$E_f^2 \approx \frac{m_p^2 c^4}{\sqrt{1-\frac{v_0^2}{c^2}}} \tag{9.8}$$

So the law of conservation of energy suggests that we can equal both total relativistic energies (9.7) and (9.8). This gives (if we ignored gravitational effects on the protons for the moment)

$$\left\langle m_p^2 c^4 + \left(p_{z_e}^2 + p_{z_p}^2\right) c^2 + c^2 |q| \hbar \mathbf{B}_z 2 \left(n_e + n_p\right) \right\rangle = \frac{m_p^2 c^4}{\sqrt{1-\frac{v_0^2}{c^2}}} \tag{9.9}$$

where the average is over all possible states. We can estimate this as follows: assume we are looking at the $n_e = n_p = 1$ and set the initial momenta in the z-direction equal to 0, i.e. $p_{z_e} = p_{z_p} = 0$ (as suggested in figure 7.2), so then one finds

$$\mathbf{B}_z \approx \frac{m_p^2 c^2}{4|q|\hbar} \left(\frac{1}{\sqrt{1-\frac{v_0^2}{c^2}}} - 1 \right) \tag{9.10}$$

So an approximate value of the magnetic field can be found since we have learned from the kinematic model of the jet in SS 433 presented in section 2.2 that the matter moves in

two exactly oppositely aligned jets with constant relativistic velocity $\beta = 0.2601$, where β is the velocity of the jet in units of speed of light c. This finally gives

$$\mathbf{B}_z \approx 1.3 \times 10^{14}\ T \tag{9.11}$$

This is huge since it equals the theoretical upper limit of magnetic field strength, which it has been estimated of around $10^{14}\ T$ for a typical neutron star in section 3.2. This suggests that some non-relativistic proton are ejected with the jets, since the approximate magnetic field is lower than the critical magnetic field $\mathbf{B}_z < \mathbf{B}^Q_{z_p}$ of $1.5 \times 10^{16}\ T$. At this magnitude of magnetic field, the electron is clearly relativist, i.e. $\mathbf{B}_z \gg \mathbf{B}^Q_{z_e} = 4.4 \times 10^9\ T$. Who knows, this result might explain why SS433 is so unique: *its magnetic field equals the theoretical upper limit of magnetic field strength, hence the formation of its jet!*

This just-developed formalism totally ignores the mechanism by which the separate electron and proton beams end up being hydrogen while would be a mixture of beam-beam interactions and radiative transitions. A better approach could be trying to establish the magnitude of magnetic field in which the observed average velocity, obtained from both estimated electron and proton velocities, that would be in the order of $0.2601c$.

The above-made calculations have considerable uncertainty. In addition to the guesses we have made for the relevant values of n_e and n_p, we have ignored gravitational effects on the protons: in this context we note that the escape velocity calculated non-relativistically is a significant fraction of c, implying that the $\mathbf{B}_z$ would need to be larger than we have calculated. In view of these uncertainties the value of $\mathbf{B}_z$ can really only be regarded as an order of magnitude estimate. However it is interesting that it lies well below the upper

limits found for neutron stars.

Considering the considerable amount of times invested for building this model, we are forced to leave this section as some future "work to be done". In this thesis, we have set up the problem with the varying field and indicated how the changing densities will affect the jet, both of which are new.

However, it is now important to stress that, although we outlined the essentials of the technique and discussed general features for building a Jet Model, a realistic model is beyond the scope of this thesis as it would involve a complex, self-consistent computer model of the jet. A realistic systematic study of this model requires a much more detailed numerical solution, where the jet density is allowed to vary and hence the transitions need to be taken into account.

Let us close up this section by saying that that we are convinced that the outcome of this work is quite reasonable for a Master of Science: we've got the ingredients assembled without quite making the cake!

Part IV

Conclusion

Chapter 10

Conclusion

10.1 Results

As a reminder, *the purpose of this work was to examine the role that the Landau States could play in explaining the origin of the astrophysical jets, in particular their geometry (i.e. narrow beam) and ejection speed (i.e. close to the speed of light) and other parameters.*

We have first proceeded with a detailed examination of SS433, in order to highlight its unusual characteristics. Once done, we undertook another survey that has taken a deeper look at the neutron star's exotic properties. We were then in position to figure out how its magnetic dipole generates the required ultra-strong magnetic fields suitable for the formation of the Landau states.

We have then initiated the core of this research in the second part of this document. We first undertook a deep exploration of the Landau states, especially about how they are created and how they behave in constant magnetic fields. We went then a step further, by

determining how these same Landau states behave in varying magnetic fields, such as the ones found in the atmosphere of the neutron star. As a reminder, this was an issue that (surprisingly) did not seem to have been discussed in the literature. This has of course given us an interesting novel result: this provided us with the required force that can propel charged particles via the astrophysical jets formed in the atmosphere of the neutron star.

Capitalizing on this interesting discovery, two models were proposed in the last part of this document: 1) a *Quasi-Realistic Astrophysical Jet Model* that explained how an astrophysical jet could be formed in the atmosphere of the neutron star, based on the current conservation principle, and 2) a *Quasi-Realistic Jet Propulsion Mechanism* that will try to explain how the photons could be emitted when the density in the Landau states changes in the vicinity of a neutron star's surface and propelled via the astrophysical jets formed in the atmosphere of the neutron star.

We have then demonstrated in this thesis that the Landau States can effectively be used for explaining the Astrophysical Jets Phenomena!

10.2 Suggestions for Further Research

As just before, we have clearly demonstrated in this thesis that the Landau States can be used for explaining the Astrophysical Jets Phenomena! However, the Jet Model we proposed is somewhat incomplete. Here are some short and long term actions that could be undertaken for completing the tasks initiated in this thesis.

First of all, the final version of the Quasi-Realistic Jet Model we proposed is non-relativistic. Since the electron density is higher than 10^6 g/cm^3 at the bottom of the atmosphere of the neutron star, and in such an environment, the relativistic regime must be used: a relativistic Quasi-Realistic Jet Model must be created as well. In this thesis, several efforts for adapting this model to the relativistic regime have been already undertaken. Consequently, we believe that with simply a marginal effort, our Quasi-Realistic Jet Model could become a relativistic one.

Some preliminary tests, using real objects' properties, should be performed on the non-relativistic (and eventually relativistic) Quasi-Realistic Jet Model(s) in order to quickly validate it (them). If some discrepancies are observed with the outcome of the Quasi-Realistic Jet Model(s) versus the astronomical observations, some series of iterative corrections will have to be implemented.

Once the Quasi-Realistic Jet Model(s) is improved and validated, a realistic model could be created. As a reminder, a realistic model was beyond the scope of this thesis, as it would have involved a complex, self-consistent computer model of the jet. A realistic systematic study of this model requires a much more detailed numerical solution, where the jet density is allowed to vary and hence the transitions need to be taken into account. This could then be pursued and achieved through a Ph.D study.

Part V

Bibliography

Bibliography

[1] 3c273: Chandra observes cosmic traffic pile-up in energetic quasar jet (`http://chandra.harvard.edu/photo/2000/0131/index.html`). Chandra X-ray Web Site, November 2000.

[2] T. N. Aeronautics and al. Cosmic Explosion among the Brightest in Recorded History.

[3] W. Baade and F. Zwicky. On super-novae. *Proceedings of the National Academy of Science*, 20:254–259, May 1934.

[4] J. H. Beall. Jets in astrophysics: A review (`http://www.lnf.infn.it/conference/vulc2008/talks/beall_jets.ppt`). , Vulcano Workshop 2008, Italy, May 2008.

[5] W. Brinkmann and al. Rosat observations of the w 50/ss 433 system. *Astronomy and Astrophysics*, 312:306–316, Aug. 1996.

[6] B. Carrol and D. Ostlie. *An Introduction to Modern Astrophysics.* Addison-Wesley, 1996.

[7] J. CHADWICK. The existence of a neutron. *Proceedings of the Royal Society of London*, Series A 136:p. 692–708, May 1932.

[8] S. Chandrasekhar. The maximum mass of ideal white dwarfs. *Astrophysical Journal*, 74:81–+, July 1931.

[9] S. Chandrasekhar. *An introduction to the study of stellar structure.* 1939.

[10] J. B. Crampton, D.; Hutchings. The ss 433 binary system. *The Astrophysical Journal*, 251:p. 604–610, December 1981.

[11] H. D. Curtis. *Pub. Lick Observatories*, (13):9–42, 1918.

[12] P. A. M. Dirac. The quantum theory of the electron. *Proceedings of the Royal Society of London*, A(117):610 - 624, 1928.

[13] Fabian and Rees. 1979.

[14] L. V. Fabrika, S. N.; Bychkova. The mass function of ss 433. *Astronomy and Astrophysics*, 240(2):p. L5–L7, December 1990.

[15] S. Gasiorowicz. *Quantum Physics.* 3rd edition, 2003.

[16] H. Goldstein. *Mécanique classique.* Presses Universitaires de France (Paris), 1964.

[17] Y. T.-M. Gottfried Kurt. *Quantum Mechanics: Fundamentals.* Springer, 2nd edition, 2003.

[18] P. Haensel, A. Potekhin, and D. Yakovlev. *Neutron Stars 1 Equation of State and Structure*, volume 326 of *Astrophysics and Space Science Library.* Springer, 2007.

[19] A. Harding and D. Lai. Physics of strongly magnetized neutron stars. *Reports on Progress in Physics*, 69:2631–2708, Sept. 2006.

[20] R. M. Hjellming and K. J. Johnston. An analysis of the proper motions of ss 433 radio jets. *Astrophysical Journal*, 246:L141–L145, June 1981.

[21] M. H. Johnson and B. A. Lippmann. Motion in a constant magnetic field. *Phys. Rev.*, 76(6):828–832, Sep 1949.

[22] W. C. Keel. The brightest quasar 3C 273 and its jet .

[23] T. Kotani. *X-Ray Observations of a Galactic Jet System SS 433 with ASCA*. PhD thesis, AA(Doctoral Thesis (Science), Department of Physics, School of Science, University of Tokyo, 1997), 1998.

[24] E. M. L. L. D. Landau. *Quantum Mechanics: Non-Relativistic Theory*, volume 3. 3rd ed. edition.

[25] D. Lai. Matter in strong magnetic fields. *Rev. Mod. Phys.*, 73(3):629–662, Aug 2001.

[26] R. Liboff. *Introductory Quantum Mechanics*. Addison Wesley, 4th edition, 2003.

[27] P. Lorrain and D. Corson. *Electromagnetic fields and waves*. Freeman, 2nd edition, 1970.

[28] B. Margon. Observations of ss 433. *Annual Review of Astronomy and Astrophysics*, Vol. 22:p. 507 – 536, 1984.

[29] B. Margon and al. *Ap. J.*, 230:L41, 1979.

[30] Milgrom. 1979.

[31] J. R. Oppenheimer and G. M. Volkoff. On massive neutron cores. *Phys. Rev.*, 55(4):374–381, Feb 1939.

[32] M. J. Rees. Black Hole Models for Active Galactic Nuclei. *Annual Review of Astronomy and Astrophysics*, 22:471–506, 1984.

[33] T. O. Sandro D'Odorico and al. Evidence that the compact object in ss 433 is a neutron star and not a black hole. *Nature*, 353:p. 329 – 331, September 1991.

[34] M. SCHMIDT. 3c 273 : A star-like object with large red-shift. *Nature*, 197(4872):1040–1040, 03 1963/03/16/print.

[35] S. Shapiro and S. A. Teukolsky. *Black holes, white dwarfs, and neutron stars: The physics of compact objects.* Research supported by the National Science Foundation. New York, Wiley-Interscience, 1983, 663 p., 1983.

[36] J. Singh. *Quantum Mechanics - Fundamentals and Applications to Technology.* Oct. 1996.

[37] G. B. T. Zwitter and S. Massaglia. Ss433: an up-to-date review. pages pp. 309–355, 1989.

[38] S. R. Vermeulen R.C., Schilizzi R.T. and al. *Astronomy and Astrophysics*, 270:p. 177, 1993.

[39] Wikipedia. Aquila Constellation.

[40] Wikipedia. Hamilton's principle.

[41] Wikipedia. Kinematics of constant acceleration.

[42] Wikipedia. SS433.

[43] Wolfram-MathWorld. Laguerre Polynomial.